UNIVERSITÀ DEGLI STUDI DI PADOVA

DIPARTIMENTO DI SCIENZE BIOMEDICHE

SCUOLA DI DOTTORATO IN SCIENZE CHIMICHE

XXX CICLO

PhD Thesis

Interspecies serum and complement-dependent mechanisms influencing the cellular uptake of nanoparticles.

Dottoranda: ALESSANDRA MARA GEFFNER-SMITH

Supervisore: PROF. EMANUELE PAPINI

December 2018

Acknowledgements

How can I convey my feelings about the people making my PhD possible on this three and a half year journey while I worked towards my PhD? Words seem paltry and I find it extremely difficult to express in these lines how grateful I am to my supervisor Prof. Emanuele Papini and tutor Regina Tavano. They have been a source of enlightening discussions and have propelled me towards my potential from a human aspect as well as from a scientific one. Without their dedicated efforts and inspiration, I would not have reached this point, and I appreciate their hard work and time in this endeavor. Thank you is an inadequate expression for how I feel but it will have to suffice.

To Prof. Fabrizio Mancin, Prof. Giorgio Arrigoni, Patrizia Polverino de Laureto, and Barbara Biondi who, through collaborations, made my dissertation possible; to Alvaro Martinez, Jakubwaldemar Trzcinski, Lucia Morillas Becerril, and Luca Gabrielli who were always dedicated to the synthesis of the nanoparticles and who were always open to interesting discussions. I also extend my gratitude and thanks.

To all the great people that shared other labs or the building; to Mox, who provided me not just laboratory equipment when needed but also tons of laughter, comradery, and most importantly, coffee. He was not just a scientific mentor but also a confidant; to Will, who through being a coffee break and Oreo buddy, made our building feel like home for me even though I was really so far from it; I also extend my warmest regards and thanks.

To Alexandria and Kyara who's lifetime of deep friendship crossed an ocean and for which I am the luckiest person alive. You both already know everything I could possibly write here and again I find myself deficient in words. But you both were always there with your confidence and belief in me even when my own in myself was faltering. You kept me going. Thank you.

To my Mom and Dad; you've provided me with unending love and support for which I am eternally grateful. To my Grandfather and all the wise things he taught me including the value of perseverance. Without you, my PhD would not have been possible.

To the people I have neglected to mention. Thank you.

Table of Contents

Abstract

Nanoparticles are utilized in a wide variety of biomedical fields and theranostic nanomedicine from imaging and sensing to drug delivery. Multifunctional nanoparticles encapsulated with imaging probes/diagnostic agents or therapeutic agents can be delivered *in vivo* via passive or active targeting, making them effective and efficient therapeutic agents. However, in order to optimize their efficacy, nanoparticle platforms must be designed in a way which limits cytotoxicity and optimizes biocompatibility for safe medical use.

The human immune system is a complex system of networks and cascade reactions which are intricate and tightly regulated. It is mainly comprised of two important reaction systems, the complement and coagulation cascade. In order to prolong the nanoparticles circulating in the bloodstream as well as enhancing sustained release of drugs to targeted tissues, surface functionalization ultimately reduces coagulation or complement activation by inhibiting the adsorption of blood proteins (stealthing) on the nanoparticles surface, called opsonization.

The most widely used surface functionalization is polyethylene glycol (PEG). The chemical conjugation of attaching this organic moiety to the nanoparticle is known as PEGylation. PEGylated particles undergo changes in physicochemical properties contributing to the overall stability and stealth ability PEG provides to nanoparticles. However, there are many drawbacks limiting the usefulness of PEGylation including complement activation or degradation.

Therefore, we have proposed and fully characterized alternative polymers, poly(2-methyl-2-oxazoline) (PMOXA) and poly(2-ethyl-2-oxazoline) (PEtOXA) which are more

biocompatible, can escape the mononuclear phagocyte system (MPS), and are easier to synthesize than PEG. Furthermore, we proposed two nanoparticle systems in order to characterize how biophysicochemical properties like surface functionalization and charge alter the way in which particles' interact with biological systems. We used two nanoparticle systems: 1) Inorganic solid silica (SiO_2-NPs) as they have become of increasing interest in controlled drug release due to their accessibility, versatility, high capacity of processing, and physical-chemical properties adapted through synthesis; 2) Gold nanoparticles (Au-NPs) due to their vast and unique optical and physical features. Au-NPs are inert, have extreme resistance to oxidation, and they are easily able to be functionalized by thiol compounds.

In the second part of my dissertation, I use two alternative animal models in order to probe and characterize the interactions nanoparticles have in non-human systems. Prior to human clinical trials, drugs were often tested *in vitro* and *in vivo* in a murine model, yet failed to be approved when proceeding with human trials. In many cases, mice responded quite differently than humans to drugs, contributing to the high failure rate of drug development. In fact, the majority of drugs never reach the marketplace following clinical trials. Therefore, it is imperative to understand the attributes which contribute to this phenomena so as to increase therapeutic applications of nanoparticles.

Chapter 1: Introduction

1. Nanoparticle's use in Bio-applications

Nanotechnology is the study and development of technology dealing with nanometer sized solid colloidal particles ranging in size from 10 to 1000 nm.[1,2] The driving force behind development of nanotechnology is the understanding of biological processes on the nanoscale level. As proteins have a typical size around 5 nm and some of the ultrasmall man-made nanoparticles are in the range of single digits as well, nanoparticles can be used as probes allowing us to study the cellular machinery with little interference. Small nanoparticles also have many other benefits over larger particles such as increased surface-to-volume ratio and increased magnetic properties. Thus there is great interest in using them in biomedical applications such as targeted drug delivery as they not only provide protection to the cargo but also enhance cellular uptake and selective delivery, hyperthermia, photoablation therapy, bioimaging, and biosensors.

1.1 Liposomes

The first NP platform was the liposome, first described in 1965 by Alec Bangham and colleagues as a model of cellular membranes establishing the basis for model membrane systems.[3] Enclosed phospholipid bilayer structures initially called 'bangosomes' consisting of a series of concentric bilayers of lipids known as lamellae, which are molecules that have a hydrophilic head group and a hydrophobic tail group, alternating with aqueous compartments within which soluble substances can be entrapped.[4] Phospholipids impulsively form closed structures when they are hydrated in aqueous solutions. Therefore, due to their self-assembling nature and thermodynamic phase properties, the appropriation by their hydrophobic sections into spherical bilayers are entropically focused making liposomes excellent payload carriers. Liposome-entrapped drugs with the anti-cancer drug cytosine arabinoside were some of the first used for demonstrations of

improved *in vivo* activity, increasing the survival of mice bearing L1210 leukemia. This form of delivery system is known as liposomal encapsulation technology (LET) where liposomes encapsulate numerous materials, forming a barrier around their contents. Due to this protection, the load is resistant to enzymes in the mouth and stomach, alkaline solutions, digestive juices, bile salts, and intestinal flora, generated in the human body, as well as free radicals and thus are protected from oxidation and degradation. This protective phospholipid barrier remains undamaged until the contents of the liposome are delivered to the exact target and the contents can be utilized. [5] The "rigidity" or "fluidity" and the charge of the bilayer are determined by the composition of bilayers themselves. Permeable and less stable bilayers can be obtained using unsaturated phosphatidylcholine species from natural sources such as egg or soybean phosphatidylcholine. However, rigid and impermeable bilayer structures can be obtained using saturated phospholipids with long acyl chains such as dipalmitoylphos phatidylcholine. Figure 1 displays the different kinds of liposomal structures which can be used to deliver lipophilic or hydrophilic drugs as well as lipids with negative or positive charges and ligand-targeted liposomes for active targeting.[6]

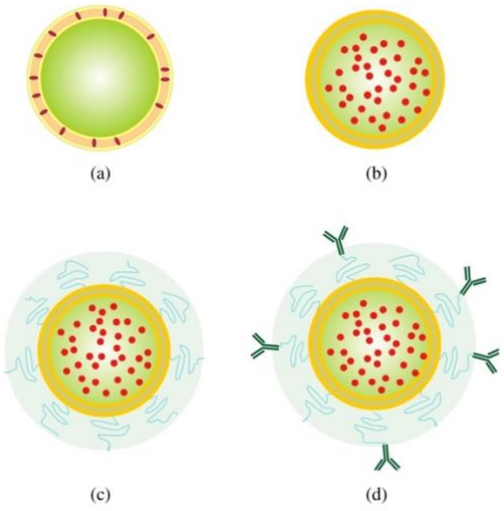

Figure 1: Structure of different liposomes. (a) classical liposome enclosing lipid soluble drugs, (b) classical liposome enclosing aqueous soluble drugs, (c) liposomes which have been sterically stabilized, and (d) ligand-targeted liposome encapsulating an aqueous soluble drug.

Taken from: *Lila, A. S. A., Ishida, T. & Allen, T. M. in Handbook of Nanobiomedical Research: Fundamentals, Applications and Recent Developments* ***3,*** *1–53 (2014).*

Over the years, development of important technical advances in liposomal research lead to remote drug loading, extrusion for homogeneous size, long-circulating (PEGylated) liposomes or "second-generation liposomes", triggered release liposomes, liposomes containing nucleic acid polymers, ligand-targeted liposomes, and liposomes containing combinations of drugs.[7] The first clinical trials of liposomal drugs were to treat patients with primary or metastatic liver cancer which was refractory to current therapies using liposomes containing doxorubicin. Phosphatidylglycerol, phosphatidylcholine, cholesterol, and DXR were intercalated in the lipid bilayer forming a liposome-associated doxorubicin (L-DXR) with a mean size of around 0.3-0.5 microns.

Although classical liposomes had unique advantages due to their diverse range of compositions, abilities to carry and protect many types of biomolecules, as well as their biocompatibility and biodegradability, they also had difficulty retaining some types of entrapped molecules in the

liposome interior when exposed to serum proteins.[8,9] In order to control the release rate of the entrapped cargo, drugs with physical characteristics amenable to retention in liposomes must be chosen. Liposomes have high permeability to hydrophobic drugs and have low permeability to hydrophilic drugs, similar to biological membranes. Therefore, highly hydrophobic drugs such as paclitaxel are very problematic when enclosed inside liposomal carriers. A way in which this was avoided was by creating drug loading in response to trans-membrane pH gradients responding to internal acidic buffers. Drugs that are weak bases possessing a primary, secondary, or tertiary amine, can be loaded in response to pH gradients and drugs such as paclitaxel which are not weak bases can be converted to weak base prodrugs thus increasing liposomal retention and encapsulation. Drug retention can be further improved by enhancing precipitation via increasing intra-liposomal drug concentrations above their solubility limits.

1.2 Surface modification of Liposomes

Another issue with classical liposomes was the rapid clearance via uptake into cells of the mononuclear phagocyte system (MPS), mostly accumulating in the liver and spleen.[10] Although diseases like leishmaniasis, in which the MPS is involved, can benefit from rapid liposomal uptake and clearance, and, in general, this response limits their ability to deliver drugs to other tissues or cells and can cause toxicity to the MPS organs, because the distribution into tissues was highly reduced by MPS capture as well as toxicities to MPS organs themselves, an alternative solution needed to be found. First attempts included blocking MPS with large pre-doses of empty liposomes before injection with drug loaded liposomes. Since the MPS would be blocked, the circulation half-life of classical liposomes would increase by evading capture of the MPS organs.[11] It was identified the surface properties of liposomes led to their premature clearance via absorption of serum proteins, opsonines, of the complement system leading ultimately to their rapid clearance. When

nanoparticles are introduced into physiological environments such as blood or inside cells, proteins, and small molecules which are at very high concentrations, they are absorbed onto the surface of the nanoparticle, forming a "protein corona" or a cloud of aggregated proteins.[12] Opsonins have been previously identified as immunoglobulins, fibronectin, beta 2-glycoprotein, C-reactive protein (CRP), and beta 2-macroglobulin. The protein corona consists of two layers, the hard and soft corona, which are the inner and outer layers of the corona, respectively. The hard corona undergoes low molecule exchange rates and high affinity to the nanoparticle's surface whereas the soft corona is composed of weakly bound proteins with high exchange rates. The soft corona being dynamic, rapidly exchanges its components based upon nearby dynamic protein concentrations and a changing proteome. The protein corona composition alters the biological identity of the nanomaterial and thus determines the physiological response including agglomeration, cellular uptake, circulation lifetime, signaling, kinetics, transport, accumulation, and toxicity. Once the nanomaterial has been identified by MPS cells such as neutrophils, monocytes, and macrophages, uptake and membrane lysis is initiated and the C5b-9 complexes, also known as the membrane attack complex (MAC), produces lytic pores inducing cell lysis or liposomal content release. Therefore, research began comparing unmodified phospholipid membranes and biological membranes with a surface layer rich in carbohydrates such as natural polysaccharides like mannan, amylopectin, and dextran thinking by increasing the surface hydrophilicity of the liposomes, the liposome would be "stealth" and avoid attracting proteins onto the surface. Such "stealthing" agents are generally enhanced by the removal of hydrogen-bond-donating groups from hydrophilic polymers.

Ultimately, classical liposomes were coated with a protective, hydrophilic barrier on the liposome surface to sterically stabilized them using inert, biocompatible substances, like

ganglioside GM1, phosphatidylinositol, or lipid-conjugated polyethylene glycol (PEG).[13–15] PEG is a linear non-ionic hydrophilic polyether diol which is biocompatibility, soluble in aqueous and organic media, nontoxic, has very low immunogenicity, and good excretion kinetics. Surface modification of liposomes with PEG can be achieved by physically adsorbing the polymer onto the surface of the vesicles, by incorporating the PEG-lipid conjugate during liposome preparation, or by covalently attaching reactive groups onto the surface of preformed liposomes.[16] However, the most widely used method is anchoring the PEG polymer in the liposomal membrane via a cross-linked lipid (ie, PEG-distearoylphosphatidylethanolamine (DSPE)).

PEGylated liposomes strongly reduced MPS uptake and prolonged circulation in the blood which subsequently improved distribution in perfused tissues. Moreover, the PEG chains improve stability avoiding vesicle aggregation. This is partially due to the molar mass of PEG chains and its uniformity "molecular cloud" but also due to its considerable conformational flexibility (Figure 2).[17] PEG stabilizes liposomes by providing a strong interbilayer repulsion that can overcome the attractive Van der Waals forces and thus avoids aggregation by increasing the repulsive barrier between two approaching particles. Elastic and osmotic restrictions contribute to stabilization. Elastic or volume restriction stems from conformational entropy loss or enthalpy gain when the available volume of two surfaces is reduced as they come closer together, resulting in particle separation due to an increase in the free energy of mixing. Osmotic contribution occurs when polymer concentrations increase as the two surfaces come closer together, causing an influx of water which ultimately forces particles apart. This mechanism is also applicable to stealthing particles against serum proteins of the complement system. As proteins approach the particle's surface, an osmotic repulsive force is created when the polymer coating undergoes a reduction in available

conformations due to interpenetration of polymer chains. Therefore, polymer density is crucial to stealth as high polymer density suggests that compression is preferred over interpenetration, while if the surface density is low, interpenetration is likely to dominate.[18]

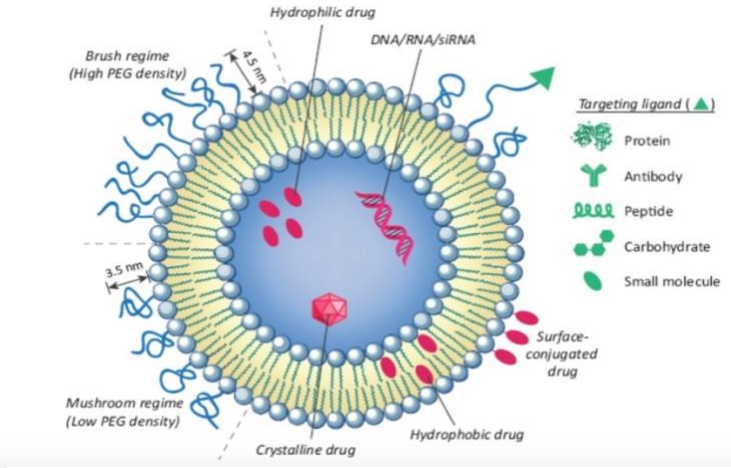

Figure 2: Liposome structure modified with low and high PEG densities for targeted delivery of active payloads.

Taken from: *MG, K., V, K. & F, H. History and Possible Uses of Nanomedicine Based on Nanoparticles and Nanotechnological Progress. J. Nanomed. Nanotechnol.* ***6,*** *(2015).*

Subsequent clinical trials in humans used PEG-liposomes as carriers of doxorubicin for the treatment of Kaposi's sarcoma in HIV patients and for demonstrating the stealthing capability of this complex. [19] Yet, antibodies against PEG produced by splenic B cells can develop after the first administration of PEGylated liposomes indicating potential immunogenic and antigenic effects. PEG can also bioaccumulate and form vacuoles in some organs, can be degraded by oxidative reactions, and is non-biodegradable. Also, anti-PEG antibodies have been reported indicating PEG has the potential to be immunogenic and antigenic. Furthermore, in order to provide effective counter phagocytosis, PEG chains typically need to have a molecular weight in excess of 2,000 Da, substantially increasing the overall hydrodynamic diameter.[20] Therefore, alternatives must be created in order to maintain the liposomal effectiveness.

Alternative polymers for PEG have been created with the hope of achieving even better control over the properties of modified drugs and drug carriers. The qualities of a polymer must be soluble, hydrophilic, have a highly flexible main chain, and high biocompatibility. Liposomes have been proposed that contain DSPE which are covalently linked to poly(2-methyl-2-oxazoline) or to poly(2-ethyl-2-oxazoline) and polymers such as polyglycerols, poly[N-(2-hydroxypropyl)meth-acrylamide)], poly-N-vinylpyrrolidones, polyvinyl alcohol, or L-amino-acid-based biodegradable polymer-lipid conjugates. Although these alternatives provided longer blood circulation time and decreased uptake by MPS, PEG still remains the gold standard in steric stabilization of liposomes.

1.3 Biodegradable polymers with Liposomal coatings

Ever since the invention of bioabsorbable sutures, the possibility of using biodegradable polymers as drug carriers became the forefront of scientific research in pharmacy, chemical engineering, biomedicine, and other disciplines. The advantages of biodegradable polymers over other carrier systems is they can deliver drugs directly in circulation as well as not needing to be removed once the drug is delivered due to their nature of degrading into nontoxic materials eliminated from the body via natural metabolic pathways.[21] Examples of such particles include inorganic mesoporous silica nanoparticles (MSNPs) which have a unique mesoporous structure preserving chemical stability, surface functionality, and biocompatibility which leads to controlled drug release and targeted delivery.[22] A biodegradable hollow mesoporous silica nanoparticle (dHMSN) was created with co-encapsulation of all-trans retinoic acid (ATRA) and doxorubicin (DOX) as well as IL-2 absorbed on the surface via electronic interaction. In order to improve the stability and biocompatibility as well as deliver a synergistic antitumor effect, dHMSNP was further coated with a lipid bilayer (dHMLB).[23] Another mesoporous silica nanoparticle carrier for

pancreatic cancer is a co delivery system for a pancreatic cancer drug, gemcitabine (GEM), and an albumin-bound paclitaxel (PTX) nanocarrier (Abraxane). This high drug loading was achieved by using a supported lipid bilayer to encapsulate the MSNPs which allowed high GEM loading and the ability to copackage PTX with no evidence of local or systemic toxicity. Drug co-delivery provided more effective tumor shrinkage than GEM-loaded LB-MSNP, free GEM, or free GEM plus Abraxane due to the ability of this co delivery system to synergistically suppress pancreatic cancer stromal volume and tumor size, and eliminated metastatic foci.[24]

1.4 Inorganic nanoparticles

Inorganic nanoparticles such as solid silica (SiO_2-NPs) and mesoporous silica nanoparticles (MSNPs) have become of increasing interest as the mean human adult intake of amorphous silica is estimated to be about 2 mg/kg of body weight per day.[25] Furthermore, silica is utilized for controlled drug release due to their high capacity for processing and physical-chemical properties adapted through synthesis. However, the loading capacity is double for MSNPs than for SiO_2-NPs due to the increase surface area via numerous meso-pores ranging in size from 2 nm and 50 nm. [26] Figure 3a shows how MSNPs physically or chemically absorb active payloads which are released using the "gatekeeper" strategy or control the binding affinity by modifying the inner surface of the pores. Whereas in Figure 3b,and c, SiO_2-NPs encapsulate or conjugate its payloads releasing its cargo via chemical linkers or the degradation of silica matrix.[27]

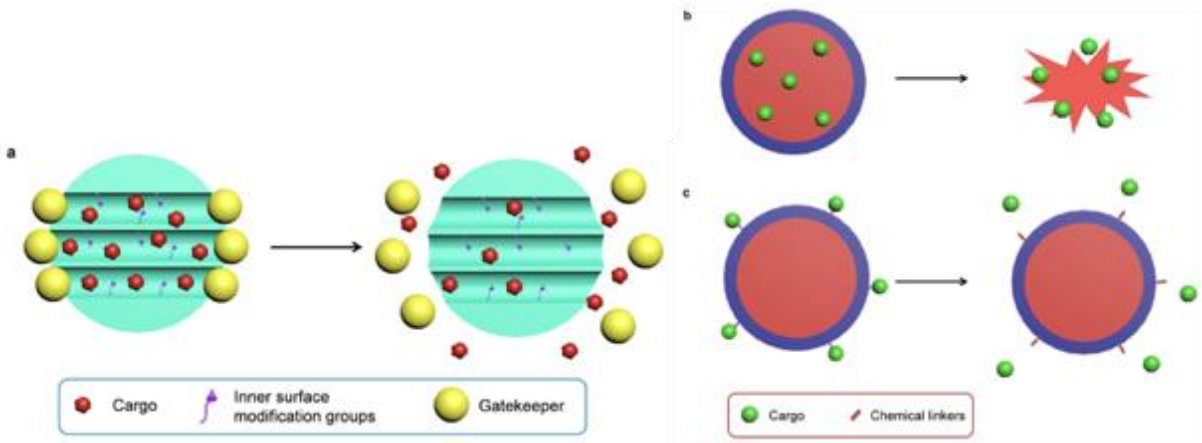

Figure 3: (a) Mesoporous silica nanoparticles and (b,c) solid silica drug loading and releasing processes.

Taken from: *Tang, L. & Cheng, J. Nonporous silica nanoparticles for nanomedicine application. Nano Today* ***8,*** *290–312 (2013).*

By exploiting versatile silane chemistry, many functional moieties can be attached to the nanoparticle's surface and therefore the desirable surface properties for biomedical applications can be tweaked based upon the targeted disease. A wide variety of polymers are used to modify the surface of the SiO_2-NPs such as cellulose derivatives and polymeric matrices based on poly(ethylene oxide) which have low toxicity, are hydrophilic, and are stable in biological pH environments. PEG has been utilized frequently as a polymer coating, providing better circulation time and targetability. However, alternative polymers such as poly(2-methyl-2-oxazoline) (PMOXA) and poly(2-ethyl-2-oxazoline) (PEtOXA) have been suggested as protein-repellent or nonfouling polymers which are easier to synthesize and can incorporate varying monomers to tailor the nanoparticle for specific applications. Although PEGylated oxazoline polymers are highly water soluble, amphiphilic, very flexible and hydrated in water, non-toxic, and may be produced with low polydispersity, PMOXA can be further tuned in size and structure using a living cationic ring-opening polymerization.[28]

2. The immune system and stealthing polymers for nanoparticles

2.1 Innate Immunity and the Complement system

Upon nanoparticle administration, blood is the first physiological environment the particle encounters thus dictating its ultimate function. Blood is composed of a cellular component of red and white blood cells and platelets suspended in a liquid component, plasma. Plasma can be isolated from anti-coagulated whole blood via centrifugation whereas whole blood lacking an anti-coagulant undergoes centrifugation and yields the supernatant fluid called the serum. Serum lacks fibrinogen, prothrombin, and other clotting proteins but is similar to plasma with regard to the concentration and composition of many small molecules including proteins and peptides like albumins, globulins, lipoproteins, enzymes, and hormones; nutrients such as carbohydrates, lipids, and amino acids; electrolytes; and organic wastes. Serum is responsible for transporting dissolved gases, nutrients, hormones and metabolic wastes, as well as regulating body temperature, pH and ion composition of interstitial fluids, limiting fluid losses at injury sites, the defense against pathogens. One of the major differences between plasma and serum is the physiological concentration of small molecules such as thromboxanes.[29]

The innate immune system utilizes complex mechanisms to defend against pathogens and to maintain homeostasis via clearance of cell debris, rapid recall of adaptive responses, and facilitating wound healing. Innate immune cells like dendritic cells, macrophages, and neutrophils as well as cells from the adaptive immune system such as T cells, express pattern recognition receptors (PRRs) which are responsible for detecting pathogen-associated molecular patterns (PAMPs). PRRs include Toll-like receptors (TLRs), the nucleotide-binding oligomerization domain (NODs)-like receptors (NLRs), the retinoic acid-inducible gene (RIG)-I-like receptors (RLRs), membrane C-type lectin receptors (CLRs), and DNA

receptors. Soluble PRRs such as surfactant proteins (SPs) and mannan-binding lectins (MBLs) are also able to recognize PAMPs.[30] The deposition of opsonic blood proteins on pathogens, called opsonization, clears the pathogens from the body by aiding recognition by macrophage receptors, such as fibronectin, immunoglobulins, and some components of the complement system which are often the first to respond.[31] The complement system is a set of unique plasma proteins which are converted to their active form through a cascade of zymogen activation where an enzyme is activated by a second enzyme, which itself has been activated by proteolytic cleavage.[32] The complement system is responsible for the initiation of the acute inflammatory response via releasing chemotactic factors and induce vasodilatation with increased permeability, mediates antibody-dependent cytolysis, removes immune complexes from the circulation, and finally induces phagocytosis by acting as an opsonin. There are three distinct pathways: classical, lectin, or the alternative pathway. The classical pathway is triggered when C1q, one of the three subunits of the first component of complement, binds to IgM or IgG complexed with antigens forming the C1-complex. The lectin pathway is triggered by the binding of mannose binding lectins to sugars on the surface of the pathogen. The alternative pathway can be spontaneously activated by absorption of C3b onto the surface of the pathogen via C3 hydrolysis. The convergence of the three complement pathways occurs around the conversion of C3 to C5 convertase activated by C3 convertase via the binding of C3b ultimately leading to the formation of the membrane attack complex (MAC). However, complement can also be activated by acting independently of C3. Complement can be activated by an additional bypass pathway acting independently of C3 or bypasses the C3 convertase. It is mediated by thrombin acting on the C5 convertase, bypassing C3 convertase.[33]

The complement systems exists in a careful state of homeostasis where activation of the inactivated proteins are closely monitored by an elaborate system of inhibitors which control activation as well as the response of the protein once activated (Figure 4a). In order to prevent complement from damaging host tissues, short half-lives of the thioester group of C3b and the C3 convertases limit their action to the site of activation. Carboxypeptidase N is a fluid phase regulator of all the complement pathways as it cleaves and partly inactivates the anaphylactic peptides C3a and C5a. C1 inhibitor (C1INH) induces the dissociation of the C1 components and C4bP displaces a component of the C3 thus regulating the classical and lectin pathways. Factor H, FHL1, and the activator protein properdin are all fluid phase regulators of the alternative pathway. CFHR1, clusterin (Apo J), and vitronectin are soluble inhibitors of the terminal pathway and CD59 preventing the assembly of the membrane attack complex. High-density lipoprotein (HDL) particles associate with clusterin (Apo J) acting as an adhesion protein and as a potent inducer of cell aggregation. Vitronectin is involved in cell attachment or spreading by binding to the extracellular matrix. Finally, properdin activates C3 convertase in the alternative pathway by directly binding to the labile C3bBb complex leading to C3bBbP. In contrast, factor H inhibits the activation of the alternative pathway by binding to C3-fragments and Apo E on HDL particles. Apo J complexes with Apo A-1 inhibiting the cytolytic activity of the C5b-9 complex. C9 polymers are prevented from inserting into the cell membrane by Apo A-I and Apo A-II. Complement receptors bound to the cell membrane include CR1 (CD35), CR2 (CD21), CD55 (DAF), CD46 (MCP), CD59 (protectin), and CRIg (vsIG4) (Figure 4b). These receptors have multiple ligands to which they bind such as fibrinogen which inhibits the alternative pathway activation by possessing binding affinity for factor H. CR1 binds C3b, iC3b, and C4b whereas CR2 binds C3d, C3dg, CD46, CD55, CD59, and CRIg. CR3 and CR4 mediate phagocytosis of C3b-opsonized particles by binding iC3b, C3dg, and C3d.

Although complement activation is best studied in its involvement in innate immunity, it also has important functions in adaptive immunity as well. For example, impaired dendritic cell differentiation and activation as well as memory B cell and regulatory T cell function are associated with C3 deficiency in humans. [34] Furthermore, inflammatory T cell responses and tolerance are enhanced by complement signaling via antigen presenting cells.

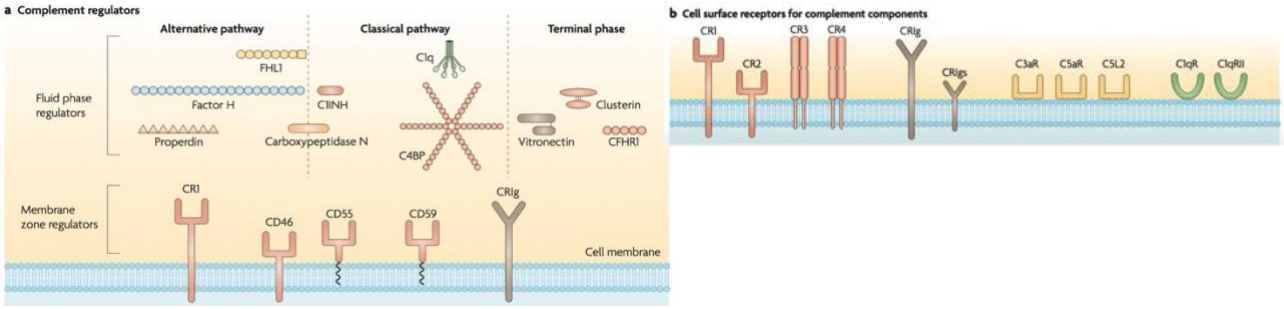

Figure 4: Complement regulators and surface receptors. (a) Complement regulators can be either fluid phase regulators or at the cell membrane regulators. (b) Complement receptors on the cell membrane.

Taken from: *Zipfel, P. F. & Skerka, C. Complement regulators and inhibitory proteins.* Nat. Rev. Immunol. ***9,*** *729–740 (2009).*

2.1.1 Classical Complement Pathway

During the classical pathway activation, C1q binds to immunoglobulins IgM or IgG complexed with antigens forming the C1-complex where one molecule of IgM or at least two molecules of IgG are required for efficient activation. In humans, IgG3 and IgG1 are strong complement activators, but IgG2 is a poor activator, and IgG4 does not activate complement. The charged residues Asp 417, Glu 418, and His 420 in the Cy3 region of IgM have been proposed to form the site to which the gClq domain binds, a 33 kDa glycoprotein, one of a number of C1q receptors/binding site. C1q (460 kDa) is produced mainly by immature dendritic cells, monocytes, and macrophages and is composed of 18 polypeptide chains (6A, 6B, and 6C) which form six globular target recognition domains (gC1q).[35] Two molecules of C1r and two molecules of C1s ultimately forms $C1qr^2s^2$, a Ca^{2+}dependent tetrameric

proenzyme complex by binding to the C1q collagen domain. C1q directly binds to the pathogens surface and undergoes a conformational change in the collagen region of Clq which in turn activates Clr and Cls which are both serine proteases. $C1r^2s^2$ forms via Ca^{2+} dependent interaction with the binding interface comprised of a Ca^{2+} binding site in the EGF domain of each subcomponent.[36] Once activated, the tetramer unfolds extending the C1s ends outside the C1q cone in order to interact with C4 and C2. C4 is cleaved producing 9 kDa C4a and 190 kDa C4b, which binds the zymogen C2 in a Mg^{2+}-dependent manner. C2 is then cleaved producing C2a, which contains a von Willebrand factor (vWf) domain and a serine protease (SP) domain and attaches to C4b making up the C3-convertase , and C2b, which is released into circulation. C3-convertase (C4b2a complex) cleaves C3 into C3a, an inflammation mediator, and C3b, an opsonin, which later joins with C4b2a to make C5 convertase (C4b2a3b complex).[37] C5 convertase cleaves C5 into C5a, interacts with C5a receptor (C5aR) to attract leukocytes, and C5b, containing binding sites for the next components in the pathway, C6, C7, C8, and C9 forming the membrane attack complex (MAC or the C5b-9 complex). C3a, C4a, and C5a are small cationic peptides also known as anaphylatoxins that bind to specific receptors on basophils and mast cells. C5b contains a binding site for C6, which becomes bound while the C5b molecule is associated with its C3b tether. The C5b6 complex may be released from C3b, or it may remain anchored until it binds a molecule of C7 forming a trimolecular complex, C5b-7, which adopts a hydrophobic and lipophilic character and associates with the membrane exposing the binding site for C8 as it burrows into the cell membrane.[38] As the complex inserts deeper into the membrane, C9 binds to C8 and undergoes conformational changes which inserts the now C5b-9 complex, or the membrane attack complex (MAC) further into the membrane as well as attracting between 12 and 18 more C9 molecules in each complex. This forms a hollow cylinder destroying the cell membrane thus leading to cell lysis and death.[39] The cell which is now

permeable to small ions but not to proteins as well as large influxes of Ca^{2+} ions, poisons the cell.

2.1.2 Lectin Complement Pathway

Lectin pathway activation occurs when sugars on the surface of the pathogen are bound by pattern recognition molecules (PRMs) either ficolins (FCNs), 35 kDa FCN1 (M-ficolin), 34 kDa FCN2 (L-ficolin), and 33 kDa FCN3 (H-ficolin), or certain collectins mannose-binding lectin (MBL), collectin (CL)-10, and CL-11 which are non-antibody, non-enzyme carbohydrate-binding proteins, as in the selectin adhesion molecules belonging to the collectin family produced by the liver.[40] MBLs bind d-mannose (Man), N-acetyl-d-glucosamine (GlcNAc), or l-fucose (Fuc), in both a calcium-dependent manner via membrane C-type lectin receptors (CLRs) whereas ficolins bind via a fibrinogen-like (fbg) domain in a calcium independent manner.[41] Ficolins are also considered to be elastin- and corticosteroid-binding proteins.[41–44] Ficolin-1 and ficolin-3 have only one binding pocket each, while ficolin-2 has four binding pockets.[45] Ficolin-1 and ficolin-2 possess ligands capable of binding to GlcNAc, N-acetyl-d-galactosamine (GalNAc), N-acetylated cysteine as well as an artificial ligand, acetylated human albumin. Ficolin 3 binds N-acetylated compounds as well as sialic acids. Mannose binds to the carbohydrate-recognition domain in a calcium dependent manner via an ASP 206 residue, a calcium ligand, and Glu 193 and Asn 205 residues, calcium ligands forming H bonds with the 4-OH group of mannose.[46] CLRs are mostly expressed on myeloid cells, functioning as pattern recognition receptors (PRRs) and reacts to ligands from non- self (pathogen-associated molecular patterns, PAMPs), damaged-self (damage-associated molecular patterns, DAMPs) or altered self (tumor-associated molecular patterns, TAMPs).[47] CLRs recognize their ligands by a carbohydrate-recognition domain (CRD) via two binding motifs: EPN motif which binds to mannose, N-

acetylglucosamine, L-fucose, and glucose; and the QPD motif which recognizes galactose and N- acetylgalactosamine.[48] These galactose recognizing CRDs bind via a glutamine-aspartic acid instead of the glutamic acid-asparagine residues which mannose recognizes. EPN motif leads to the formation of a complex with protease zymogens called Mannose-binding lectin Associated Serine Protease MASP1, MASP2, MASP3, MBL-associated protein of 19 kDa (MAp19), and MBL-associated protein of 44 kDa (Map44), truncated alternative splice products of the MASP2 and MASP1/3 genes.[49] MASPs are structurally and functionally similar to C1r and C1s where MASP2 cleaves C4 and C2 into C4a, C4b, C2a, and C2b forming the C3-convertase (C4b2a complex) as in the classical pathway. Therefore, the activation of the lectin pathway via C3 and C5 convertase complexes is impossible without MASP2. C3 can be directly activated by MASP1, bypassing C4 and C2, by direct cleavage of complex-bound MASP-2 or cleavage of C4b-bound C2. MASP3 does not have an identifiable substrate thus far. MASP-1 activates MASP2 as well as factor D, which is a component of the alternative pathway which indicates that MASP-1 is an initiator of the alternative pathway.[50] Collectins bind the same C1q receptor and are thus able to activate the classical pathway by directly activating the $C1r_2C1s_2$ tetramer in the absence of C1q.

2.1.3 Alternative Complement Pathway

In plasma, during normal physiological conditions, the dominant active complement pathway is the alternative, monitoring for pathogen invasion by maintaining a low level of constitutive activation by a process known as tick-over. Despite the name, the alternative pathway accounts for up to 80–90% of total complement activation. The alternative pathway can be spontaneously activated by absorption of C3b onto the surface of the pathogen via C3

hydrolysis. C3 is mildly unstable in water, thus causing the internal thioester bond to breakdown forming C3(H_2O) and binding factor B to form activated C3(H_2O)B or fluid-phase C3 convertase. C3(H_2O) can also non covalently bind to the pathogen's surface and bind factor B and D to cleave C3 but on C3(H_2O)B convertase cleaves C3 into C3a and C3b which following binding to the surface of the pathogen, binds to factor D to form C3bBb, stabilized by properdin (P) (Figure 5).[51,52] Once bound, properdin (P) can recruit fluid-phase C3b, independent of covalent binding, to form the convertase C3bBbP thus directing activation in such a way as MBL does in the lectin pathway. Complement factor D cleaves complement factor B to Ba and Bb activating the Alternative pathway. A positive feedback loop is established, regulated by factor H and I, as the convertase C3bBbP also cleaves C3 into C3a and C3b, building up more C3b onto the surface of the pathogen. Factor H inhibits the alternative pathway by disrupting Bb in the C3 convertase as well as behaving as a cofactor for Factor I which cleaves C3b and C4b. C4b-binding protein (C4BP) is involved in inhibiting the classical and lectin pathways via binding C3b, decaying C3 convertase, and being a cofactor for Factor I.

Furthermore, C3bBbP forms C5-convertase ($(C3b)_2BbP$) by binding additional C3b, and converges with the two other pathways where C5 convertase cleaves C5 into C5a, interacts with C5a receptor (C5aR) to attract leukocytes, and C5b, interacting with C6, C7, C8, and C9 forming the membrane attack complex (MAC) or the C5b-9 complex. The MAC complex forms transmembrane channels destroying the cell membrane leading to cell lysis and death.[37] However, on normal cells, C3b is rapidly deactivated to iC3b by factor I via innate regulatory mechanisms suppressing complement activation as uncontrolled activation can induce tissue damage and the pathogenesis of various conditions like autoimmune diseases, sepsis, and transplant rejection are caused by the inappropriate activation of complement.[53]

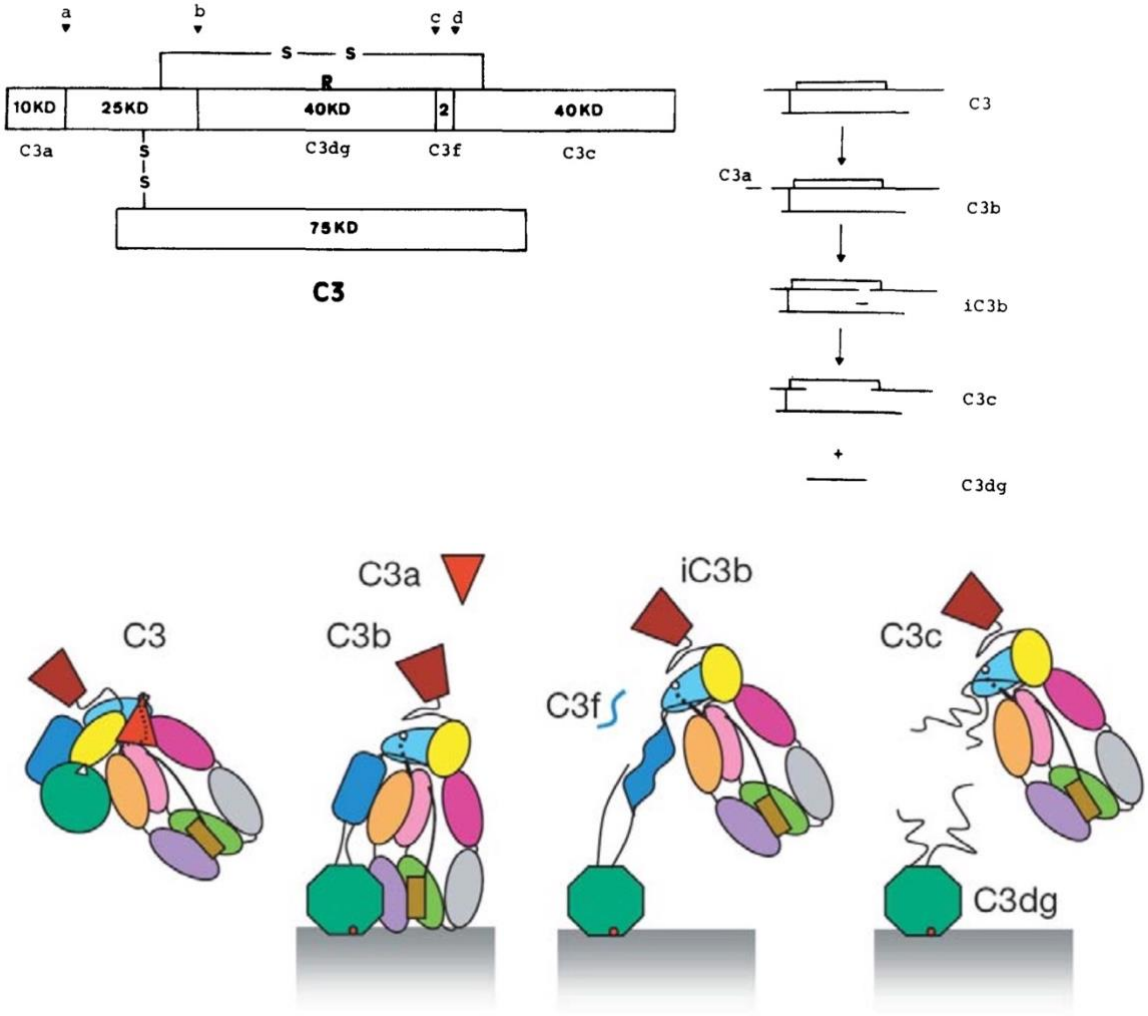

Figure 5: Schematic diagram of complement C3 protein as well as its cleavage sites and subsequent fragments upon C3 activation.

Taken from: *Seifert, P. S., Messner, M., Roth, I. & Bhakdi, S. Analysis of complement C3 activation products in human atherosclerotic lesions.* Atherosclerosis ***91,*** *155–162 (1991).*

Janssen, B. J. C., Christodoulidou, A., McCarthy, A., Lambris, J. D. & Gros, P. Structure of C3b reveals conformational changes that underlie complement activity. Nature ***444,*** *213–216 (2006).*

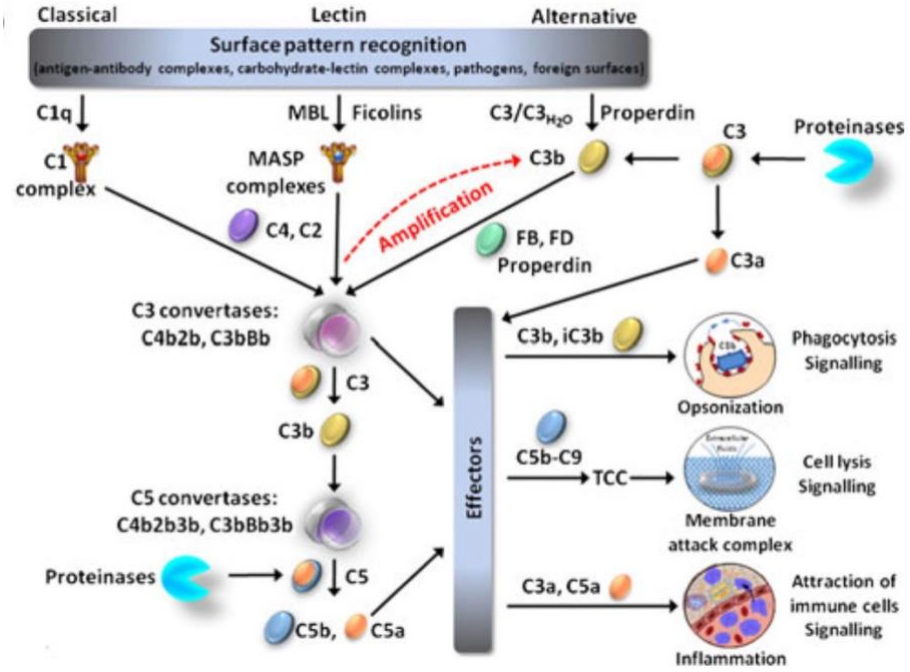

Figure 6: The complement system is divided into 3 pathways: Lectin, Alternative (Mg^{2+}), and classical (Ca^{2+}). Whichever pathway is taken, it leads to C3 convertase and cell lysis via an amplification loop.

Taken from: *Oikonomopoulou, K., Ricklin, D., Ward, P. A. & Lambris, J. D. Interactions between coagulation and complement—their role in inflammation.* Semin. Immunopathol. ***34,*** *151–165 (2012).*

2.2 Coagulation Cascade and the Complement system

Many enzymatic cascades control a wide range of biological functions where three protein networks play dominant roles including the complement system (discussed above), the coagulation cascade, and the fibrinolytic system. These three pathways all consist mainly of serine proteinases with trypsin-like activity, together with their activators and inhibitors. The complement and the coagulation systems are two distinct protein networks, however, they both are involved in the first line of defense against pathogens and the inflammatory response as well as having a few points in the cascade which link these two pathways together. Hemostasis is continuously active at low levels in the body, terminating bleeding and slightly favoring an anticoagulant state, and as in the complement system, the procoagulant factors are activated in tightly controlled conditions and regulations. Hemostasis not only supports

blood clotting (coagulations), but also is involved in fibrinolysis, the dissolution of blood clots, and is activated by either an intrinsic or extrinsic cascade (Figure 6). Following tissue damage, the functions of blood cells, the vascular system, several soluble plasma proteins, aggregation of platelets, and low molecular weight components are all involved in the regulation of hemostasis. For example, effective hemostatic responses depend greatly on the regulation of mediators such as the activated and aggregated platelets which provide a negatively charged surface in areas in which the clotting cascade is initiated.[54]

Upon tissue damage, platelets are activated via adhesion to the extracellular matrix by collagen binding to either platelet GP Ia/IIa and GP VI receptors or by binding to platelet glycoprotein (GP) Ib-IX-V receptor complex via a bridge produced by Factor XV or the von Willebrand factor. Platelet adhesion can be inhibited by high density lipoprotein (HDL) and Apo A-1 which prevents von Willebrand factor (vWF) self-association and prevents circulating vWF binding to adherent vWF fibers, respectively.[55] Thrombin also activates platelets through protease-activated receptors (PAR) on the platelet surface via G protein-coupled receptors (GPCR). Platelet degranulation releases thromboxane A_2 (TXA_2) which triggers platelet activation through GPCR leading to an increase in cytosolic calcium concentrations.[56] Coagulation is initiated and TXA_2 being unstable, quickly hydrolyzes into the stable and inactive thromboxane B2 (TXB_2). TXA_2 is a prostanoid, an oxygenated lipid, produced by the metabolism of arachidonic acid (AA) released from membrane phospholipids by phospholipase A_2 (PLA2) through the cyclooxygenase (COX) pathway. Phospholipase A_2 catalytically hydrolyses the Sn2 ester bond of phospholipids releasing a free polyunsaturated omega-6 fatty acid, AA, and a lysophospholipid. COX-1 and COX-2 convert AA to prostaglandin (PG) intermediate PGH_2 which is then converted to five primary

bioactive prostanoids PGD_2, PGE_2, PGF_{2a}, PGI_2, and thromboxane A2 (TXA_2). Stimulated platelets also activate further platelets creating a feedback loop promoting clot formation.[29,57]

During the extrinsic pathway, tissue factor (TF) tightly binds the serine protease FVIIa circulating in the blood forming the TF-FVIIa complex which in turn increases the catalytic activity of FVIIa by roughly 30,000-fold.[58] TF-FVIIa complex activates the downstream serine protease factor X (FX) and factor IX (FIX), thus initiating the coagulation cascade and where the extrinsic and intrinsic pathways of the coagulation system converge.[59] FX can also be activated by IXa (FIXa) forming a complex with its cofactor protein, factor VIIIa (FVIIIa). Activated FX or FXa binds FVa forming prothrombinase which converts prothrombin to thrombin (FIIa) allowing thrombin to activate platelets, FV, factor VIII (FVIII), and factor XI as well as cleavage of fibrinogen to fibrin.[60]

During the intrinsic pathway, the negative charges of the aggregated platelets initiates plasma FXII, an 80 kDa glycoprotein, to be converted to the protease FXIIa in a plasma kallikrein-high molecular weight kininogen (HMWK)-dependent fashion (contact system). This contact-activation complex, formed by prekallikrein, FXI, HMWK, and FXII, brings all the factors into reactive proximity thus triggering the reaction cascade. HMWK is a 120 kDa nonenzymatic cofactor of FXII which circulates in complex with prekallikrein, an 80 kDa protein. FXII cleaves prekallikrein into two subunits, a 46 kDa heavy chain and one 36 or 33 kDa light chain. Activated kallikrein can now activate FXII, plasminogen, and factor IX. Either FXIIa catalyzes the activation of FXI, 160 kDa glycoprotein, to FXIa or FXI can also be activated by thrombin or FXIa, leading to the activation of FIX and subsequent thrombin generation. At this step, the extrinsic and intrinsic pathways of the coagulation system converge with the activation of factor X (FX).[61]

Coagulation is resolved by fibrinolysis, which leads to the degradation of fibrin, the product of the coagulation cascade. Plasminogen, the zymogen of the serine proteinase plasmin which can be found on HDL, is activated by tissue plasminogen activator (tPA) and urokinase plasminogen activator (uPA) which generates active plasmin on the fibrin surface and soluble plasmin, respectively. HDL is both an activator and inhibitor of the fibrinolysis pathway. Kallikrein is also found on HDL which suggests HDL activates plasmin by promoting the interaction of plasminogen and kallikrein but HDL also binds alpha- 2-antiplasmin and alpha-2-macroglobulin.

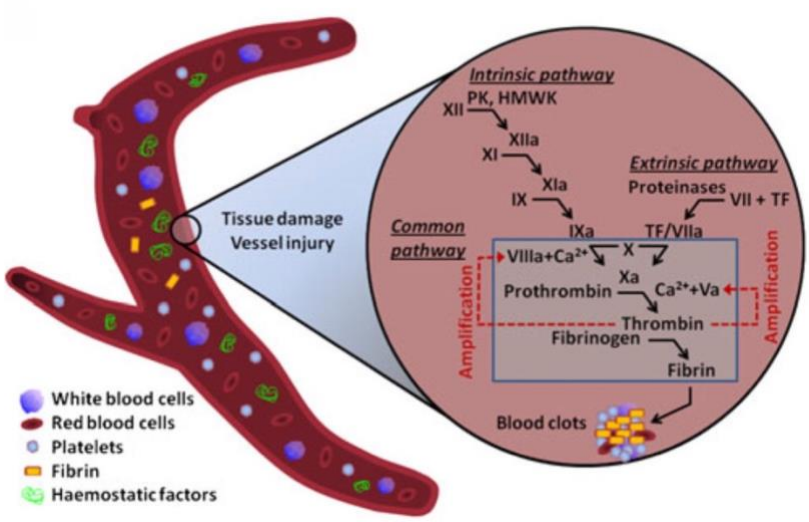

Figure 7: The coagulation cascade depicting the Intrinsic and Extrinsic pathways as well as the part of the cascade in which they both have in common.

Taken from: *Oikonomopoulou, K., Ricklin, D., Ward, P. A. & Lambris, J. D. Interactions between coagulation and complement—their role in inflammation.* Semin. Immunopathol. ***34,*** *151–165 (2012).*

The coagulation, complement, and fibrinolysis pathways are linked in intricate and tightly regulated ways having some shared activators and inhibitors (Figure 7). It has been established that the rapid activation of the coagulation cascade following trauma is accompanied by a very early onset of an uncontrolled, progressive inflammatory response which can end in lethal repercussions, indicating coagulation components can activate

components of the complement cascade. C3a and C5a, the activated form of C3 and C5 respectively, of the complement cascade, can be formed via kallikrein activation of factor B in the coagulation cascade. Activated platelets can phosphorylate C3 by releasing a serine/threonine protein kinase leading to a phosphorylated C3b which is not susceptible to deactivation to iC3b. This causes an increase in C3b deposition and CR1 receptor binding inducing the alternative complement pathway.

Thrombin activation can proteolytically generate C5a triggering the complement pathway and inducing the expression of the decay accelerating factor (DAF) in a PAR_1-dependent manner, reducing C3 deposition thus inhibiting the complement pathway. Both C3 and C5 can be activated by FIXa, FXa, FXIa, thrombin, and plasmin as well as being inactivated by thrombin-activatable fibrinolysis inhibitor (TAFI) generated by a thrombomodulin–thrombin complex. TAFI also can inhibit the plasmin-mediated fibrinolysis, inhibiting fibrin degradation. Chondroitin sulfate on platelet surface can also contribute to binding of C1q (which itself can also be activated by XIIa), as well as the complement regulators C1 inhibitor (C1INH), C4b-binding protein (C4BP), and factor H. C3 and C4 activation can occur with the interaction of fibrinogen/fibrin with recognition molecules that trigger initiation of the lectin pathway.

Complement cascade components can activate components of the coagulation pathway (Figure 8). Thrombin activation can occur via MASP2, which itself along with C1r/s and C3b can be inhibited by C1-esterase. Kallikrein and XIIa are also inhibited by C1-esterase. While the membrane attack complex (MAC) or the C5b-9 complex associates with the cell membrane, changes in the membrane- associated components are triggered which in turn affects platelet activation and thus the coagulation pathway. Platelet activation and aggregation is further induced by activated C3 whereas tissue factor (TF) activity is induced

by activated C5, triggering the extrinsic coagulation pathway. Furthermore, a C5a receptor (C5aR)-TF has been found demonstrating obvious cross-talk between the two pathways.[59]

Fibrinolysis, which leads to the degradation of fibrin, the product of the coagulation cascade, generates the fibrinolytic proteinase plasmin via C5 activation of the complement system leading to upregulation in the coagulation cascade component plasminogen activator inhibitor 1 (PAI-1). PAI-1 can inhibit the enzymatic activity of the serine protease tissue plasminogen activator (tPA). However, plasmin can also activate C3 and C5.

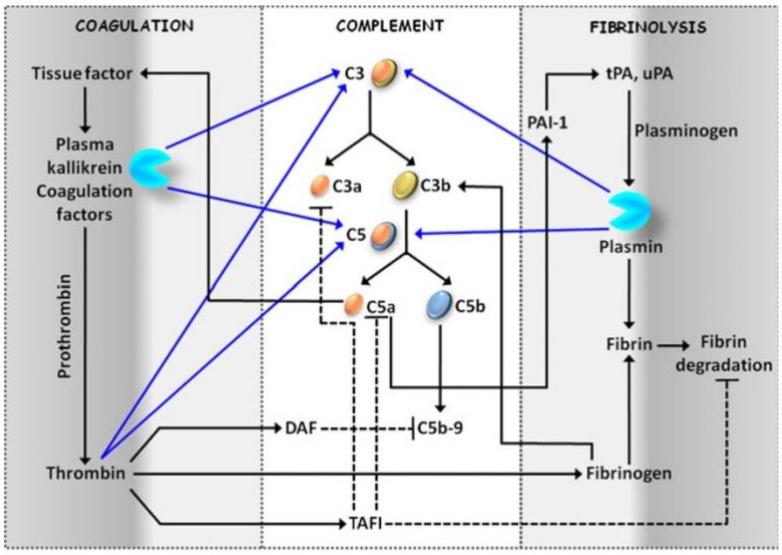

Figure 8: Intercommunication between the coagulation, complement, and fibrinolysis cascades.

Taken from: *Oikonomopoulou, K., Ricklin, D., Ward, P. A. & Lambris, J. D. Interactions between coagulation and complement—their role in inflammation.* Semin. Immunopathol. ***34,*** *151–165 (2012).*

2.3 Hepatic lipid pathway and complement activation interplay

Lipoprotein metabolism functions as a fuel transport system where insoluble hydrophobic fat becomes soluble in the form of lipoproteins for delivery to peripheral tissues. Very-low-density lipoprotein (VLDL) are produced hepatically, functioning as triglyceride (TG) transporters. Lipoproteins include chylomicrons (CM), VLDL, intermediate-density lipoproteins (IDL), low-density lipoprotein (LDL), and high-density lipoproteins (HDL) organized by their core lipid density composition. Further structural characteristics include surface phospholipids, cholesterol, and apolipoproteins which function either as structural (apolipoproteins B and AI), or exchange between different lipoprotein particles (apolipoproteins AII, C, and E).[62] Apolipoproteins are multifunctional, important in both lipoprotein metabolism via receptor-binding regulation and controls enzyme activity. Apolipoprotein A-I (Apo AI) is a 29 kDa protein and is a major component of high-density lipoprotein (HDL) cholesterol (70-80%) as well as Apo AII, a 17 kDa protein, which makes up about 20% of HDL. Both Apo AI and AII are involved in lecithin cholesterol acyltransferase (LCAT). Apo AI interacts with lipid transfer proteins and specific receptors and Apo AII regulates lipoprotein lipase (LPL) activity as well as regulating the reactivity of HDL towards lipid transfer proteins, enzymes, and receptors. Apo AIV is a 44 kDa protein which activates Apo CII lipoprotein lipase and lipoprotein modifiers such as LCAT, but to a lesser degree than Apo AI. Apo AIV also interacts with Apo CII, and Apo E mediates the binding, internalization, and catabolism of lipoprotein particles as well as being a ligand for the LDL (Apo B/E) receptor and for the specific Apo E receptor. Apo E also binds LDL receptors with a higher affinity than Apo B-100. Apo B-100 functions as a recognition signal for low-density lipoprotein (LDL) as it contains the LDL receptor binding domain.

Components of the lipid metabolism and complement pathway have been shown to crosstalk. Apo E interacts via domains 5–7 with Complement factor H (FH) reducing alternative pathway activation and iC3b formation. FH induces platelet aggregation, thrombin production, and an associated platelet procoagulant response by forming a complex with heparin via electrostatic interactions as well as binding glycosaminoglycans. Complement factor H is released from platelet α-granules upon platelet activation and platelet FcγIIa receptors cross link with subsequent immune complexes composed of FH-heparin complex and IgG molecules. However, FH also functions as a complement inhibitor of the alternative pathway as it inactivates C3b via factor I and increases C5 and C3 convertase dissociation.[62,63] Furthermore, Apo A1 is involved in the MAC complex assembly. Both Apo A1 and Apo AII have specific binding sites on the surface of C9 which can disrupt the formation of the C5b-9 complex which inserts into the cell membrane. Apo AI also disrupts the formation of the C5b-9 complex by forming together with clusterin, a high density lipoprotein complex as well as hydrophobically associating with C3. Therefore, Apo AI and AII can be associated with complement down regulation.[64]

2.4 Mononuclear phagocyte system

Once inside the bloodstream, the mononuclear phagocytic system (MPS) targets and clears nanoparticles via cells such as monocytes circulating in the blood, macrophages, and dendritic cells (DCs) which are derived from hematopoietic bone marrow stem cells and are present in tissues like the liver, spleen, lung (alveolar macrophages), and bone marrow. Dendritic cells are also found in lymphoid and nonlymphoid tissues and are responsible for activating T cells in an antigen-dependent manner. Current literature indicates that unlike previously accepted, tissue-specific macrophages are in fact first derived during

embryogenesis instead of bone marrow-derived monocytes accumulating in the tissues and replenishing their populations by self-renewal. Being a part of the innate immune system, macrophages phagocytose dead and damaged cells and organisms and release cytokines which may activate other cells such as lymphocytes and eosinophils. Concerning the acquired immune system, macrophages are responsible for removing opsonized cells and particles as well as antigen processing, presentation, and T lymphocyte priming.[65] Macrophages have several responsibilities in the upkeep of normal homeostasis such as removing dead and dying cells during normal tissue cell turnover or are recruited during an inflammatory response where they differentiate from circulating blood monocytes. Macrophages have four different stages in their life cycle: differentiation, priming, activation, and resolution. The first stage occurs when monocytes differentiate from bipotential stem cell (CFU-GEMM) via stimulation by growth-stimulating cytokines such as interleukin 3 (IL-3), stem cell factor (SCF), granulocyte-macrophage colony-stimulating factor (GM-CSF), retinoic acid, lipoproteins, and macrophage colony-stimulating factor (M-CSF), and factor increasing monocytopoiesis (FIM). Because the capillaries in the lung are only 6.5 μm, circulating monocytes are roughly 7-8 μm whereas monocyte derived macrophages are 15-20 μm.[66] Macrophage priming is accomplished by the different cytokine milieus during their continuous recruitment into tissues which ultimately impacts their innate immune response. Two categories of macrophages exists, M1 with classical activation or M2 macrophages with an alternative activation. M1 macrophages are characterized by inflammatory cytokine secretion and produce nitric oxide (NO), by metabolizing arginine, induced by intracellular pathogens, lipoproteins, bacterial cell wall components, and cytokines such as interferon gamma (IFN-Ɣ) and tumor necrosis factor alpha (TNF-α). M2 macrophages produce trophic polyamines and are subdivided based on their stimuli M2a, M2b, M2c, and M2d. M2 macrophages are induced by parasites, fungal cells, apoptotic cells,

immune complexes, complements, and MCSF. [67] More specifically, M2a is activated in response to IL- 4 and IL-13, the M2b to immune complexes and bacterial lipopolysaccharide (LPS), the M2c to glucocorticoids and TGF-β, and the M2d to IL-6 and adenosines. M2 macrophages not only clear apoptotic cells, mitigate inflammatory responses, and encourage wound healing but they also produce extracellular matrix (ECM) components, angiogenic and chemotactic factors, and IL-10.

Monocytes are differentiated from bipotential stem cell (CFU-GEMM) and express cell surface markers CD14 (LPS co-receptor), CD16 (FcɣRIII), CD64 (FcɣRI), and the chemokine receptors CD192 (CCR2) and CX_3CR1 (fractalkine receptor).[68] Similar to macrophages, monocytes are also subdivided into three categories of classical monocytes ($CD14^{++}CD16^{-}$) which are responsible for about 80–90% of peripheral blood monocyte population, non-classical monocytes ($CD14^{+}CD16^{++}$), and intermediate monocytes ($CD14^{++}CD16^{+}$) which are found primarily in the circulation, bone marrow, and spleen.[69] Monocytes can be further distinguished based upon their differential expression of surface markers as well as the pathogenic stimuli each subset responds to where classical and intermediate monocytes preferentially express CD11b and CD62L and respond to bacteria-associated signals whereas CD11c and CX3CR1 are expressed on the non-classical monocytes and respond to virus-associated signals.[66,70] SIRPα, an inhibitory receptor that suppresses phagocytosis, DC differentiation and maturation, and cytokine production, is preferentially expressed on non-classical monocytes. Circulating monocytes represent 5-10% of leukocyte populations circulating in blood.

Classical monocytes are responsible for phagocytic and microbial activity with low pro-inflammatory cytokine production. They express high levels of chemokine receptor 2 (CCR2), chemokine receptor (CXCR) 1, 2 and 4, and CD62L (L selectin). CX3CR1

(fractalkine receptor) and CCR5 (the receptor for the following chemokines: CCL3, CCL4, CCL8, and CCL3) are expressed at low levels. Classical monocytes also produce the cytokines and chemokines upon lipopolysaccharide (LPS) stimulation including IL-10, IL-6, IL-8, TNF-α, IL-1β, and CCL2. They also express CD64, the opsonin receptor FcϒRI, but not CD16 (FcϒRIII) as well as expressing integrins CD11a/CD18 and CD11b/CD18 but not CD11c/CD18. Non-classical monocytes are responsible for anti-inflammatory and constitutively produces IL-1RA. They express high levels of CX3CR1 but not CCR2 and CD62L and when stimulated with LPS, they produce high levels of TNF-α and IL-1β. In addition to their low phagocytic capacity, non-classical monocytes express CD16 (FcϒRIII) but little of CD64 (FcϒRI). Intermediate monocytes are responsible for Pro-inflammatory function and actively produces TNF-α (in response to LPS), IL-1β, and IL-6. They express high levels of CCR1, CCR2, and CXCR2 similar to classical monocytes, as well as CX3CR1, similar to non-classical, and they uniquely express CCR5. Intermediate monocytes further express both opsonin receptors CD64 (FcϒRI) and CD16 (FcϒRIII), CD36 scavenger receptor, and high integrin expression of CD11a/CD18, CD11b/ CD18, and CD11c/CD18.[71]

2.5 Mechanism for Nanoparticle uptake by MPS

Just like nanoparticles are engineered to function in a specific manner, they too can be engineered to avoid opsonization by the MPS thus increasing their efficacy and prolonging their circulation time. The molecular features on nanoparticles such as surface charge, corona molecules, size, and shape of the nanomaterials impact immune activation highly. Opsonization or the recruitment of serum proteins bound to the surface of the particles, leads to the formation of a biomolecular corona on the particle. The surface functionalities which are determined by the size and shape of the nanoparticle, interacts with biological systems

with their uptake highly dependent on the cell type, therefore utilizing different uptake routes or targeting different organelles.[72] These interactions are dependent on thermodynamic exchanges between the nanoparticle surface and the biological surface, colloidal forces, as well as dynamic biophysiochemical interplays. Therefore, the protein corona is not just a function of the specific material of the nanoparticle or the surface modification, but also of time. Once formed, the corona will change the distribution, macrophage and reticular endothelial system uptake, blood coagulation, and complement activation, however, the composition of the corona is dynamic, changing overtime in relation to their association strengths and rate constants.[73]

The issue of the formation of a protein corona is twofold. Firstly, opsonization of the particle occurs via complement protein absorption and activation eventually clears the pathogens from the body by aiding recognition by macrophage receptors, such as fibronectin, immunoglobulins, and complement proteins themselves as discussed above. Therefore, the particle's function and identity are impaired and altered than the intended chemical design. Secondly, phagocytosis of nanoparticles happens when opsonization of particles by iC3b and immunoglobulin G (IgG) occur which is mediated by either the CR or FCɣR receptors. MPS phagocytosis ultimately leads to the accumulation of nanoparticles in the tissues of the MPS which causes inflammation, release of toxic byproducts by biodegradation, and uncontrolled and unpredictable localization.

However, it is not just the composition of the corona which dictates the nanoparticle's ultimate biological function, but also the structure of the proteins adsorbed on the nanoparticle. Protein absorption on the particle's surface can cause denaturation, changing the structure of the protein. Examples of this phenomena can be seen by lysozyme and

chymotrypsin losing their secondary structure and activity following adsorption by 10 nm gold nanoparticles as well as cytochrome c upon binding to sulfonated polystyrene and magnetic nanoparticles. Loss of secondary structure can also be caused by the surface charge of a particle not just its material. BSA binds to anionic particles but conserves its structure and ability to bind to native albumin receptors. However, when BSA binds to cationic nanoparticles, the subsequent denaturation of the protein structure causes the BSA to bind to scavenger receptors.[74]

Particles larger than 100 nm are sequestered by Kupffer cells, macrophages lining hepatic sinusoids in the liver, together with marginal zone and red pulp macrophages in the spleen via phagocytosis, eliminating particles through the hepatobiliary system. Hepatocytes endocytose and enzymatically break down particles usually between 10-20 nm and depending on their composition, expelling them into the bile through biliary excretion whereas Kupffer cells of the MPS remove particles through intracellular degradation. Particles less than 5 nm are subjected to renal filtration by passing through the pores of the glomerulus in the kidneys thus rapidly cleared from the circulatory system. The glomerular capillary wall is composed of three layers where glomerular filtrate flows through the fenestrate, across the glomerular basement membrane, and through the filtration slits.[75] Nanoparticles of around 50 nm undergo the most efficient uptake through the receptor-mediated endocytosis in contrast to particles smaller and larger than 50 nm as there is, respectively, insufficient free energy to efficiently wrap the nanoparticle with cell membrane lipids or wrapping the nanoparticles takes too long as more time is needed to diffuse the receptors of the cell membrane around the nanoparticle.[20] However, in general smaller particles of the same composition absorb less complement proteins than larger particles and thus the blood concentration decreases with increasing size. A likely explanation of why particles around 50 nm induce more

immunogenic and cytotoxic responses is likely due to an inherent, conserved immunogenic signal stemming from the nano-size range bearing great similarity to viral particles. Other physical properties which are affected by particle size such as zeta potential and available surface area also contribute to the ultimate fate and clearance of the particle. Particles with a negative surface charge and hydroxylation of the surfaces are found to increase activation of the complement and therefore a more rapid clearance. Even the shape of the surface is known to activate complement in different ways, for example spheres and short filomicelles are more rapidly taken up by cells than longer filaments example under fluid flow conditions, because longer filaments are extended by the flow.[76] This indicates the internalization of nonspherical particles occurs via different mechanisms of endocytosis.

Surface charge of a particle can directly affect the fate of the nanoparticle. Renal filtration can be dictated by interactions between charged molecules and fixed charges within the glomerular capillary wall. Particles within the 6-8 nm range who are unable to undergo normal filtration due to their size, depending on their surface charge, may still undergo renal filtration.[75] Opsonization of a particle occurs predominantly by hydrophobic and ionic interactions, although the process can be more complex given the heterogeneous surface. Complement activation is increased as hydroxylation of the surface on more negatively charged particles increases. This indicates that complement activation is party caused by C3b covalently binding to hydroxyl groups. Thus hemolysis and complement activation increases with more negatively charged particles. Inflammatory signaling and phagocytic uptake are mediated through receptors such as class B SRs, SR-B1, and CD36, preferentially expressed on macrophages, which bind anionic lipids and lipoproteins, in particular, phosphatidylserine and phosphatidylinositol liposomes. Furthermore, both anionic and cationic nanoparticles are internalized via CD64 on macrophages. Conversely, cationic liposomes favorably interact

with DCs and had significantly slower uptake of phosphatidylserine liposomes.[31] Therefore, a particle with a more hydrophilic polymeric coating will be less likely to induce protein corona-mediated complement activation.

3. Stealthing polymers for nanosystems

Once introduced to biological fluids following internalization by cells, nanoparticles are typically localized inside highly acidic endosomes and/or lysosomes, being exposed to and ultimately stabilized by negatively charged groups. This leads to agglomeration due to the loss of charge, and the reduced pH enhances nanoparticle corrosion inducing toxic ion release. Furthermore, during internalization by cells and in the subcellular compartments, the polymers coating hydrophobic nanoparticles can be dissociated from the surface as well as the nanoparticle's protein corona enzymatically degrading, altering the surface chemistry of the particle.[77,78] Therefore surface modification and ultimately stealth properties of nanoparticles are designed to 1) increase the circulation lifetime and to prevent or reduce nonspecific interactions with the MPS, 2) targeting and therapeutic molecules can be conjugated to the nanoparticle, 3) prevent aggregation, 4) protect the payload from detrimental effects during transport, 5) release effective quantities and facilitate elimination of the payload following administration, and 6) reduce cytotoxicity.

Nanoparticles are coated with polymers in order to grant stealth behavior from opsonins, which is achieved by osmotic pressure (crowding of polymer chains in any fixed space), elastic restoring forces, Van der Waals attraction, ionic forces, and hydrophobic/hydrophilic forces. Higher osmotic contribution or higher elastic contribution is associated with a longer equilibrium layer thickness or a shorter equilibrium layer thickness, respectively.[79] As the

surface density of the polymer increases and the chain length increases, the greater the repulsion force and thus the better at resisting protein interactions. For example, PEG which is the most widely studied stealth polymer to date, has a hydrophilic and flexible nature which lends it its “brush” conformation. The polymer chains exert steric repulsive force as the chains extend from the particle surface and interact with one another at high polymer densities. This conformation causes absorbed opsonins to compress the chains leading the polymers to condense lending to a higher energy conformation. Therefore, the attractive forces between opsonins and nanoparticles are counterbalanced by the subsequent repulsive forces caused by polymer-protein interaction.

Not only can modifying the surface of the nanoparticle reduce the likelihood of absorbing complement proteins and activating phagocytosis, but chemically engineering nanoparticles enhances desirable surface properties for biomedical applications based upon the targeted disease.

3.1 Targeted drug delivery

Targeted drug delivery is composed of a wide range of approaches with the ultimate goal to enhance a drug delivery system (DDS) with better specificity, increased circulation lifetime, and decrease toxicity. This is achieved via a few methods involving passive targeting, active targeting, contact-facilitated drug delivery, or biological barrier delivery.

Passive targeting, utilized extensively in tumor therapeutics, is realized by conjugating a therapeutic agent to a nanoparticle which then passively reaches the target organ via blood circulation thus depending highly on circulation time. Many tumors and vascularized solid

tumors display an enhanced permeability and retention (EPR) effect where leaky vasculature and absent or impaired lymphatic drainage can be exploited by roughly 20-500 nm drug-loaded nanoparticles or high molecular weight molecules (polymers) to accumulate within the tumor site (Figure 9).

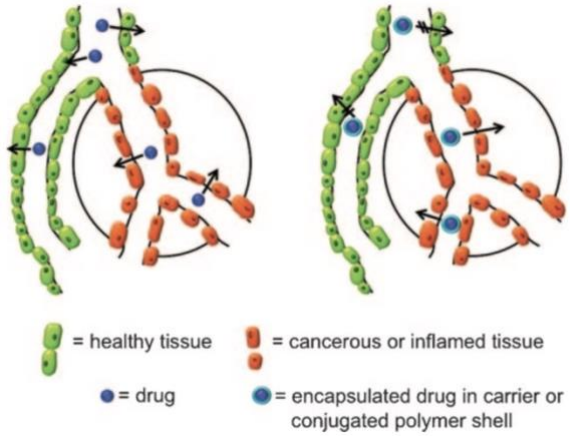

Figure 9: Schematic representation of enhanced permeability and retention (EPR) effect where leaky vasculature and absent or impaired lymphatic drainage can be exploited.

Taken from: *Knop, K., Hoogenboom, R., Fischer, D. & Schubert, U. S. Poly(ethylene glycol) in Drug Delivery: Pros and Cons as Well as Potential Alternatives.* Angew. Chemie Int. Ed. ***49,*** *6288–6308 (2010).*

On the other hand, active targeting involves tissue or cell-specific ligands conjugated to the therapeutic particle which interacts with its complementary membrane-bound receptor. However, active targeting begins with passive accumulation of the DDS therefore an active carrier must also be biocompatible, stable in circulation, long circulating, and appropriate diameter permitting efficient extravasation and accumulation in tumors as passive DDS are required to be for effective treatments.[80,81] In order to achieve controlled, localized delivery of a particle's payload, stimulus-responsive nanoparticles can be further designed to release their content in response to a trigger such as pH, ultrasound, UV light, temperature, biological microenvironment (protease). [82]

Contact-facilitated drug delivery involves transferring lipid-prodrugs following particle docking to a cell surface receptor and releasing the lipid surfactant components into the outer

leaflet of the target cell membrane. The drug would then be distributed throughout the intracellular membranes following translation from the outer lipid leaflet into the inner lipid leaflet.[83] These types of enhanced lipid-lipid exchanges can exhibit prolonged release kinetics and long persistence at the target site.

Another type of sustained delivery of therapeutic agents involves crossing biological barriers such as the blood brain barrier (BBB) which controls the exchange of hydrophilic compounds, small proteins, and charged molecules between the plasma and the CNS. Drugs which cannot cross this barrier are extremely limited but when conjugated to a nanoparticle, they become more lipid-soluble, providing greater CNS penetration, slower drug release in the brain, and decreasing peripheral toxicity. Drugs can be directed across the BBB via passive diffusion or receptor-mediated endocytosis as well as active site-directed delivery where high-affinity ligands for these transporters are placed on the surface of the NPs.[84]

3.2 Silica nanoparticles

Silica is the second most abundant material on earth after oxygen, frequently found bonded in the form of silicon dioxide (SiO_2) also known as silica, occurring naturally as crystalline quartz sand, rocks, and clays which are then used as industrial silica products like silica gel, precipitated silica, silica sol (colloidal silica), and fumed silica.[85] Crystalline silica is known to cause silicosis, a progressive fibrotic lung disease, when inhaled, via the production of ROS leading to DNA damage or oxidative membrane damage, which in turn spurred the use of amorphous silica instead. Amorphous silica occurs naturally in the form of diatomaceous earth, opal, and silica glass or as human-made products like additives to cosmetics, drugs, printer toners, varnishes, and food. Amorphous silica may present some short-range order but

lacks long-range order in three dimensions and does not exhibit a sharp x-ray diffraction pattern. Whereas crystalline silica exhibits long-range order in all dimensions and produces a sharp x-ray diffraction pattern.[86] Inorganic nanoparticles such as solid silica (SiO_2-NPs) and mesoporous silica nanoparticles (MSNPs) have become of increasing interest as the mean human adult intake of amorphous silica is estimated to be about 2 mg/kg of body weight per day.[25] Furthermore, they are utilized in controlled drug release due to their accessibility, versatility, high capacity of processing, and physical-chemical properties adapted through synthesis. The structure of silica is rigid, inert, and stable as it does not swell or change porosity with solvent or pH variation. Silica contains negatively charged isolated, vicinal and geminal silanol groups, silicon-bonded hydroxyl groups, giving rise to a strongly negative zeta potential at physiological pH. Vicinal silanol groups, one hydroxyl group per tetrahedron less than three nm apart from one another, interacts strongly with water molecules whereas germinal silanol groups, two hydroxyl groups per tetrahedron, interact with water molecules with less affinity. As the number of silanol groups increases, the hydrophilicity increases as well as its ability to form H bonds with water molecules. Amorphous silica has a concentration of 4-5 hydroxyl groups on the surface per square nanometer.[86]

Synthesis of silica nanoparticles occurs via the Stober protocol, in reverse microemulsions, or in aqueous micellar solutions. [87] The Stober method is a sol-gel approach of synthesizing silica involving silicon alkoxides such as tetraethylorthosilicate (TEOS) combined in a mixture of water, alcohol, and ammonia and agitated to form monodisperse particles ranging in size from 50 nm–2 μm. The size of the silica nanoparticles is controlled by the concentration of the solvents and silicate additives such that as the amount of TEOS increases, the particle size decreases forming uniform particles (Figure 10).[88] The reaction includes hydrolysis and condensation reactions:

Hydrolysis: $Si(OR)_{4(aq)} + 2H_2O_{(l)} \rightarrow Si(OH)_{4(aq)} + 4R\text{-}OH_{(l)}$

Condensation: $(HO)_3\ Si\text{-}OH_{(aq)} + HO\text{-}Si(OH)_{3\ (aq)} \rightarrow (HO)_3Si\text{-}O\text{-}Si(OH)_{3(sol)} + H_2O_{(l)}$

where R represents either a methyl (CH_3) or ethyl (CH_2CH_3) moiety in the case of TEOS. The "sol" phase of the reaction is the formation of small colloidal particles from the initial condensation of two hydrolyzed organosilane molecules. The "gel" phase is the formation of discrete, solid particles following a continued condensation of particles.

Reverse microemulsion synthesizes silica spheres around 30-60 nm with better average monodispersity than using the Stober protocol. TEOS is added to a reverse water-in-oil microemulsion, resulting in the hydrolysis of the alkoxide, via the diffusion of the alkoxide into the water droplets, as well as the formation of oxy-hydroxy-silicate species and alcohol.[89] Aqueous micellar solution synthesis involves micellar aggregates encapsulating polymerized lipophilic organosilane derivatives in the hydrophobic core.

Controlled polymerization of organosilane derivatives produces amorphous silica materials (ORMOSIL) where the Si atom is covalently bonded to an organic moiety. ORMOSIL conserves stability and physical features and properties as with inorganic SiO2-NPs but they have a larger chemical versatility because of the organic substitutions and are biologically inert, biocompatible, and are chemically and mechanically resistant. Therefore, they present an interesting alternative to the already established and more common organic delivery systems such as liposomes, micelles, dendrimers, and polymeric particles. It also produces electrostatic repulsion between the negative charges of the deprotonated silanol groups which stabilizes the particle but unfortunately also causes particle aggregation and precipitation when exposed to biological fluids such as human serum which is a high ionic strength media.

Furthermore, complement can be activated by opsonization via the adsorption of proteins on the surface by exploiting both hydrogen bonding and electrostatic interactions.[87] Even surface silanol groups are directly involved in hemolysis and in alveolar epithelial cell toxicity. Therefore, surface passivation is a necessity in order to avoid capture of the MPS using such strategies as coating particles with hydrophilic and neutral species like poly(ethylene) glycol (PEG).

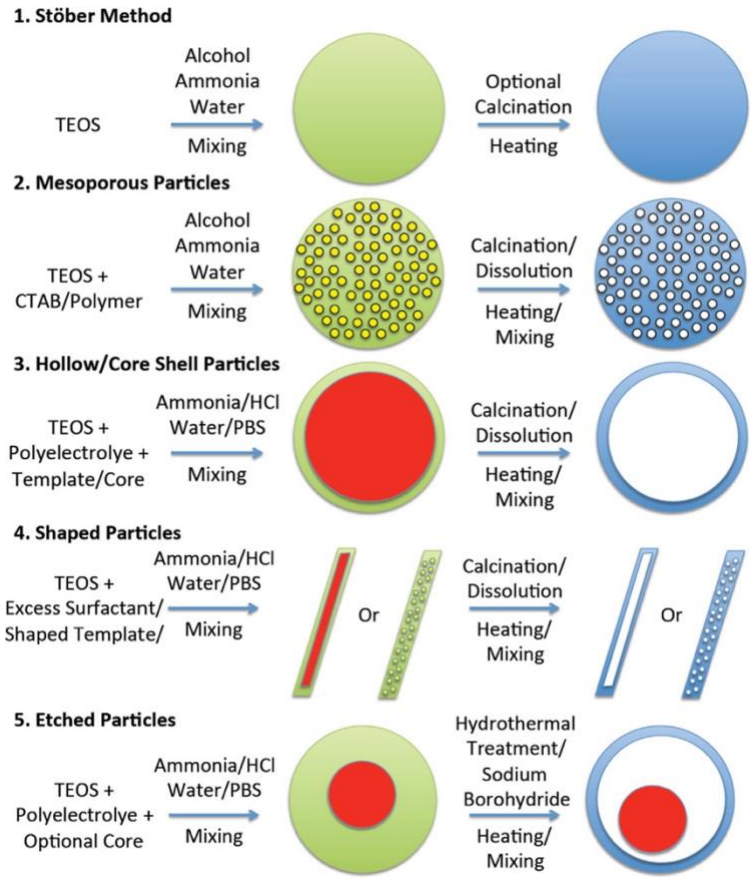

Figure 10: Popular methods to synthesize silica nanoparticles.

Taken from: *Liberman, A., Mendez, N., Trogler, W. C. & Kummel, A. C. Synthesis and surface functionalization of silica nanoparticles for nanomedicine.* Surf. Sci. Rep. ***69,*** *132–158 (2014).*

3.3 Gold nanoparticles

Gold nanoparticles (Au-NPs) or colloidal gold have been of great interest throughout history from being used as a coloring pigment back in the middle ages to today in the biomedical field, due to their vast and unique optical and physical features. Au-NPs are inert, have extreme resistance to oxidation, have a large surface-to-volume ratio, high X-ray absorption coefficient, excellent biocompatibility, low toxicity, and they are easily able to be functionalized by thiol compounds. Current applications of gold nanoparticles include organic photovoltaics, sensory probes, therapeutic agents, drug delivery, electronic conductors, and catalysis. Gold nanoparticles can be directly conjugated with drug molecules via ionic or covalent bonding, or by physical absorption thus changing its surface chemistry. Optical and electronic properties can be altered by changing the size, shape, or aggregation state.[90] Ranging from 1-100 nm, gold nanoparticles in solution exhibit size-dependent range of colors with red indicative of smaller particles and blue/purple for larger or aggregated particles. Size dependent changes to the physical and chemical properties of the nanoparticle can possibly occur due to the number of surface atoms. For example, take an iron 1cm cube where 10^{-5} % are surface atoms, but taking just 10 nm of that cube results in 10% surface atoms while 1 nm results in every atom being a surface atom. Even slight changes in size from a couple of nanometers can trigger size dependent alterations in the particle's properties. [91]

Gold nanoparticle are particularly unique due to their optical properties which are used extensively in diagnostics. Gold nanoparticles will undergo a change in their physicochemical properties upon molecular binding to itself. Such changes include surface plasmon resonance, conductivity, and redox behavior, which all lead to detectable signals. Surface plasmon resonance (SPR) is the phenomena when plasmons, oscillations of the free

electrons, occurs in response to oscillating electromagnetic field of the incident light (Figure 11).[92] This causes a coordinated dipole oscillation of electron charge formed around the particle's ionic lattice in resonance with the frequency of visible light. The SPR is when the amplitude of such oscillations at a specific frequency reaches maximum.[93] Plasmon oscillation in small nanoparticles undergo non-propagating excitations called localized surface plasmons (LSPs) distributed over the whole particle volume but SPR is absent in particles less than 2 nm or for bulk material. When the photons are confined to a small particle, radiative and nonradiative properties of the nanoparticles are enhanced by the SPR thus making Au-NPs highly useful for biological and medical applications. SPR reflectivity measurements can be used to detect molecular adsorption, such as polymers, DNA, or proteins via detecting the changes in the surface plasmon waves due to the alteration of the local index of refraction by the absorbed molecules. SPR can be modified based on the size and shape of the particle thus allowing for greater tuning and control. For example, <10 nm Au-NPs conjugated with short-chain thiolated ligands causes the native SPR to be dampened. Furthermore, nanospheres with the size of 2–50 nm show only one plasmon band at ~520 nm, while for cylindrical Au-NPs, two SPR bands appear.[94] Furthermore, quenching of fluorophores occurs by either the surface plasmon band overlapping with the emission spectrum of excited fluorophores known as fluorescence resonance energy transfer (FRET) or by the photoinduced electron transfer (PET) where Au-NPs act as electron acceptors.

As synthetic protocols became more robust and controllable, various shapes of Au-NPs can be achieved including nanorods, nanoshells, nanocages, and nanospheres.[95] Nanospheres of gold ranging between 5 to 100 nm are produced in various ways, some of the most common being the reduction of chloroauric acid $HAuCl_4$ and sodium citrate into boiling water.[96] Reducing particle size leads to different physical and optical properties due to the effect on

the energy level spacing as the system becomes more confined. The bandgap energy increases with size reductions and the onset of the bandgap transition is shifted to higher frequencies.[91] A red-shifted SPR is seen for aggregated particles due to interparticle plasmon coupling and the broadening of the surface plasmon band.

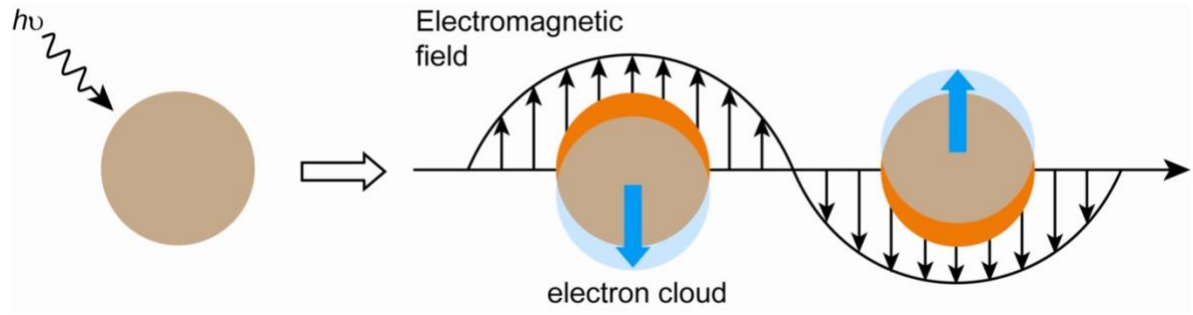

Figure 11: Schematic representation of Surface plasmon resonance (SPR). This phenomena occurs when plasmons, oscillations of the free electrons, occurs in response to oscillating electromagnetic field of the incident light.

Taken from: *Yeh, Y.-C., Creran, B. & Rotello, V. M. Gold nanoparticles: preparation, properties, and applications in bionanotechnology.* Nanoscale ***4,*** *1871–1880 (2012).*

Because of the versatility and physicochemical properties of gold nanoparticles, new opportunities for therapeutic treatments have been of increasing focus. At first, when the nanoparticles are introduced into circulatory system, the plasma proteins are the first to form the corona dominated by albumin, the most abundant protein in serum (55%) along with apolipoproteins, fibrinogen, and immunoglobulins. However, similar to silica nanoparticles, when exposed to plasma or serum, unwanted side effects occur from protein interactions with the particle's corona triggering immunogenicity, cytotoxicity, platelet aggregation, or altering blood coagulation pathways.[97] Gold particles themselves can trigger coagulation as the van der Waals forces between two metal nanoparticles leads towards coagulation or they can trigger coagulation via interactions with plasma proteins based on their surface charge where anionic surfaces initiate coagulation due to the fact that the intrinsic coagulation pathway is activated by anionic physiological surfaces, extracellular matrix, or aggregated platelets.

Nanoparticle modification and surface passivation via alterations of the surface of the gold nanoparticle is a necessity in order to avoid triggering coagulation as well as increasing positive surface attributes and efficacy using such strategies as direct conjugation with antibiotics or other drug molecules via ionic or covalent bonding, or by physical absorption. Ionic bonding is weaker than covalent bonding but allows for efficient release of drug payloads once it has reached the target zone whereas covalent bonding offers high stability. Instead, functional ligands can be utilized to alter the surface charge of the particle by exploiting non-covalent binding. Agglomeration can also be avoided depending on the synthesis of the modification. Polyelectrolytes such as poly(sodium-4-stryrenesulfonate; PSS), poly(diallydimethyl ammonium chloride; PDADMAC), and poly(allylamine hydrochloride; PAH) have already been employed for this purpose. Stabilization can occur via electrostatic stabilization, where negatively charged ions are attracted to the Au-NPs forming a second layer with positive counterions, or by steric stabilization where polymers made of long alkyl chains bind to the surface thus physically preventing two particles from getting too close to one another.[90] However, altering the surface charge, the size, or the surface with polymers will ultimately change how the particle interacts with plasma proteins. For example, sulphonated chitosan 13 nm and pyrimidine 10 nm Au-NPs inhibited coagulation and platelet aggregation whereas 220 nm carboxylated polystyrene NPs show an increased thrombogenicity. Therefore, since Au-NPs synthesis greatly affects biodistribution, it is crucial to evaluate and modify Au-NPs synthesis to promote favorable *in vivo* blood circulation times and biodistribution of the NP.

3.4 PEG Coatings

PEG is a linear non-ionic hydrophilic polyether diol which is biocompatible, soluble in aqueous and organic media, nontoxic, and has very low immunogenicity and good excretion

kinetics. PEGylation is the surface modification and polymer conjunction of a molecule by the linking of one or more 5-60 kDa polyethylene glycol (PEG) chains resulting in changes in physicochemical properties such as increased size, hydrophilicity, and molecular weight as well as changes in surface charge, solubility, stability, and steric hindrance of intermolecular interaction (Figure 12). Aggregation of PEG is also prevented by steric stabilization following the formation of a sterically hindering cloud, thereby producing nanoparticle platforms with increased stability during storage and applications.[98] This cloud of PEG polymers depends on the molar mass of the PEG polymers, the surface density, and the way the PEG is attached such as brush-like or mushroom-like conformations. An increased size and molecular weight can influence and decrease renal glomerular filtration favoring a hepatobiliary route, as well as the hydrodynamic volume which is dependent on the architecture of the polymer. These alterations ultimately leads to an enhanced pharmacokinetic and immunological profiles, extended circulation time, increases their bioavailability, modifies their biodistribution profiles, and altered tissue localization and cellular uptake.[99]

Surface modification of silica is easily achievable using a condensation reaction. Alkoxysilanes bind silanol groups on the surface by forming one to three Si–O–Si links which can coordinate with two to three water molecules per oxy-ethylene (-OCH_2CH_3) unit. This results in a loss of the overall positive protein charge, loss of the protein glycosilic functions involved in the galactose-receptor-mediated uptake, loss of protein pairing with haptoglobin, and a high hydrodynamic volume. These PEGylated alterations contribute to prolonging the body's exposure to proteins. PEGylated ORMOSIL can be achieved by the polymerization of lipophylic organosilane derivatives in the hydrophobic core of detergent micelles.[100] On one end of the PEG polymer, functional groups can bind the N-terminal amine, lysine, cysteine, and other amino acids.[101] For protein modification, the thiol group of

cysteine is an excellent anchoring site due to the infrequency in amino acid sequence and that disulfide bonds require two cysteine residues allowing for only one, if present, to be used for selective PEGylation. Stealth properties are provided by a reduction in their zeta potential as the thiol groups are masked. However, the most widely used synthesis method is PEGylation of the α- amino of the N terminus where differences in pKa between the *ε*-amino group of Lys and the α-amino of the N terminus are exploited to site selectively bind PEG molecules to the N terminus.[99] Amino group modification was among the first proposed methods due to the fact that amine groups are the most represented groups in proteins. Conjugation strategies include alkylation (forming a secondary amine group) or acylation which either maintains the positive charge of the starting amino group or loses its charge, respectively.[102]

Although PEG is the gold standard for polymer stealthing, there are many drawbacks that limits the usefulness of PEGylation. Firstly, complement can be activated by PEG, inducing specific and non-specific interactions with blood proteins leading to opsonization. This can ultimately lead to hypersensitivity reactions (HSR) which can lead to anaphylactic shock. Secondly, due to its polyether and hydrophilic behavior, PEG is prone to oxidative degradation resulting in the molecular weight deterioration and cleavage of the polymer chain.[103] This process leads to a loss in coating functionality thus reducing its hydrophilicity, charge masking ability, and resistance to non-specific adsorption. PEG is also known to autocatalytically degrade in bulk (solid state), surface-bound state, and in dilute solutions.[104] Thirdly, antibodies against PEG produced by splenic B cells can develop after the first administration of PEGylated liposomes indicating potential immunogenic and antigenic effects. Fourthly, PEG can also bioaccumulate and form vacuoles in some organs. PEG is non-biodegradable, and anti-PEG antibodies have been reported indicating that PEG has the potential to be immunogenic and antigenic.[105] Furthermore, in order to provide effective

counter phagocytosis, PEG chains typically need to have a molecular weight in excess of 2,000 Da, substantially increasing the overall hydrodynamic diameter.[20] Finally, PEG is synthesized via an exothermic, living anionic ring-opening polymerization of ethylene oxide, which is highly toxic, explosive, and gaseous at room temperature.[106] Therefore, in combination with the limitations of PEG as a stealthing agent, alternative polymers have been proposed which are more biocompatible, can escape the MPS, and are easier to synthesize.

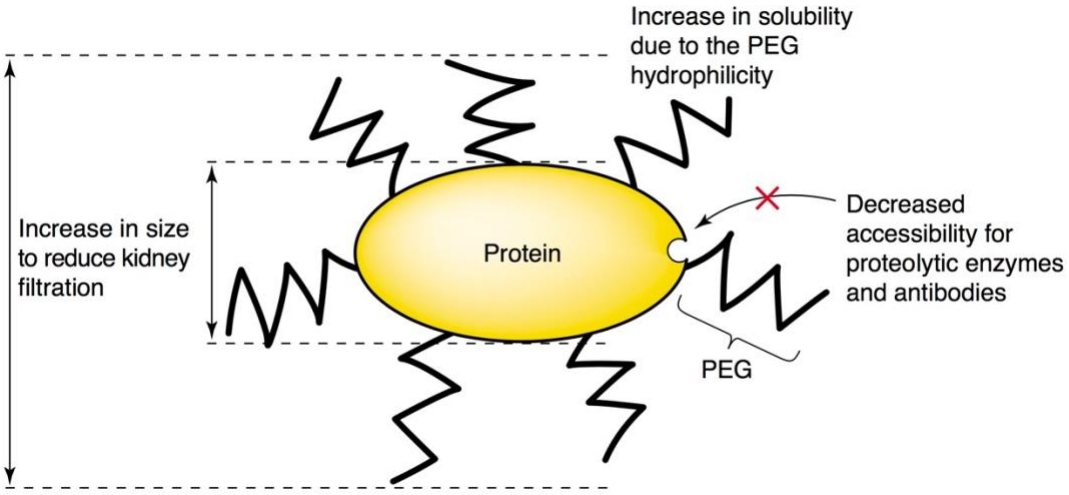

Figure 12: PEG polymer-protein conjugate. The protein is shielded by PEG polymer chains preventing binding and degradation by steric hindrance as well as increasing solubility via PEG hydrophilicity. Furthermore, the particle's size decreases renal glomerular filtration of the PEGylated protein.

Taken from: *Veronese, F. M. & Pasut, G. PEGylation, successful approach to drug delivery.* Drug Discov. Today ***10,*** *1451–1458 (2005).*

3.5 Poly(2-oxazoline) polymers

Alternative polymers for PEG have been created with the hope of achieving even better control over the properties of modified drugs and drug carriers. The qualities of a polymer must be soluble, hydrophilic, have a highly flexible main chain, and high biocompatibility. Poly(2-oxazoline) (POZ) has been proposed as an alternative polymer for PEG given that they are easier to synthesize and can incorporate varying monomers to tailor the nanoparticle for specific applications.

Oxazolines are hydrophilic, tertiary polyamides with the amide group in the side chain, as well as being structural isomers of polypeptides. [107] Three isomers of oxazolines exist depending on the location of the double bond, 2-, 3-, and 4-oxazoline, where 2-oxazoline is by far the most studied. They can be further substituted on the 2, 4, or 5 position of the 2-oxazoline ring, however substitution on the 4th or 5th position is more difficult to polymerize due to steric crowding. POZs have structural similarities to PEG and polypeptides due to having (C-C-N) backbone repeat units and amide side chains. POZ has higher chemical stability due its N-vicinal C–H bond causing a lower polarization compared to PEG which has an O-vicinal C–H bond. Although PEGylated polymers are highly water soluble, amphiphilic, very flexible and hydrated in water, non-toxic, and may be produced with low polydispersity, POZ can be further tuned in size and structure using a living cationic ring-opening polymerization (CROP) as well as facile surface functionalization and fluorescent labeling via click chemistry thus overcoming PEGs low drug loading capacity.[28] CROP utilizes a thermodynamically favorable isomerization of the imino ether group to the amide which results in a stable polyamide, due to ring strain, and narrow average molecular weight distributions.[108] POZ is highly biocompatible and behaves as an entropic spring in a crowded environment giving rise to its antifouling and stealth effect to particles.

Several monomers can be synthesized namely poly(2-methyl-2-oxazoline) (PMOXA) and poly(2-ethyl-2-oxazoline) (PEtOXA). In a one pot synthesis, sequential monomers may be added giving rise to a well-defined block copolymer, allowing for complex multifunctional architectures together with tunable physicochemical properties.[109] PEtOXA is slightly more lipophilic and has a smaller intra-chain flexibility than PMOXA and PEG, and is also significantly less viscous than PEG. PEtOXA is also stable against hydrolysis in acidic conditions and/or in the presence of enzymes but most importantly, hydrolysis does not lead

to molecular weight deterioration or cleavage of the polymer chain.[110] Furthermore, since the 2-ethyl-2-oxazoline repeating unit is significantly spatially larger than ethylene glycol giving rise to steric hindrance, PEtOXA will bind less to the nanoparticle surface compared to PEG, ultimately giving rise to a smaller coated particle.[111]

4. Interspecies comparison

Nanomedicine, like most scientific fields, employ the mouse model, *Mus musculus*, as an experimental tool to probe human biology and disease whether it be *in vitro* or *in vivo*. The mouse has many features which make it an attractive scientific model such as their phylogenetic relatedness, physiological similarity, and genetic homologies to humans as well as their ease of breeding and producing many inbred strains with fast generation turnover. However, in many cases, experimental interventions in mice are responded to quite differently than in humans thus contributing to the high failure rate of drug development where the majority of drugs never reach the marketplace following clinical trials. Therefore, it is imperative to understand the attributes which contribute to this phenomena so as to increase therapeutic applications of nanoparticles.

There are many similarities between humans and different species concerning the immune system. Pigs (*Sus scrofa*) share anatomical and physiologic characteristics with humans. Studies done to compare the orthology preservation of familial gene expansion deriving from family member expansion analysis revealed that in total, humans and pigs share 42 genes that are not found in mice; mice and humans share 14 genes that are not found in pigs; and mice and pigs share 7 genes that are not found in humans.[112] Human and porcine macrophages

produce pro-inflammatory cytokines such as TNF-α, IL-1β, IL-6, IL-8, and IL-12 via the production of indoleamine 2,3-dioxygenase (IDO) upon LPS activation instead of NO synthase as with murine macrophage cells. Mouse and human complement proteins C2, C3, C4, and factor B have a very high degree of similarity[113] 9 out of 12 Toll-like receptors in mice and 9 out of 10 human TLRs are conserved between species.[30] Roughly 80% for TLR1, 3, and 10; 85% for TLR7; and 73% for TLR8 are homologous between porcine and humans as well as sharing typical functional TLR domains. Porcine NOD 1 and 2 have an 83.8% and 81.6% amino acid sequence conserved with human NOD2, respectively.[114] Mouse C3 has 79% identity to human C3 at the nucleotide level and 77% identity at the amino acid level.[115]

Although there are quite a number of similarities between mice and humans, there are quite a number of limiting factors which make the mouse model not always appropriate for nanomedicine. Firstly, the most obvious difference between the two species is size where mice are about 2,500 times smaller than humans. Size is correlated with metabolic rates and the variations between mice and humans can manifest in anatomic, physiologic, and biochemical differences. Higher metabolic rates in small mammals can be attributed to thermoregulation and heat-loss where not only is capillary and mitochondrial density increased in tissues, but metabolically active tissues, such as liver and kidney are found in higher amounts. Mouse cells also have a higher content of fatty acid composition of their membrane phospholipids such as readily oxidizable polyunsaturated fatty acid docosahexaenoic (DHA), an omega-3 (n-3) with 22 carbons and 6 double bonds, thus also contributing to higher rates of oxidative damage.[116] DHA is highly active and flexible due to the low potential barriers of rotation around the carbon-carbon single bonds between the double bonds, despite no rotation around the cis double bonds.[117]

Secondly, serum and plasma protein compositions differ between species where human (HS), mouse (MS), pig (PS), and fetal calf serum (FCS) are the most commonly utilized experimentally. The protein hard-corona formed in FCS is uniquely different from that formed in human plasma (HP) where coagulation and complement components, immunoglobulins (IgG), and lipoproteins are defective in FCS compared to HP.[118] Albumin, which is the most abundant protein in blood, is the predominant component of the corona. Human serum albumin (HSA) and bovine serum albumin (BSA) differ in amino acid composition and charge, BSA: -17 and HSA: -15, which can affect protein absorption based on conformational changes. The interspecies homology between BSA and HSA is largely restricted to the Fab portion of bovine IgG, however bovine IgGs are unable to bind murine Fc-receptors which do recognize human IgG.[119] Complement and coagulation factor proteins are species specific with many proteins only present in human serum and not in bovine. Apolipoprotein B-100 in not present in FCS which is responsible for binding and internalization of low-density lipoproteins (LDL) and Alpha 1-antitrypsin inhibitor. Complement component C3c, C4a, and C4b which are all involved in complement activation as well as coagulation factor II (thrombin) which cleaves fibrinogen to fibrin.[120]

Thirdly, different composition and properties of cellular components results in different strategies in immune responses. In C57BL/6 mice, there is a 10–25% neutrophils, 75–90% lymphocytes, and about 2% monocytes and for CD-1 mice there is 15–20% neutrophils and 50–70% lymphocytes whereas for humans have 50–70% neutrophils and 20–40% lymphocytes. Furthermore, the size and phagocytic capability of the cells are distinct where human pulmonary alveolar macrophages (PAMs) are larger and are able to sequester foreign particles with regard to size as compared to mice.[121] The expression of inducible NO-synthase and arginase is enhanced in activated murine macrophages which is barely found in

human macrophages. Mast cells in mice release serotonin whereas human mast cells release histamine. Complement receptor 1 (CR1, CD35), which bind C3 and C4, are present on erythrocytes, macrophages, neutrophils, B cells, follicular dendritic cells, and some T cells whereas complement receptor 2 (CR2, CD21), regulates B cells activation as well as binding CD59, is present on B cells, follicular dendritic cells, and some T cells.[122] Human CD59 highly inhibited lysis by human and pig complement with an AA conservation level of 48% whereas with mouse complement, it was only moderately effective and shared only 34%. Furthermore, human CD59 inhibits human complement to a higher degree than pig complement and pig CD59 inhibits pig complement to a higher degree than human complement.[123] Human platelets lack CR1 whereas human blood monocytes express CR1.[124] However, mouse CR1 is not present on the membrane of erythrocytes, macrophages, neutrophils, B cells, follicular dendritic cells, and some T cells therefore indicating an alternative to CR1 for an immune adherence receptor which is a single receptor able to bind C3 but seen separately by human CR1 and CR2.[113] Furthermore, mouse Kupffer cells do not express CR3. Natural killer cells (NK) are responsible for lytic activity and production of cytokines such as IFN-γ. The CD3 T-cell receptor and CD4, CD5, and CD6 T-cell co-receptors are lacking in porcine NK cells but they do express CD2, CD8α, CD16, CD45RC, and perforin.[114]

Chapter 2: Results and Discussion

Section 1: Silica

Physiochemical characterization of SiO_2-NPs

With the express purpose of gaining a more in-depth and thorough insight into the role played by polymers who coat vinyl-triethoxysilane-derived organically modified silica nanoparticles (ORMOSIL) influencing serum protein corona and cell interactions, we first prepared coated and non-coated amorphous silica materials (ORMOSIL) particles. The following protocols are also outlined in the Methods section for additional information. Using the Stober protocol, in collaboration with Professor Fabrizio Mancin of the Department of Chemistry at the University of Padova, the particles were labeled with (10 mM in DMSO) Rhodamine B triethoxysilane with loadings in the 0.1-0.3% w/w range (Figure 13). All NP types presented comparable UV−visible spectra (Figure 52 in the appendix section) and NMR data of both PEG and PEMOXA- coated NPs showed all signals belonging to nanoparticle-grafted species, where a diffusion filter removed free molecules (Figure 53 in the appendix section). Transmission electron microscopy analysis (TEM) and dynamic light scattering analysis (DLS) of uncoated ORMOSIL particles showed a diameter of 115 nm with the most negative zeta potential of all the SiO_2-NPs, -6. Not only did all the coated particles retain similar diameters, 100 nm, but also similar ζ-potentials, -4, and number of polymer chains (n), 44. This indicated although the addition of coatings changes the surface of the uncoated NPs, it does not change other physiochemical properties such as charge, size, grafting-density and so on. Thermogravimetric analysis (TGA) revealed another major difference between the coated particles which are their polymer footprints. Polymer footprints divulges the average space occupied by one polymer chain on the NPs' surface. Using the data obtained by TGA, the

footprints ie the grafting densities, of PEG coated ORMOSIL was calculated to be ~ 3 nm^2, whereas PMOXA coated ORMOSIL has a footprint of ~ 2.4 nm^2, and PEtOXA coated ORMOSIL has a footprint of ~ 4.6 nm^2. Therefore, particles of the same diameter but having different footprints will have a different amount of polymer chains which are able to occupy the surface of the nanoparticle. PEtOXA (2-ethyl-2-oxazoline) repeating unit is significantly spatially larger than PEG (ethylene glycol), hence a smaller number of polymer chains will reach the particle's surface and be able to bind compared to PEG. This is an important characteristic of a nanoparticle given the intricate balance at minimizing the free energy of the system by balancing low area per molecule which induces steric clashes among ligand chains and too high an area per molecule which exposes the nanoparticle to water. Furthermore, this optimal coverage must also impart colloidal stability thus preventing particle aggregation which is vital to biomedical applications of nanoparticles.

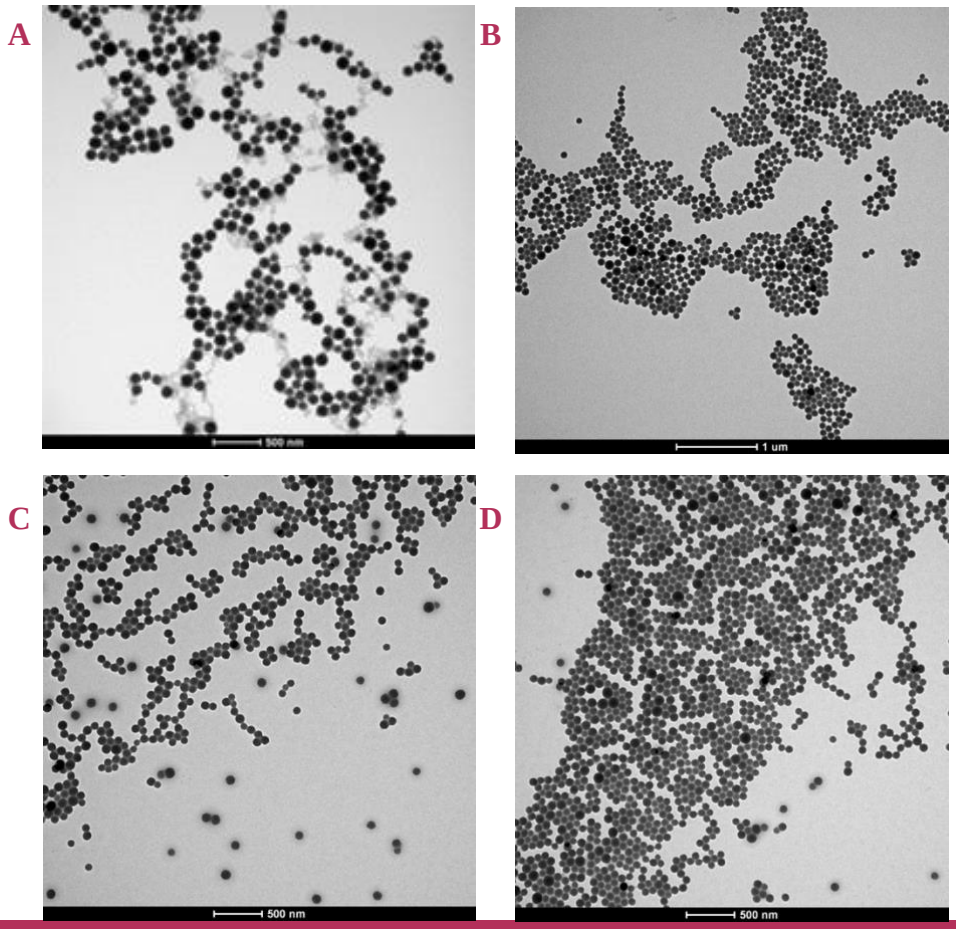

Table 1: Physiochemical properties of ORMOSIL nanoparticles either uncoated NPs or coated by PEG, PMOXA, or PEtOXA.

Nanoparticle	# polymer chains (n)	MW (Da)	Diameter (nm)	ζ-potential (mV)	Footprint (nm^2)	m
ORMOSIL	-	-	115 ± 23	-6	-	-
PEG-ORMOSIL	44	2000	100 ± 10	-4	3.0	10,000
PMOXA-ORMOSIL	44	3800	100 ± 6	-4	2.4	13,000
PEtOXA-ORMOSIL	44	-	100	-4	4.6	-

Figure 13: TEM analysis of silica ORMOSIL nanoparticles coated with either (A) Uncoated (B) PEG (C) PMOXA (D) PEtOXA. TEM analysis, performed using FeiTecnai 12, 100 keV, yielded 100 nm diameter particles in good agreement with the DLS size (samples prepared by spreading a droplet of the nanoparticles diluted in PBS buffer (~ 1 mg/mL) onto standard carbon-coated copper grids (200 mesh). Image J software was used for dimensional analysis).

Nanoparticle	n	MW (Da)	Diameter (nm)	ζ-potential (mV)	Footprint (nm^2)	m

Characterization of SiO_2-NPs' capture by human monocytes and macrophages in serum from varying species

In order to probe the impact of serum from multiple species on coated nanoparticle cellular association with phagocytes, flow cytometry was performed with primary human monocytes isolated from healthy blood donors and macrophages differentiated from monocytes. Figure 14A demonstrates the effect on cellular uptake by human monocytes when 70% (v/v) human serum (HS), pig serum (PS) and mouse serum (MS), is incubated with 800 μg/mL uncoated, PEGylated, PMOXA-coated, and PEtOXA-coated NPs first in the absence of cells for 20 min at 37 ℃ and then incubated with cells after a 10-fold dilution in protein-free culture medium for 3 hours at 37 ℃. Uncoated and PEGylated particles had a reduced phagocytic effect, whereas PMOXA-coated NPs had the highest cellular capture by human monocytes with 77 times more cellular association than uncoated and 49 times more than PEGylated NPs. PEtOXA-coated NPs, while still inducing phagocytosis by 22 times and 15 times over uncoated and PEGylated, respectively, have a reduced cellular association by 70% compared with PMOXA-coated NPs. In mouse serum, all nanoparticles display a universal lack of cellular association with human monocytes. This may indicate either a stealth effect by the coating or a molecular mismatching between non-orthologous cells and serum. Interestingly, the same trend is seen in pig serum as with human serum where the coated particles are captured more than PEGylated or uncoated particles. Similarly to HS, PEGylated NPs were captured 41% more than uncoated NPs in PS. Furthermore, in PS PEtOXA-coated NPs, while still inducing phagocytosis by 7 times and 4 times over uncoated and PEGylated NPs, respectively, had a reduced cellular association by 80% compared with PMOXA-coated NPs.

In human macrophages with human serum (Figure 14B), the trends seen with monocytes is only in part reproduced. In fact, the macrophages' capture of PMOXA-coated NPs was 17 times more intense than that of PEG-coated NPs, which was captured 1.3 times more than uncoated NPs. However, the most interesting effect was seen by PEtOXA-coated NPs, which induced cellular association of NPs with macrophages 28% more compared to PMOXA-coated NPs. This observation was not expected given the fact that uncoated, PEGylated, and PMOXA-coated NPs associate with monocytes and macrophages in a similar fashion. Similarly, in mouse serum there was an increase capture of PEtOXA-coated NPs two times over PMOXA-coated NPs, which has a similar capture to uncoated and PEGylated NPs. Another interesting observation concerns pig serum where PMOXA-coated NPs cellular association is highly reduced, just 2.4 times more than PEG which is roughly 14 times less than with human monocytes. Furthermore, PEtOXA- coated NPs capture in PS is 58% more than PMOXA-coated NPs which is 30% more than in HS.

These results taken together suggest circulating monocytes and human macrophages showed preferential tendency to capture PMOXA-coated and PEtOXA-coated NPs, compared with uncoated and PEGylated NPs.

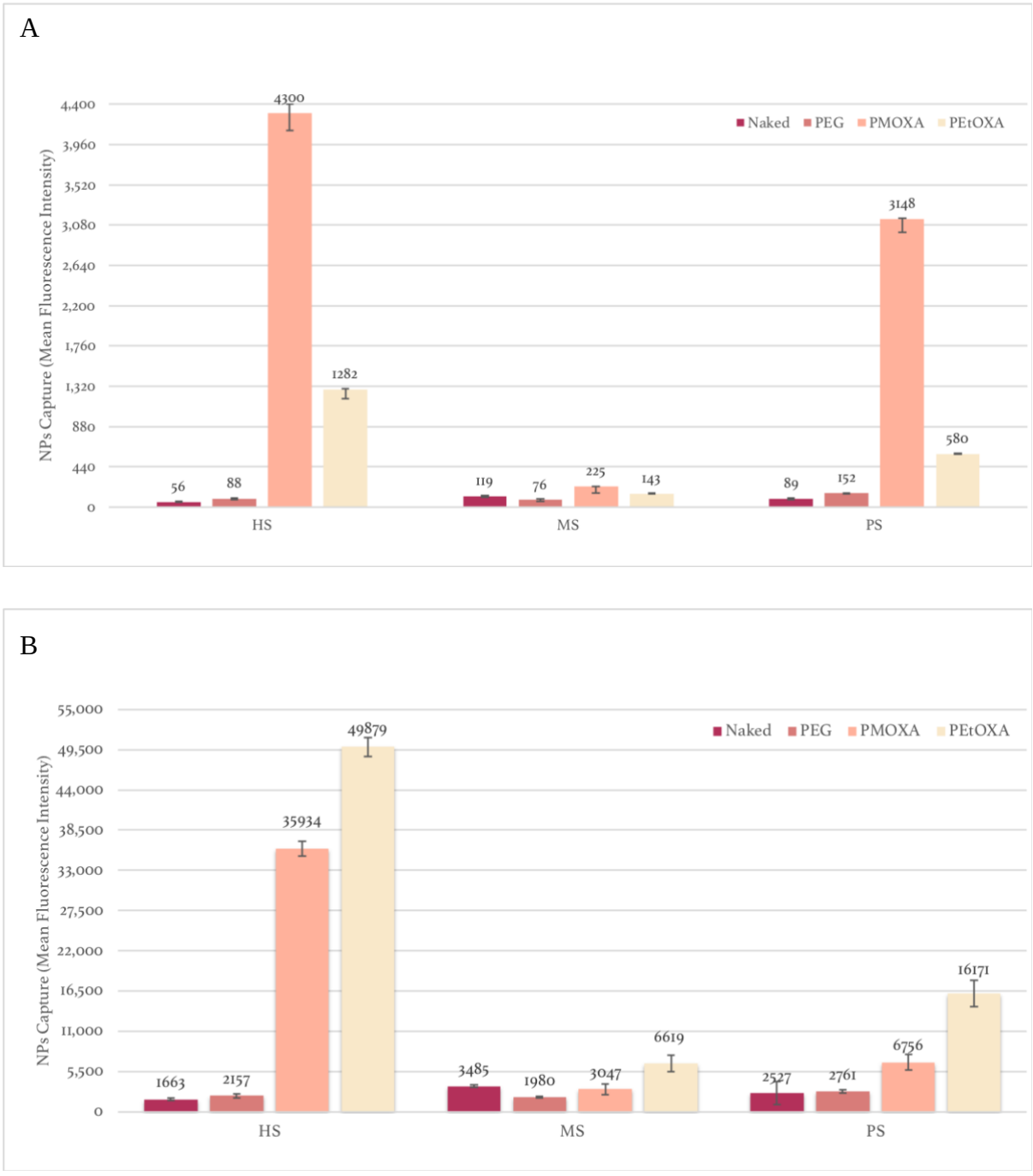

Figure 14: The effect of serum proteins from multiple species on SiO_2-NPs cellular association. Following a 20 min incubation at 37 °C in 70% serum, 80 µg/ml SiO_2-NPs were incubated for 3 hours at 37 °C with human (A) monocytes and (B) macrophages for 3 hours. The cells were subsequently analyzed by flow cytofluorimetry to measure nanoparticle-associated fluorescence. Data are mean ± standard error of the mean (n = 3). Values above the bars indicate cell association expressed as the mean Fluorescence Intensity

Moreover, these studies demonstrate the differences of nanoparticle uptake by human phagocytic cells in the presence of serum from varying species. In contrast to our unpublished previous studies performed with PEGylated NPs in FCS (Figure 15), this polymer did not provide stealth properties in HS but it also didn't increase the uptake of the nanoparticles either.

PEtOXA-coated particles have different behaviors in macrophages versus monocytes yet the trend is the same in both human and pig serum indicating the cell interacts independently of protein differences in species' serum composition. The lack of cell interaction in both human monocytes and macrophages with MS could be attributed to different cellular receptors' characteristics, which could lead to molecular mismatching. In this case, although MS might act the same as HS, opsonic receptors on human cells might be unable to interact with proteins from MS. Furthermore, the fact that particles behave similarly in PS as they do in HS indicates that pig serum opsonic proteins likely interact similarly with human cell receptors as with equivalent human serum opsonins. Additionally, data may also suggest that the protein composition of the pig serum-derived corona is similar to that of human serum-derived. This is fascinating due to the possible experimental implications for testing particles as drug delivery carriers in preclinical models. Data suggests pigs and pig serum better predict the behavior of NPs in the human context, therefore being a more effective alternative model for *in vitro* testing, compared to FCS or MS which produced trends not reproducible in humans.

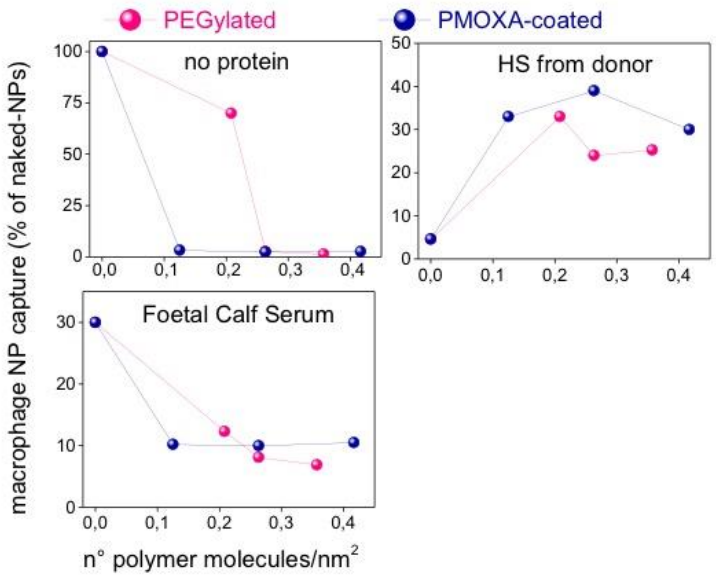

Figure 15: The effect of serum proteins from fetal calf serum (FCS) on PEG and PMOXA SiO_2-NPs cellular association.

Characterization of the cellular affinity and uptake of SiO_2-NPs in orthologous species and cells.

In order to investigate why human phagocytes do not favor coated particles in the presence of mouse serum unlike in human serum and whether that is due to a molecular mismatch between non-orthologous serum and cells, we decided to probe the nanoparticles in mouse serum with orthologous mouse macrophage RAW cell line as well as bone marrow derived mouse macrophages (BMM). Figure 16 demonstrates the effect of serum proteins from multiple species on SiO_2-NPs cellular association in RAW and BMM cells. Following a 20 min incubation at 37 °C in 70% serum (v/v) and a 10 fold dilution in culture medium, 80 µg/mL SiO_2-NPs were incubated for 3 hours at 37 °C with (A) RAW 264.7 mouse macrophage cell line with MS and (B) primary mouse macrophages with MS for 3 hours. The cells were subsequently analyzed by flow cytofluorimetry to measure nanoparticle-

associated fluorescence. In addition, we also probed the possible complement involvement in particle capture by mouse cells with human and pig serum.

The data showed uncoated NPs were captured more by RAW and BMM cells in MS compared to PEGylated and PMOXA-coated particles. This supports the idea the lack of capture seen by MS in human cells is due to molecular mismatching between non-orthologous serum and cells. In addition, all NPs in HS and PS showed little cellular capture in mouse cells as compared to capture by human cells, further supporting the idea that NP capture is dependent on the serum protein and cell interactions which are species specific.

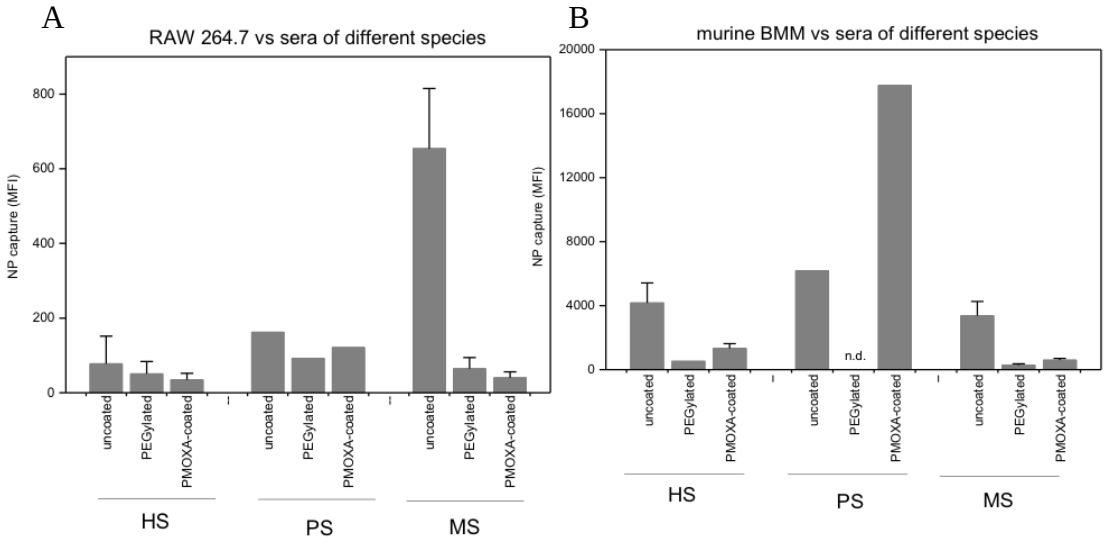

Figure 16: The effect of serum proteins from multiple species on SiO_2-NPs cellular association with orthologous macrophages. Following a 20 min incubation at 37 ˚C in 70% serum, 80 µg/ml Si_O2-NPs were incubated for 3 hours at 37 ˚C with human (A) RAW 264.7 mouse macrophage cell line with MS and (B) primary mouse macrophages with MS for 3 hours. The cells were subsequently analyzed by flow cytofluorimetry to measure nanoparticle- associated fluorescence. Data are mean ± standard error of the mean (n = 3). Values above the bars indicate cell association expressed as the mean Fluorescence Intensity.

Localization of SiO_2-NPs in primary human macrophages

Localization of SiO_2-NPs in primary human macrophage cells was visualized using fluorescence microscopy after 3 hour incubation. Cells were incubated with 75 nM Lysotracker DND-26 (Invitrogen, CA, USA), a green fluorescent dye that stains acidic compartments in live cells (green, λ_{exc} 504 nm and λ_{em} 511 nm). Co-localization of nanoparticles with Lysotracker and rhodamine indicates endocytosis by cells and accumulation in acidic endolysosomal/phagosomal vesicles via cell internalization. Cells were incubated for 3 hours at 37 °C in HS, PS, and MS, in the presence of nanoparticles diluted in culture medium, and then inspected. In HS (Figure 17A), the uncoated particles showed little cell internalization indicated by the stark decrease in fluorescent cytoplasmic signal as well as little co-localization evidence of reduced accumulation in acidic endolysosomal/phagosomal vesicles. However, PMOXA-coated particles demonstrated an increased cell internalization as compared to uncoated, clearly seen by the striking increase in fluorescent signal as well as high co-localization. Furthermore, PEtOXA-coated NPs demonstrated an even greater cell internalization and co-localization. Similarly, in PS conditions, Figure 17B, uncoated nanoparticles showed little cell internalization and co-localization, similar to the HS conditions, whereas PMOXA-coated and PEtOXA-coated NPs showed an equally similar increase in fluorescent and Lysotracker signals. The trends between coated and non-coated particles are consistent for both human and pig serum where coated particles were captured by phagocytic cells and uncoated particles were stealth.

At variance, in MS (Figure 17C), uncoated particles showed the greatest cell internalization and co-localization, whereas the coated particles showed decreased cell internalization, which

is in contrast to NP capture in human and pig serum. Thus, coated particles are in fact not stealth but were recognized by the immune system in MS.

These results further support previous flow cytometry data where PMOXA-coated and PEtOXA-coated NPs induce cellular phagocytosis in HS and PS whereas uncoated NPs increase cellular capture in MS.

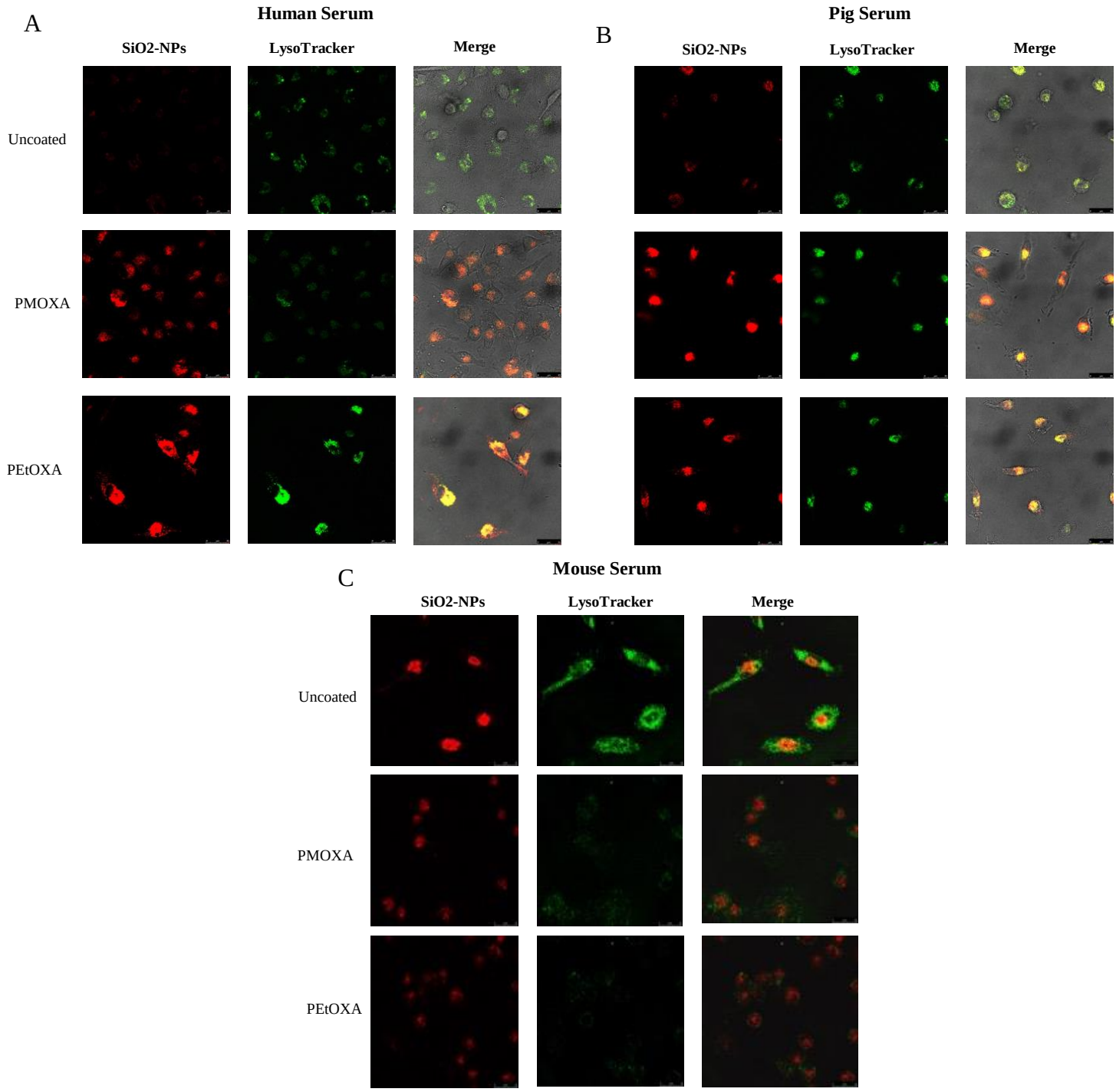

Figure 17: Effect of human macrophage capture on the transport of SiO_2-NPs in HS, PS, MS to acidic endolysosomes. Confocal images of human macrophages treated at 37 °C for 3 hr with 80 µg/ml SiO_2-NPs in (A) HS (B) PS (C) MS in RPMI medium (indicated to the left of the boxes), stained with LysoTracker green. Merge fields indicate SiO_2-NPs/acidic compartments co-localization

Next, we decided to look at whether we could distinguish between the classical and alternative complement pathways in order to discern a possible mechanism by which the coated and non-coated particles use to activate the immune response. Due to the fact that the classical complement cascade is calcium dependent and the alternative complement cascade is magnesium dependent, we used 10 mM EDTA and 10 mM EGTA supplemented with 2.5 mM magnesium in order to probe this effect. EGTA has a lower affinity for magnesium than EDTA, making it more selective for calcium ions where EDTA chelates both calcium and magnesium. When supplemented with additional magnesium, EGTA can selectively inhibit the classical pathway, allowing for the alternative pathway to remain active, whereas EDTA inhibits both pathways. In addition, in order to determine which situation is responsible for the low cellular capture by coated particles, we decided to probe the nanoparticles in mouse serum with orthologous mouse macrophage RAW cell line. As we have already demonstrated particles behave similarly in pig serum as they do in human serum with human cells, we wanted to further probe complement involvement by deactivating the complement system via calcium chelation with human cells and pig serum, and mouse serum and mouse cells (Figure 18).

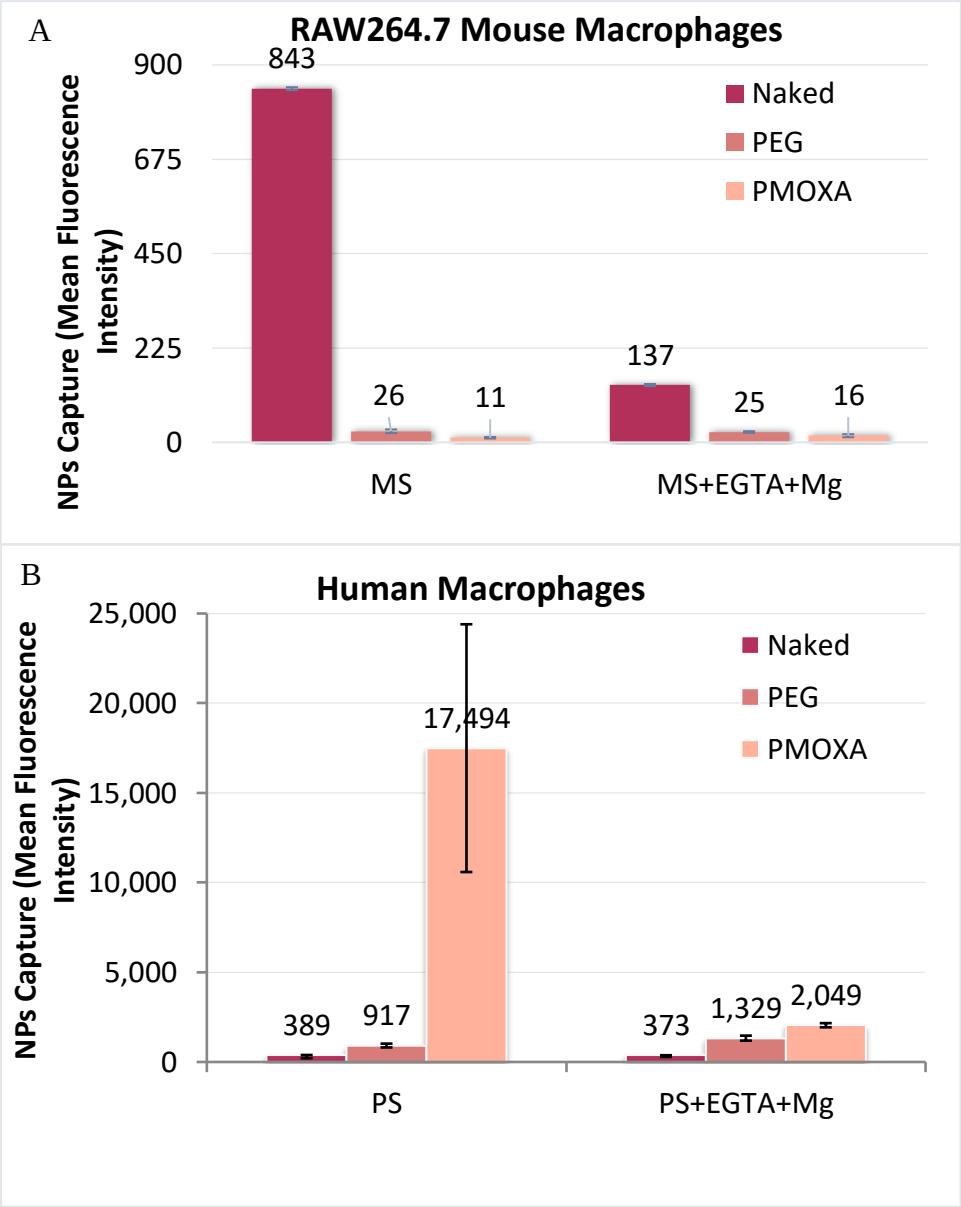

Figure 18: The effect of serum proteins from multiple species on SiO_2-NPs cellular association with orthologous macrophages with calcium chelating agents. Following a 20 min incubation at 37 °C in 70% serum, 80 µg/ml SiO_2-NPs were incubated for 3 hours at 37 °C with human (A) RAW 264.7 mouse macrophage cell line with MS and (B) human macrophages with PS for 3 hours. The cells were subsequently analyzed by flow cytofluorimetry to measure nanoparticle- associated fluorescence. Data are mean ± standard error of the mean (n = 3). Values above the bars indicate cell association expressed as the mean Fluorescence Intensity.

In congruence with previous confocal images with human macrophages, when uncoated, PEGylated, and PMOXA-coated particles are incubated with mouse serum and incubated

with RAW mouse macrophage cell line, uncoated NPs had a higher uptake compared to the coated particles. With the chelation of calcium, uncoated NPs were captured 6 times less compared to normal calcium supplemented serum. PEGylated and PMOXA-coated NPs showed no change in nanoparticle uptake in EGTA conditions, which when taken together with previous findings and the fact that the particles behaved as seen in FCS, indicate that the coated particles are stealth, there is a lack of cellular recognition and internalization in orthologous non-human cells and serum, and this phenomena is calcium dependent.

We wanted to demonstrate this effect of calcium chelation on the transport of SiO_2-NPs in PS and MS to acidic endolysosomes in human macrophages. Figure 19 demonstrates the comparison between non-coated particles, PEGylated, and PEtOXA-coated NPs in mouse and pig serum with human macrophage cells. We used PEtOXA-coated NPs due to the fact that it had the highest cytoplasmic signal and co-localization compared to the other PMOXA-coated particles. Furthermore, we wanted to compare PEtOXA-coated NPs to an already established polymer coating for stealthing particles, PEG. Finally, because interspecies comparison is of great interest to us, we wanted to compare pig serum (PS) and mouse serum (MS) in order to compare the effect of cell internalization and to probe the efficacy of coated nanoparticles' surface. Non-coated particles and PEtOXA-coated particles incubated with PS (Figure 19A) supported previous finding in Figure 17B where uncoated NPs had a low cytoplasmic signal and co-localization whereas PEtOXA-coated NPs had high cytoplasmic signal and co-localization. In addition, PEG, which has been shown to be captured by macrophages previously in this lab, was seen to induce phagocytosis, however, less than that of PEtOXA-coated NPs. The three particles were analyzed in PS supplemented with 10mM EGTA and 2.5mM Mg^{2+} (Figure 19B). Images indicate PEtOXA had a reduced cell internalization given the reduced cytoplasmic signal but PEGylated NPs in fact had an

increase in fluorescence and co-localization. Furthermore, when comparing MS, (Figure 19C) images indicate a reverse trend as seen with PS and even HS. Uncoated particles had an increase fluorescence comparable to that in the PEtOXA-coated NPs and PS conditions, and both PEGylated and PEtOXA-coated particles evaded phagocytosis by human macrophages. Furthermore, similar to PS, when 10 mM EGTA and 2.5 mM Mg^{2+} (Figure 19D) were supplemented to MS, there was a slight decrease in signal in the uncoated NPs conditions, although there was no remarkable reduced signal either with PEGylated or PEtOXA-coated NPs.

These results further indicate that PEtOXA-coated particles induce cellular capture by human macrophages in PS and this trend is calcium dependent. Furthermore, cellular capture by mouse cells in MS is increased by uncoated particles and is also calcium dependent. These observations may suggest a likely role for complement activation in NP recognition by human phagocytic cells with pig serum, as well as mouse phagocytic cells and mouse serum.

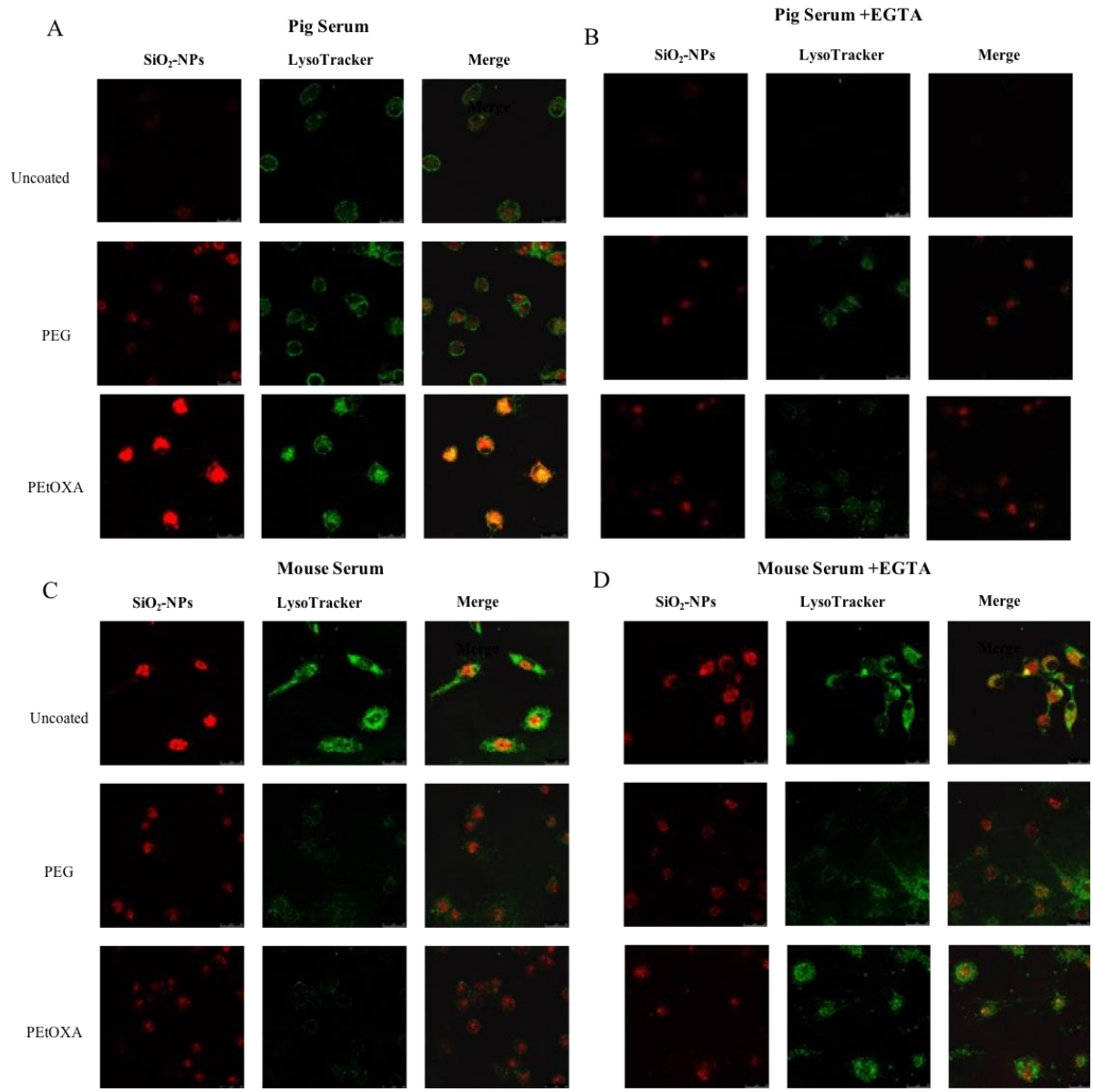

Figure 19: Effect of calcium chelation on the transport of SiO_2-NPs in PS and MS to acidic endolysosomes in human macrophages. Confocal images of human macrophages treated at 37 °C for 3 hr with 80 µg/ml SiO_2-NPs in (A) PS (B) PS+EGTA (C) MS (D) MS +EGTA in RPMI medium (indicated to the left of the boxes), stained with LysoTracker green. Merge fields indicate SiO_2-NPs/acidic compartments co-localization.

Characterization of the SiO_2-NPs corona composition by gel electrophoresis and LC MS/MS.

Given the observed difference between the four ORMOSIL nanoparticles in affecting SiO_2-NPs' cellular uptake as well as differences between serum species, it is reasonable to conclude given past studies[118,125] the difference lies in the protein corona composition

between particles, altering the ability of phagocytes to interact with them. Therefore, we analyzed the protein corona formed on uncoated, PEGylated, PMOXA-coated, and PEtOXA-coated nanoparticles incubated for 20 min at 37 °C in 70% (v/v) human, mouse, and pig serum in order to elucidate the protein differences. Following NP recovery and thorough ultracentrifugation washings, gel electrophoresis under non-reducing conditions was performed, where the proteins were revealed by silver nitrate staining and further analyzed by densitometry. We first began to characterize the protein corona in 70% (v/v) human serum, where the major electrophoretic bands with uncoated SiO_2-NPs are shown in Figure 20 corresponds to p220, p60, p50, p20, p35, p33, and p8. However, in the mock NP free samples, there are bands belonging to certain proteins such as p60, p50, and p20 indicating that these proteins could be remnants from serum. The p60 also demonstrates an inverse correlation to particle amount, seemingly getting more intense as the uncoated ORMOSIL concentration decreases. In human serum, p50 and p60 are at the same intensity in the mock as in the samples with NPs (Figure 20A). It is apparent that the major bands of p35 and p33 proteins vary in intensity directly proportional to the concentration of nanoparticles, decreases as the particle amount decreases. In addition, p20 seems to be slightly concentration dependent, only slightly reducing its relative intensity even at 25 μg/mL versus 800 μg/mL.

In contrast, the pattern of the main proteins strongly associated with PEGylated NPs (Figure 20B) varies considerably with much of the predominant bands being concentration dependent. Below 100 μg/mL, p20, p35, p40, p80, p100, and p120 proteins almost entirely disappear yet p80, p65, p60, and p10 are not only more intense at higher concentrations such as 800, 400, and 200 μg/mL but are located within the context of a more complex set of bands than uncoated. This is supported by our previous results from confocal imaging, cellular uptake assay with FACS, as well as LC MS/MS. Furthermore, coated PMOXA-

coated SiO_2-NPs (Figure 20C) showed a similar band pattern and intensity with p20, p33, and p35 yet with a further increase in band intensity. They are also concentration dependent, decidedly visible at higher concentrations, tapering off to a fraction of the amount at low particle amounts. Furthermore, p60 and p65 which were very prominent in PEG conditions, but was highly reduced with PMOXA even at the highest tested concentrations. The most striking difference between PMOXA-coated and PEGylated NPs is the band between 45 kDa and 30 kDa.

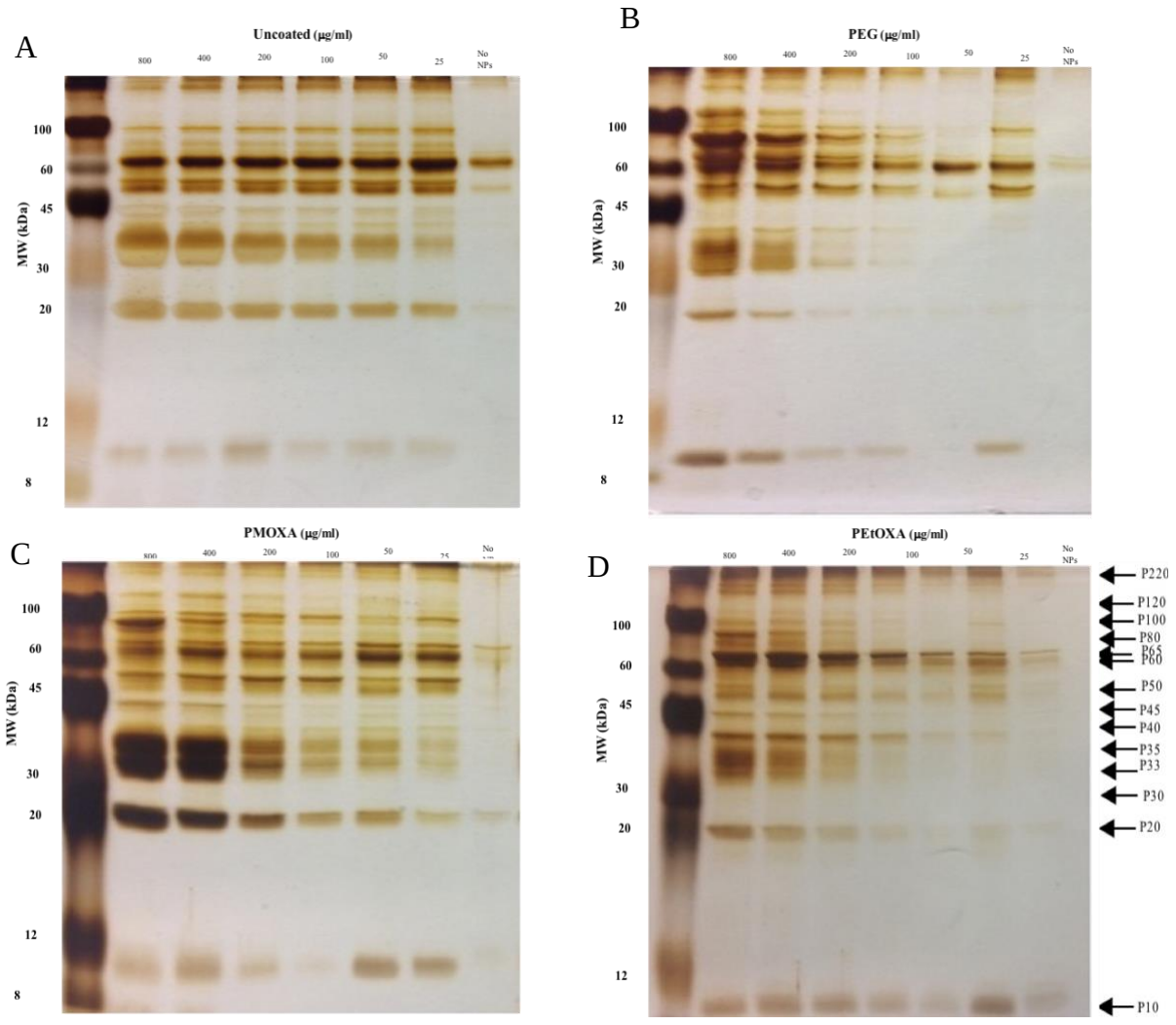

Figure 20: SDS-PAGE analysis of the pattern of HS with clot activator and HS without clot activator proteins adsorbed on SiO_2-NPs. (A) Uncoated (B) PEG (C) PMOXA (D) PEtOXA SiO_2-NPs were incubated at the indicated concentrations for 20 minutes at 37 °C in 70% HS, washed and analyzed by SDS-PAGE (12%). Equal sample volumes were loaded onto an SDS-PAGE and stained by silver nitrate, where a semi-quantitative estimation of the relative amount of the main protein bands found (arrows), labeled by their rough apparent molecular weight in kDa (pxx), were determined by densitometry and represented in histograms. On the left-hand side of each image, the values indicate the MW in kDa of the molecular weight standard polypeptides used in the gel.

Although the band pattern once again changes for PEtOXA-coated nanoparticles (Figure 20D), where p65 increased intensity compared to PMOXA-coated NPs and p35, p33, and p20 have decreased band intensities, the patterns are more complex compared to uncoated NPs which is in line with the other coated particles. From the gel, it seems the band between 45 kDa and 30 kDa is in higher amount in PMOXA-coated and PEtOXA-coated, compared to PEG and uncoated NPs.

These results indicate that the corona composition is not only concentration dependent but is quite different between particles. Thus, NP capture and cellular affinity is most likely due to the proteins identified here.

Because we observed differences between the four ORMOSIL nanoparticles in affecting SiO_2-NPs' cellular uptake as well as differences among serum species, we decided to next characterize the protein corona in 70% (v/v) pig serum (Figure 21). Furthermore, all the bands were quantified using densitometry methods and are displayed in Figure 22. The major differences between particles incubated in pig serum than in human serum are mainly for p120, p100, and a significant amount of the high molecular weight proteins which are absent in uncoated and PEGylated nanoparticles. In addition, the bands corresponding to p80 are much more intense in all four NPs compared to HS conditions. p18 is present in PS but is not found in HS, and at concentrations of 50 μg/mL and 25 μg/mL, the band signal is equivalent to the background mock serum condition (without particles) (Figure 21A). The bands at p15 and p18 are found in only pig serum conditions as well as p30, which is seen in small traces in human serum. The bands at p33 and p35 are highly reduced in pig serum as well as p60 and p65, which are interestingly dose dependent in PS but not in HS. This phenomena is also found to be the case for p20 which decreases with decreasing particle dosage but is relatively stable in HS. Certain bands in the mock NP free samples correspond to certain proteins such

as p60, p50, and p20 indicating the proteins could be remnants from serum. However, p15 is found in PS and not in HS. According to densitometry quantitative measurements, p100, p50, p40, p35, p33, p30, p20, p18, P15, and p10 in conditions of 50 μg/mL and 25 μg/mL have equivalent signal seen in the nanoparticle-free mock, serum-only control samples.

As for coated nanoparticles, the protein corona pattern is relatively the same for PEGylated NPs (Figure 21B) as was for uncoated however, bands corresponding to p80 and p10 are highly more intense and p35 and p33 are slightly more intense. p15 was reduced in PEGylated NPs by 80%, with only traces of protein, equivalent to the mock samples, indicating it might be a remnant from PS. The doublet at p50 and p20 was also reduced by 11% and 35%, respectively. p18 increased by 16% in PEGylated NPs compared to uncoated NPs.

However, PMOXA-coated and PEtOXA-coated NPs (Figure 21 C and D, respectfully) have a much more complicated corona formation in PS. All major protein bands are evident where P120 as well as the other high molecular weight proteins that were absent on uncoated and PEGylated NPs are now present and more intense. The most striking difference between PMOXA-coated and PEtOXA-coated NPs is the band between 30 kDa and 45 kDa which is not present in PEGylated NPs or uncoated NPs. The band at p12 which was also absent in uncoated and PEGylated NPs is also present in PMOXA-coated NPs but is once again reduced in PEtOXA-coated NPs by 50%. Compared to PEGylated, PMOXA-coated NPs proteins increased by: p10 (25%), p12 (100%), p18 (55%), p20 (50%), p30 (24%), p33 (12%), p35 (57%), p40 (52%), p50 doublet, p60, and p80 (69%). This patter predominates in the corona pattern for both PMOXA-coated and PEtOXA-coated NPs. Below 400 μg/mL, p33 bands disappear for PMOXA-coated NPs whereas it is still present at 100 μg/mL for PEtOXA-coated NPs. The major differences between PMOXA -coated and PEtOXA-coated

NPs are as follows: p100 and p120 appears as well as p15 (53%) and p18 (23%) increases in intensity for PEtOXA as well as the doublet at p50 (56%) but also appears to become a singlet at 400 μg/mL. The band at p20 deceases by 17% in intensity compared to PMOXA-coated NPs and p12 and p30 almost entirely disappears. It is obvious to conclude from these gels that the protein corona becomes more complex and elaborate for the two oxazoline coated particles than for uncoated NPs and even PEGylated particles which is in line with densitometric analysis data.

These results indicate the corona composition is not only concentration dependent but is quite different between particles and between species. Thus, the differences in NP capture and cellular affinity between species is most likely due to the proteins identified here.

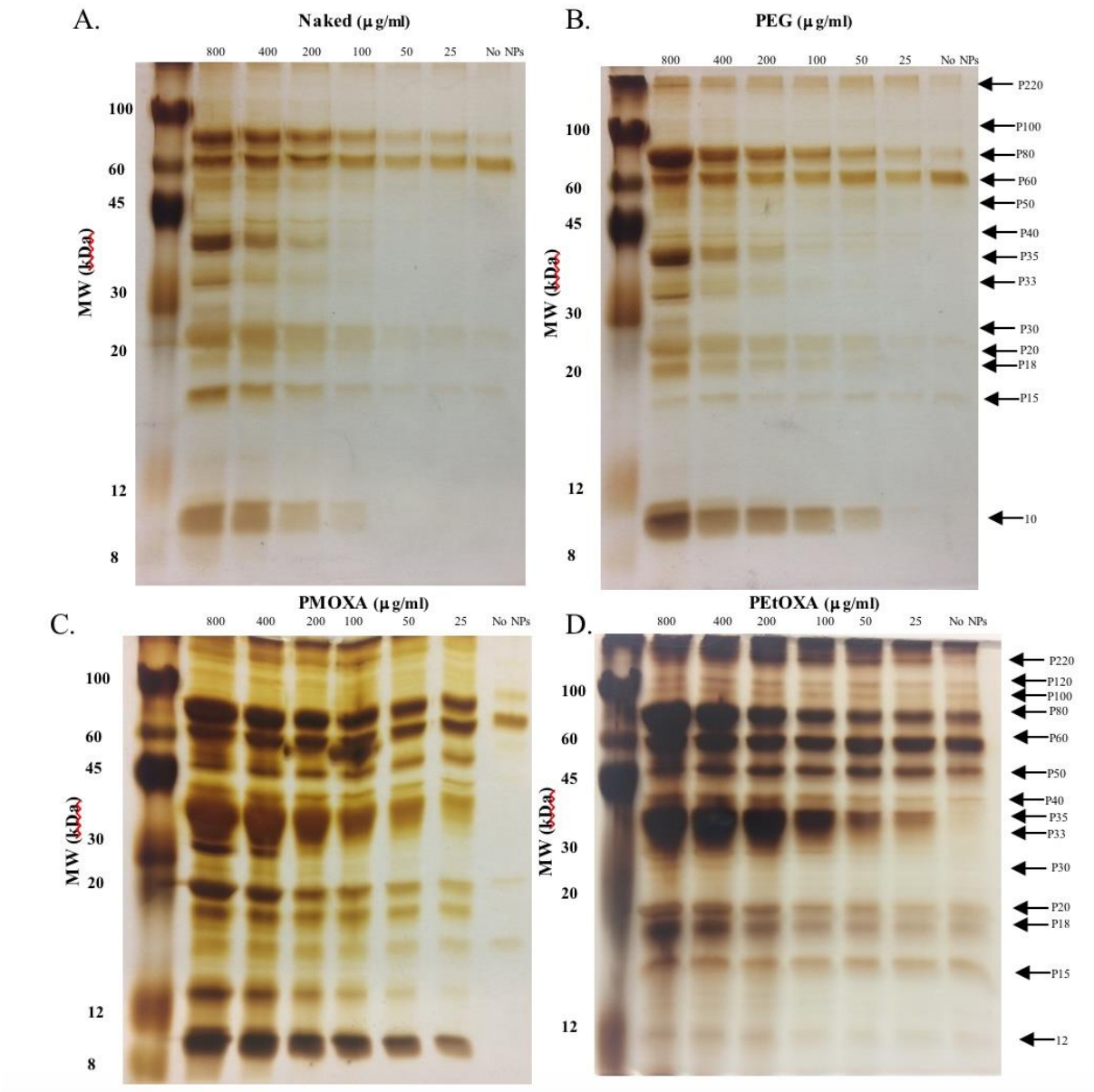

Figure 21: SDS-PAGE analysis of the pattern of PS proteins adsorbed on SiO_2-NPs. (A) Uncoated (B) PEG (C) PMOXA (D) PEtOXA SiO_2-NPs were incubated at the indicated concentrations for 20 minutes at 37 °C in 70% PS, washed and analyzed by SDS-PAGE (12%). Equal sample volumes were loaded onto an SDS-PAGE and stained by silver nitrate. On the left-hand side of each image, the values indicate the MW in kDa of the molecular weight standard polypeptides used in the gel.

Figure 22: Densitometric analysis to examine the corona protein levels absorbed onto ORMOSIL SiO_2-NPs. Following silver staining, a semi-quantitative estimation of the relative amount of the main protein bands found (arrows), labeled by their rough apparent molecular weight in kDa (pxx), were determined by densitometry.

Given the fact PEtOXA-coated NPs showed unusual cellular behavior as shown in Figure 14 and the complex corona composition elucidated by gel electrophoresis Figure 20 and Figure 21, we decided to perform semi-quantitative estimations by label-free methods after liquid chromatography-tandem mass spectrometry (LC-MS/MS) analysis for determining the polypeptide composition of proteins bound to PEtOXA-coated NPs in the presence of HS, MS, and PS (Table 2 and Figure 23). The main corona components included the expected common circulating blood proteins, coagulation and complement factors, and protease inhibitors. Proteins bound to PEtOXA-coated NPs in human serum included Albumin, Apolipoprotein A1, Apolipoprotein E, Clusterin, and Complement C3. In pig serum, the most abundant polypeptides were found bound to the surface of PEtOXA-coated NPs included Complement C3, Prothrombin, Albumin, Ficolin 1, Ficolin 2, Apolipoprotein A1, Apolipoprotein E. For mouse serum, the major polypeptide components include Antithrombin-III, Prothrombin, and Apolipoprotein E. The major differences between the human and the pig serum is the lack of Clusterin in PS and the lack of Ficolin 1 and 2 in HS. Clusterin, also known as Apolipoprotein J, is a 75- to 80-kDa heterodimeric glycoprotein consisting of an α-chain and a β-chain, linked by five disulphide bridges. It has been shown in past studies[126,127] that clusterin, a dysopsonic protein, provides stealth effects against phagocytes by inhibiting complement, preventing protein aggregation, and by inducing apoptosis of inflammatory cells. This phenomena could explain why there was a reduction in band intensities with PEtOXA-coated NPs in HS as seen in Figure 20 and why PEtOXA-coated NPs had a reduced capture by human macrophages in HS compared to PS (Figure 14). However, clusterin also mediates and accelerates sC5b-9 formation as well as complexing with HDL and ApoA1. Our data shows even when complement is inhibited, clusterin deposition is still present in the corona composition, thus indicating direct HDL binding to the surface of the particle is required or clusterin complexed with Apo A1 is transferred from

HDL to the surface. However, despite the complement inhibitory effects and the ability to remove opsonization molecules, clusterin does not seem to inhibit complement activation in human serum by PEtOXA-coated NPs.

The other major difference between the two sera is the presence of Ficolin 1 and 2 in PS. Ficolins are involved in the lectin complement pathway by binding via a fibrinogen-like (fbg) domain.[41] ficolin-1 and ficolin-3 have only one binding pocket each, while ficolin-2 has four binding pockets.[45] Ficolin plasma levels in pig (30 pg/ml) are relatively higher than in mouse (1-2 pg/ml) or human (4.13 pg/ml) and are comprised of two ficolin 12-mers connected face-to-face by their fbg domains.[128] It has been shown that repeated freeze-thaw cycles of plasma and serum can reduce complement and ficolin concentrations by repeated clotting, degradation of ficolin, or salting-out during freezing.[129] Therefore, experiments were performed with either fresh or once-frozen samples thus ensuring the activation and presence of ficolin proteins. Therefore, the lack of ficolin in human serum with PEtOXA-coated NPs is directly related to complement activation, or lack thereof by ficolin association, instead of inactivated serum samples ensuring accurate quantitative ficolin amounts. Ficolin may be directly involved in complement activation via the lectin pathway by PMOXA-coated and PEtOXA-coated nanoparticle which is species specific to pigs.

Both pig and mouse serum show specificity for prothrombin which when activated by FXa bound to FVa forming prothrombinase, converts into thrombin (FIIa) allowing thrombin to activate platelets, FV, factor VIII (FVIII), and factor XI as well as cleavage of fibrinogen to fibrin. Thrombin activation can proteolytically generate C5a activating the complement pathway as well as inducing the expression of the decay accelerating factor (DAF) in a PAR_1-dependent manner which reduces C3 deposition thus inhibiting the complement pathway. Therefore, the roles in pig and mouse serum might be quite varying, either inhibiting or

initiating complement. However, taken together with the fact that both human and pig serum showed complement C3 fragments either native C3 or covalently bound C3 with molecular weight greater than native C3, thus indicating complement activation, we can suggest that, possibly, prothrombin plays some role in complement activation in pigs. However, given the lack of Complement C3 protein in mouse as well as the presence of another major polypeptide components for antithrombin III, which is an inhibitor by neutralizing the enzymatic activity of thrombin, it was imperative to look further into C3 specificity among the three species.

Table 2: Serum proteins from different species bound to PEtOXA-coated amorphous silica nanoparticle surface identified by tandem mass spectrometry analysis.

Bands	Species	Accession #	Protein name	Mass (Da)	Score	Peptides	Sequence coverage %	EMPAI
1	pig	P01025	Complement C3	188,229	130	15 (7)	4	0.16
2	pig	P01025	Complement C3	188,229	159	8 (1)	0	0.02
3	pig	Q19AZ8	Prothrombin	**71,447**	216	5 (4)	8	0.24
4	pig	P08835	Albumin	**71643**	194	9 (2)	4	0.12
	pig	P01025	Complement C3	188,229	128	7 (7)	4	0.19
5	pig	Q29041	Ficolin 2	35,173	302	7 (6)	18	0.97
	pig	Q29042	Ficolin 1	35,680	270	5 (4)	12	0.56
	pig	P01025	Complement C3	188,229	266	7 (5)	3	0.11
6	pig	Q29041	Ficolin 2	35,173	316	6 (6)	18	1.11
	pig	P18650	Apolipoprotein E	36,634	186	7 (2)	5	0.27
	pig	Q29042	Ficolin 1	35,680	245	4 (4)	12	0.64
7	pig	P18650	Apolipoprotein E	36,634	206	6 (2)	7	0.24
8	pig	P18648	Apolipoprotein A1	30,307	282	10 (1)	3	0.16
9	mouse	P32261	Antithrombin-III	52,484	449	11 (5)	4	0.44
	mouse	P19221	Prothrombin	71,649	237	5 (4)	5	0.24
10	mouse	P08226	Apolipoprotein E	35,901	562	12 (8)	28	1.39
11	human	P01024	Complement C3	188,569	476	14 (7)	4	0.16
12	human	P01024	Complement C3	188,569	525	17 (7)	4	0.17
13	human	P02768	Albumin	71,317	377	13 (7)	12	0.46
	human	P01024	Complement C3	188,569	1,431	35 (28)	20	0.77
14	human	P10909	Clusterin	53,031	62	2 (1)	2	0.08
	human	P01024	Complement C3	188,569	337	10 (5)	3	0.12
15	human	P02649	Apolipoprotein E	36,246	61	2 (1)	2	0.1
	human	P10909	Clusterin	53,031	174	5 (3)	9	0.22
16	human	P02649	Apolipoprotein E	36,246	52	5 (0)	n.d.	n.d.
17	human	P02647	Apolipoprotein A1	30,759	270	11 (3)	14	n.d.

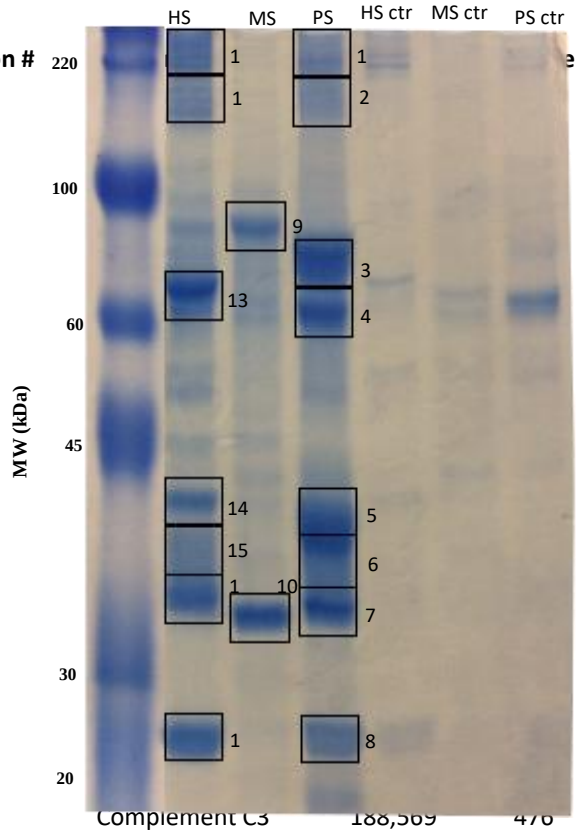

Bands	Species	Accession #	Peptides	Sequence coverage %	EMPI
1	pig	P01025	15 (7)	4	0.16
2	pig	P01025	8 (1)	0	0.02
3	pig	Q19AZ8	5 (4)	8	0.24
4	pig	P08835	9 (2)	4	0.12
	pig	P01025	7 (7)	4	0.19
5	pig	Q29041	7 (6)	18	0.97
	pig	Q29042	5 (4)	12	0.56
	pig	P01025	7 (5)	3	0.11
6	pig	Q29041	6 (6)	18	1.11
	pig	P18650	7 (2)	5	0.27
	pig	Q29042	4 (4)	12	0.64
7	pig	P18650	6 (2)	7	0.24
8	pig	P18648	10 (1)	3	0.16
9	mouse	P32261	11 (5)	4	0.44
	mouse	P19221	5 (4)	5	0.24
10	mouse	P08226	12 (8)	28	1.39
11	human	P01024	14 (7)	4	0.16

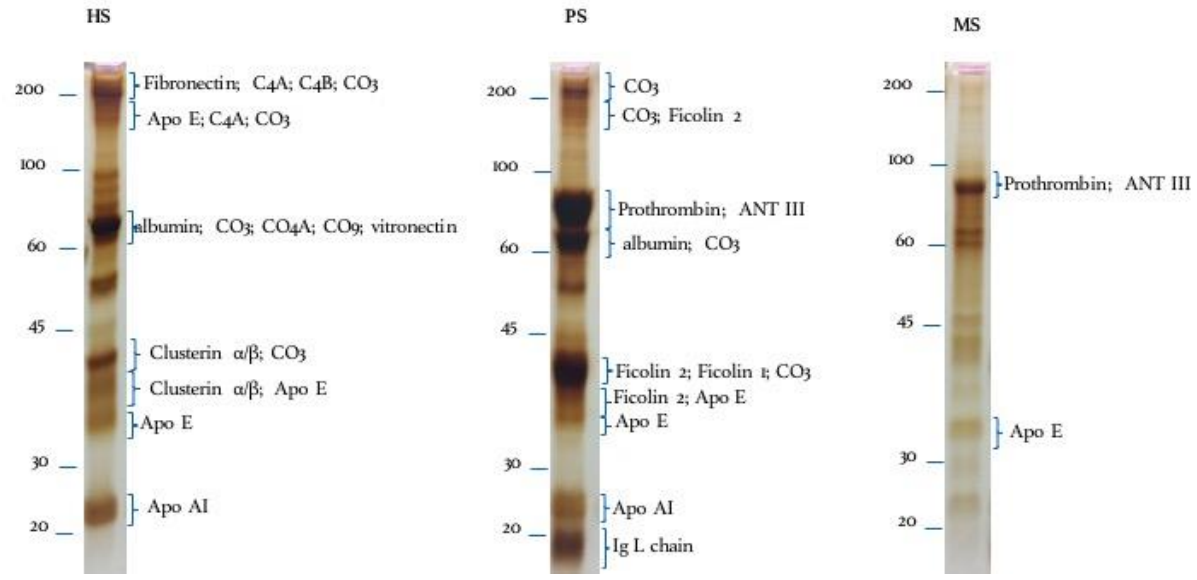

Figure 23: Serum proteins from different species bound to PEtOXA amorphous silica nanoparticle surface identified by tandem mass spectrometry analysis. Major complement proteins and lipoproteins in HS, MS, and PS are identified and shown with their band identified by silver staining following gel electrophoresis.

One of the more interesting aspects of the MS/MS results is the fact that the readout analyzed multiples peptides corresponding to different molecular weights as Complement C3 (180 kDa). C3 is composed of two chains, α and β, connected by a disulphide bond, which is reduced in the presence of β-mercaptoethanol. Upon C3 activation, cleavage forms C3b and C3a which is released into solution. C3b contains an exposed thioester bond in the C3dg region which allows C3b to covalently bind to foreign cells via hydroxyl (-OH) and amine (-NH2) groups on the cell's surface. C3b is further inactivated by Factor H and I to form C3f and iC3b, which is further degraded into C3c, C3d, and C3g. Peptide mapping was performed with human serum and pig serum (Figure 24) in order to identify which C3 fragments were present by mapping the identified peptide sequences onto the full C3 protein sequence. The three peptide fragments identified corresponds to the molecular weight 180->200 kDa, 70 kDa, and 38 kDa in both human and pig C3. Mapping these peptides onto the C3 sequence revealed the peptide corresponding to 70 kDa mapped as C3β which is about 80 kDa and is in line with reduced C3. The peptide at 180->200 kDa mapped to the region C3b containing C3dg bounded to the particles. The native fragment is about 80 kDa, but since it's covalently

bound to the particle, the molecular weight will be much higher, therefore this is the reason why this fragment is seen at such a higher than expected MW. This fact is interesting because it indicates that C3 is in fact activated pointing to complement activation by the nanoparticles. Furthermore, the final peptide associated with 38 kDa, was mapped to C3c α' fragment 1 at the corresponding 39 kDa which occurs upon C3b inactivation. Thus not only is C3 activated in human and pig serum by PEtOXA coated nanoparticles, but it is also inactivated thus indicating opsonization by C3 leading to complement activation and phagocytosis.

It is known that C3 and C4 are homologous and share the same receptor, CR1, which is not only involved in complement activation, but also involved in inhibiting the classical and alternative pathway C3/C5 convertases as well as being a cofactor for the cleavage of C3b and C4b by factor I.[130] Therefore, we performed peptide mapping with C4a as it was done with C3. In congruence with the C3 findings, C4 was activated, bound to the particle, and then inactivated further supporting the idea of complement activation.

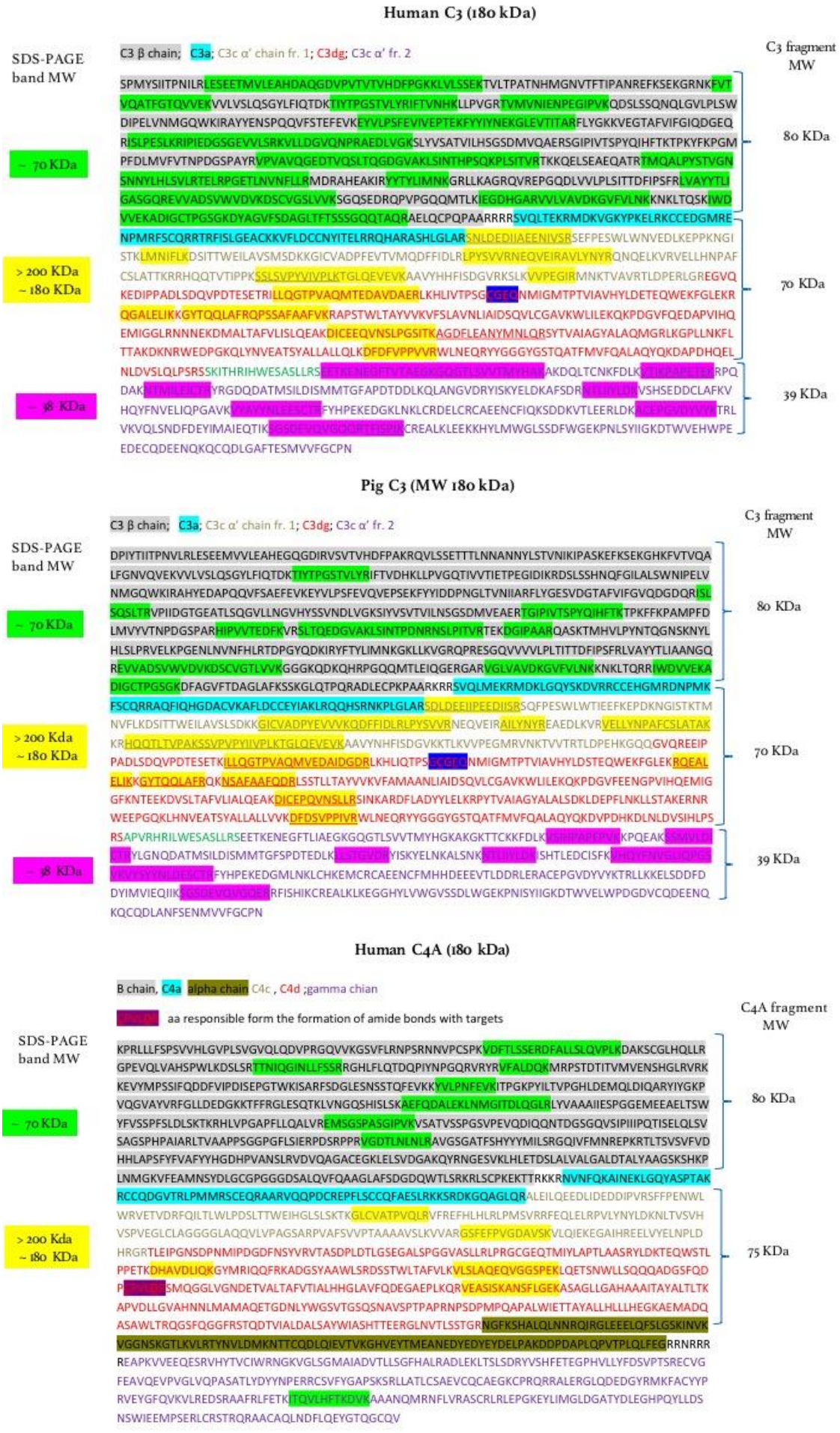

Figure 24: Peptide mapping of key conserved residues and motifs found in the amino acid sequence of human and pig C3 and human C4A. On the left hand side, the molecular weight of the peptide found in the SDS PAGE gel is indicated while on the right hand side, the predicted fragments of the protein of interest. The dark blue highlighted portion represents the amino acids which form the amide bond to the target particles.

Polypeptide abundance in complement activation in human, mouse, and pig serum with SiO_2-NPs.

To obtain a more in-depth examination of the proteins involved in complement activation upon particle introduction into serum, shotgun proteomics analysis was performed via analyzing peptides released through proteolytic digestion of intact proteins. As it is possible to observe in Figure 25, the logarithmic distribution displays the molar amount (iBAQ) for each protein which is the summed intensity for each protein divided by the number of theoretically observable peptides in serum. The theoretically observable peptides are considered to be all tryptic peptides between 6 and 30 amino acids long. The peptides listed are in descending abundance corresponding to uncoated SiO_2-NPs after the elimination of proteins with peptide number <4 and elimination of contaminants (keratins, dermicidins, and hornerin).

The greatest difference between uncoated particles and coated ones concerned properdin, platelet F4, C3, and C4b. Polypeptide molar abundances relative to uncoated for Properdin are 5.99E+07 for PEtOXA-coated NPs and 1.56E+07 for PMOXA-coated NPs compared to 5.56E+06. Furthermore, the molar abundances of C3 and C4b respectively for uncoated are 1.81E+07 and 1.08E+06, for PEGylated NPs 1.47E+07 and 6.87E+05, for PMOXA-coated NPs 2.81E+07 and 9.70E+05, and for PEtOXA-coated NPs 9.64E+07 and 1.91E+07. Properdin is a major player in enhancing the Alternative pathway by stabilizing C3 and C5 convertases by binding C3b and to Bb which prevents their spontaneous or induced activation. Complement C4b is a 193 kDa glycoprotein comprised of modified C4 α-chain (α') and intact β- and γ-chains which binds to target cell surfaces by a covalent ester bond. Inflammatory cell CR1 complement receptor can be bound by C4b bounded to the surface, leading to opsonic and immune adherence activities. Although non-enzymatic, C4b is an

essential component of the classical complement pathway. Properdin also aids in the uptake of immune complexes which can directly activate the Alternative pathway. C9 which is increased in PEtOXA-coated NPs, is part of the MAC complex which is the terminal component of all three complement pathways. Therefore, increased amounts of the complement factors may suggest a major role that the Alternative and classical pathway play in complement activation by PMOXA-coated and PEtOXA-coated NPs in human serum. However, as we have demonstrated that C3 is activated and then inactivated upon nanoparticle introduction, therefore it would make sense that factors involved in complement inhibition would be present at higher levels in the coated particles as well. The polypeptide abundance of Complement factor H (FH) bound to PEtOXA-coated NPs is 5.23E+06 and 4.60E+05 for PMOXA-coated NPs compared to 1.24E+05 for uncoated. As factor H is both a coagulation initiator and a complement inhibitor, FH plays a crucial role in the intricate balance and regulation of the two pathways as well as suggesting C3 is involved in nanoparticle uptake.

The most striking difference in pig serum (Figure 25B) is the high abundance of ficolin 1 and especially ficolin 2 for PMOXA-coated and PEtOXA-coated NPs compared to PEGylated NPs and uncoated particles. This is in congruence with previous in gel digestion data where Ficolin 1 and 2 (Table 2) was found bound to PEtOXA-coated NPs only in pig serum and not in human or mouse as well as gel electrophoresis where ficolin was also only found in pig serum and not in mouse or human serum (Figure 23). These findings may further support the role of lectin pathway in complement activation in pig serum with coated particles.

However, in mouse serum (Figure 25C), Complement C3 peptide abundance is much lower than in human serum, 1.30E+07 for PMOXA-coated NPs which is 2 times lower than in

human serum, 8.91E+06 for uncoated NPs, 5.08E+06 PEtOXA-coated NPs which is almost 19 times lower than in human serum, and 4.11E+06 for PEGylated.

The most abundant polypeptides found in human serum (Figure 26A) are associated with the apolipoproteins: Apo AI, AII, AIV, CII, CIII, E; Clusterin; Complement C3, truncated C1, and C4b; and properdin. Complement proteins C3, truncated C1, C4b, FH, and C9 were all in much higher abundance for PMOXA-coated and PEtOXA-coated particles than for uncoated and PEGylated NPs. Apo CIII was more abundant with uncoated particles compared to coated ones which is congruent with the fact that Apo CIII (8.8 kDa) inhibits the activity of lipoprotein lipase and disturbs lipids as well as interfering with the binding of Apo E to hepatic receptors. Therefore, reduced amount of Apo CIII indicates an increase in amount of Apo E for coated particles. Apolipoprotein E, which is 1.40E+08 for PEtOXA-coated NPs is about one and a half times less abundant than PEtOXA-coated NPs in human serum at 1.92E+08. Apo AIV, Coagulation factor V, C3, properdin, and clusterin are in higher abundance for coated PMOXA-coated NPs than uncoated NPs whereas Apo AIV, prothrombin, Coagulation factor V, and antithrombin III are higher for PEtOXA-coated NPs compared to uncoated. Apo AIV is the only protein higher in abundance for PEGylated NPs. The reduced protein amount of complement activation associated proteins in mouse serum compared to human as well as the reduced relative abundance between the four particles indicate that complement, while still possibly activated, does not have the same specificity to the same degree in mouse serum to the particles as does human serum. Furthermore, because uncoated NPs has a greater abundance of complement activating proteins such as prothrombin, Apo AI, AII, CII, and clusterin which are all proteins which can be associated with complement downregulation.

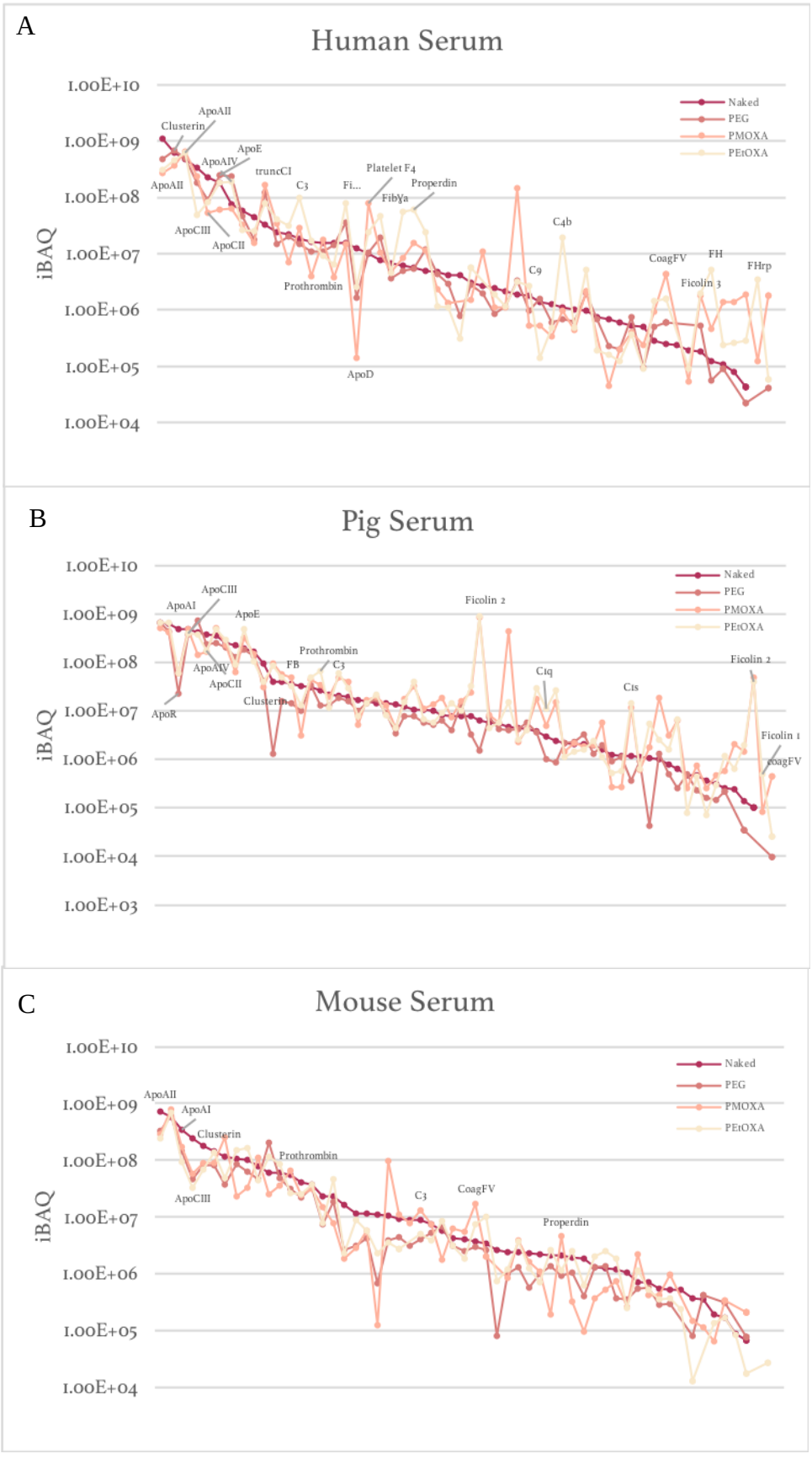

Figure 25: Polypeptide abundance of SiO_2-NPs in human, mouse, and pig serum. The iBAQ score on the left of the graph corresponds to the sum of all the peptides intensities divided by the number of observable peptides of a protein. The peptides listed are in descending abundance corresponding to serum with Uncoated SiO_2-NPs after the elimination of proteins with peptide number <4 and elimination of contaminants (keratins, dermicidins, and hornerin).

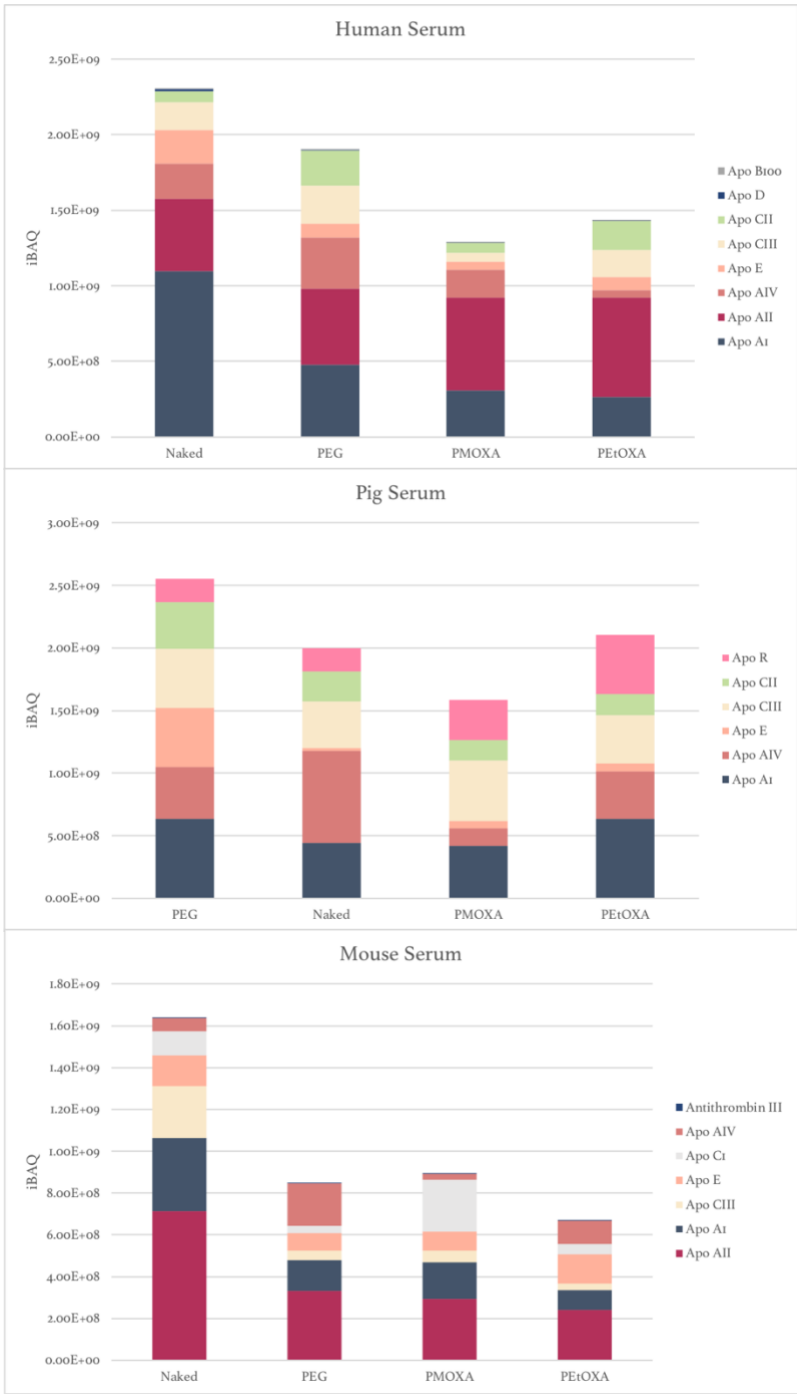

Figure 26: Apolipoprotein polypeptide abundance of SiO_2-NPs in human, mouse, and pig serum. The iBAQ score on the left of the graph corresponds to the sum of all the peptides intensities divided by the number of observable peptides of a protein. The peptides listed are in descending abundance corresponding to serum with Uncoated SiO_2-NPs after the elimination of proteins with peptide number <4 and elimination of contaminants (keratins, dermicidins, and hornerin).

Due to the fact that the classical complement cascade is calcium dependent and the alternative complement cascade is magnesium dependent, we decided to look at whether we could distinguish between the two pathways in order to discern a possible mechanism by which the coated and non-coated particles use to activate the immune response. In order to probe this effect, we wanted to discern the protein abundance of the corona for the particles in the presence of calcium chelating agents. The addition of EDTA prevents complement activation and C3b opsonization of the NPs for the classical and lectin pathways. It has already been established that ficolins bind MASPs via a fibrinogen-like (fbg) domain in a calcium independent manner and C1q interacts with $C1r^2C1s^2$ via Ca^{2+} binding domains. For most of the proteins identified in uncoated NPs (Figure 27A) incubated in human serum, their abundance does not seem to be affected by the addition of calcium chelating agents. However, complement C3 in much higher abundance in PEtOXA-coated but it also showed a significant decrease upon calcium chelation. C9, C4b, Apo B, and FH saw a substantial reduction in protein abundance as well (Figure 31). As discussed previously, $C1r^2s^2$ forms via Ca^{2+} dependent interaction with the binding interface comprised of a Ca^{2+} binding site in the EGF domain of each subcomponent.[36] Once activated, the tetramer unfolds extending the C1s ends outside the C1q cone in order to interact with C4 and C2. C4 is cleaved producing 9 kDa C4a and 190 kDa C4b, which binds the zymogen C2 in a Mg^{2+}-dependent manner. Therefore, both C3 and C4b polypeptide content in the protein corona would be reduced if there is a lack of calcium as well as C9 which is part of the MAC formation. In contrast to complement proteins, in all nanoparticles, clusterin, lipoproteins, and other predominantly deposited species are all slightly affected on divalent cation chelation.

The removal of calcium and subsequent reduction in proteins which are calcium dependent in the protein corona not only affects the composition of the corona directly but also indirectly. Because the corona is highly dynamic and constantly changing given the environment and surroundings, the lack of certain proteins may allow for the physical opportunity of other proteins to bind which might not have the steric space to do so in the presence of other, more abundant proteins.

The protein abundance pattern for PEGylated NPs (Figure 27B) was more complicated than uncoated NPs where not only was C4b and C3 reduced with the addition of calcium chelation; but slightly more than with uncoated particles. Furthermore, Apolipoprotein A1, AII, AIV, Apo E, Apo CII, and Complement component C9 were also reduced.

Not only was the abundance in normal human serum for complement component C9 higher for PMOXA-coated NPs (Figure 27C), but in HS with EDTA, the amount of protein was significantly reduced. Additionally, Apo D was also slightly reduced without the presence of calcium.

For PEtOXA-coated NPs (Figure 27D), it is interesting to note the fact that properdin abundance was undetectable in EDTA conditions and C3 and C4b was highly reduced. Apo A1, AII, AIV, E, CII, and C9 decreased upon EDTA administration.

Unlike in human serum, mouse serum presented quite a different polypeptide pattern. Figure 28 and Figure 32 demonstrates how mouse complement proteins were highly reduced in the protein corona in all particles compared to HS and PS. However, complement proteins were the most prevalent in the mouse serum derived corona of uncoated nanoparticles compared to coated particles. This indicates, in contrast to the effect induced in human and pig serum,

complement activation is inhibited by coatings in mouse serum compared to uncoated particles in agreement with previous phagocyte capture experiments.

On the other hand, pig serum revealed a protein pattern quite similar to that found in humans (Figure 29). High abundance of complement proteins such as C3, clusterin, C1s, and FB can be found primarily in the coated PMOXA and PEtOXA particles and less so in the uncoated NPs which is in congruence with the human serum (Figure 33). However, the main difference as seen with the in gel digestion, is the absence of properdin, C4b, and C9 with the presence of Ficolin (Figure 30). Not only is Ficolin 2 the highest abundant protein in the corona for both PMOXA-coated and PEtOXA-coated NPs, but it is specific for only pig serum and is not found in human nor mouse serum.

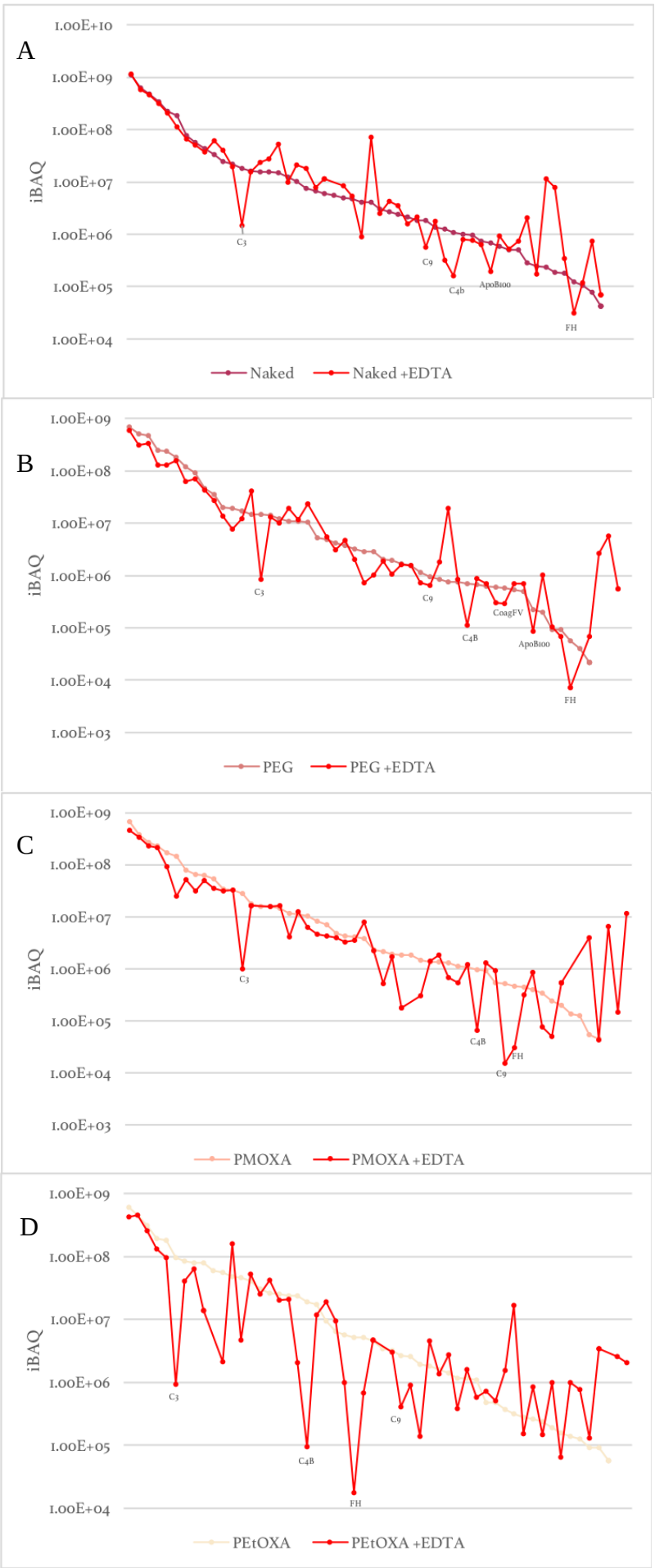

Figure 27: Polypeptide abundance of SiO_2-NPs in human serum with chelating agents (EDTA). The iBAQ score on the left of the graph corresponds to the sum of all the peptides intensities divided by the number of observable peptides of a protein. The peptides listed are in descending abundance corresponding to serum with SiO_2-NPs without EDTA after the elimination of proteins with peptide number <4 and elimination of contaminants (keratins, dermicidins, and hornerin).

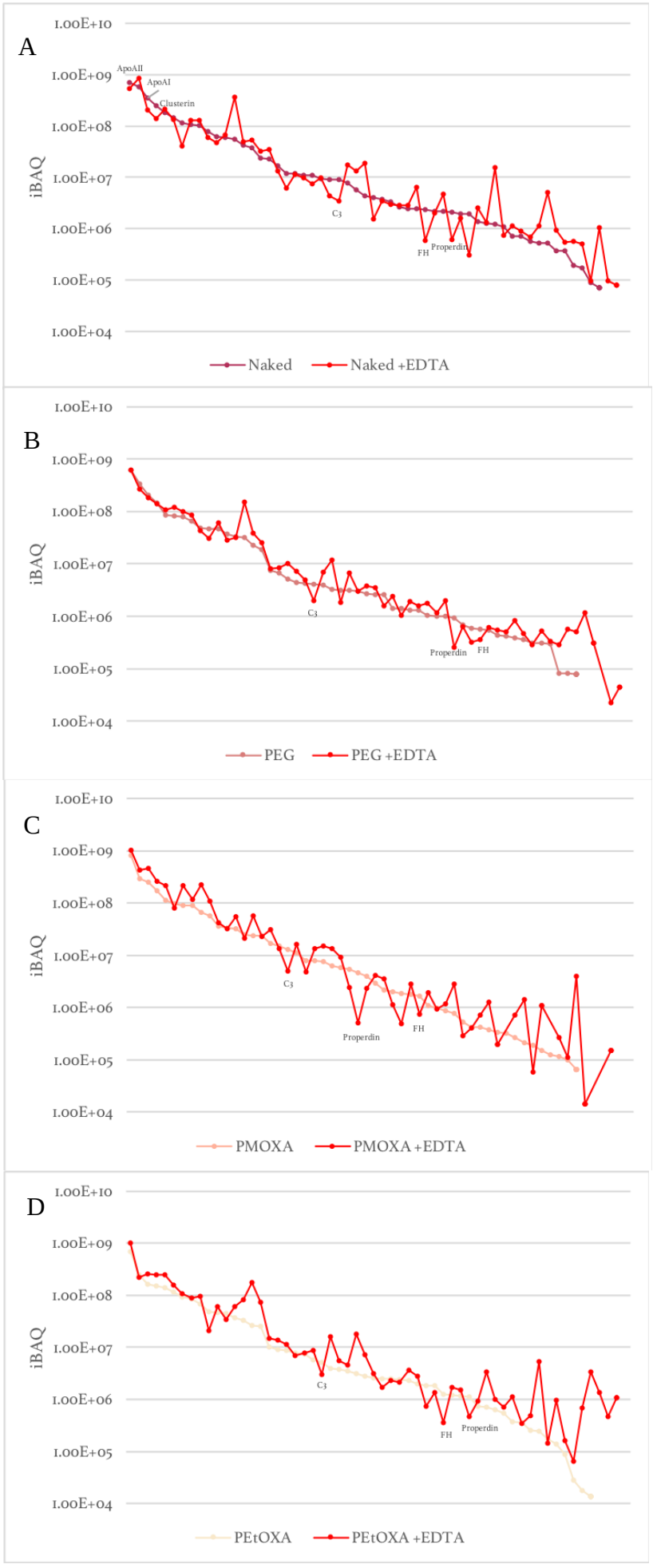

Figure 28: Polypeptide abundance of SiO_2-NPs in mouse serum with chelating agents (EDTA). The iBAQ score on the left of the graph corresponds to the sum of all the peptides intensities divided by the number of observable peptides of a protein. The peptides listed are in descending abundance corresponding to serum with SiO_2-NPs without EDTA after the elimination of proteins with peptide number <4 and elimination of contaminants (keratins, dermicidins, and hornerin).

Figure 29: Polypeptide abundance of SiO_2-NPs in pig serum with chelating agents (EDTA). The iBAQ score on the left of the graph corresponds to the sum of all the peptides intensities divided by the number of observable peptides of a protein. The peptides listed are in descending abundance corresponding to serum with SiO_2-NPs without EDTA after the elimination of proteins with peptide number <4 and elimination of contaminants (keratins, dermicidins, and hornerin).

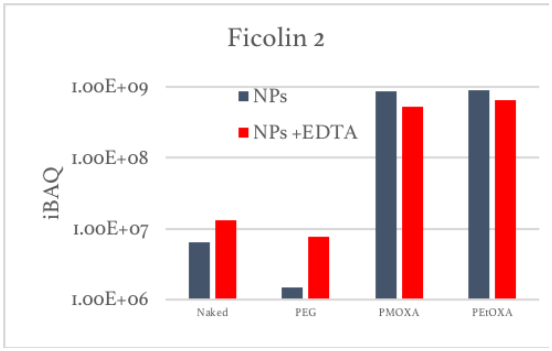

Figure 30: Specific polypeptide abundance of Ficolin 2 with SiO_2-NPs in pig serum with chelating agents (EDTA). The iBAQ score on the left of the graph corresponds to the sum of all the peptides intensities divided by the number of observable peptides of a protein. The peptides listed are in descending abundance corresponding to serum with SiO_2-NPs without EDTA after the elimination of proteins with peptide number <4 and elimination of contaminants (keratins, dermicidins, and hornerin).

*Figure 31: Specific polypeptide abundance of certain complement proteins and clusterin with SiO_2-NPs in human serum with chelating agents (EDTA). The panels on the left represent the change in abundance between the human serum and serum supplemented with EDTA. On the right, panels indicate the difference between particles with HS and particles with HS+EDTA (**Δ**). The iBAQ score on the left of the graph corresponds to the sum of all the peptides intensities divided by the number of observable peptides of a protein. The peptides listed are in descending abundance corresponding to serum with SiO_2-NPs without EDTA after the elimination of proteins with peptide number <4 and elimination of contaminants (keratins, dermicidins, and hornerin).*

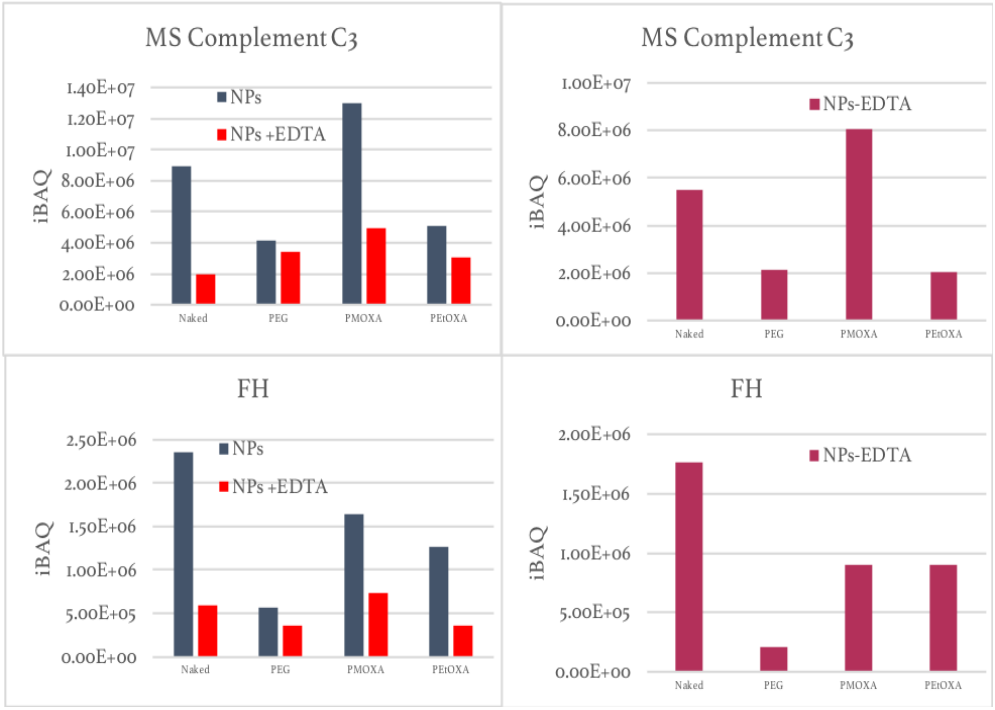

Figure 32: Specific polypeptide abundance of certain complement proteins with SiO_2-NPs in mouse serum with chelating agents (EDTA). The panels on the left represent the change in abundance between the mouse serum and serum supplemented with EDTA. On the right, panels indicate the absolute value when normalized against EDTA. The iBAQ score on the left of the graph corresponds to the sum of all the peptides intensities divided by the number of observable peptides of a protein. The peptides listed are in descending abundance corresponding to serum with SiO_2-NPs without EDTA after the elimination of proteins with peptide number <4 and elimination of contaminants (keratins, dermicidins, and hornerin).

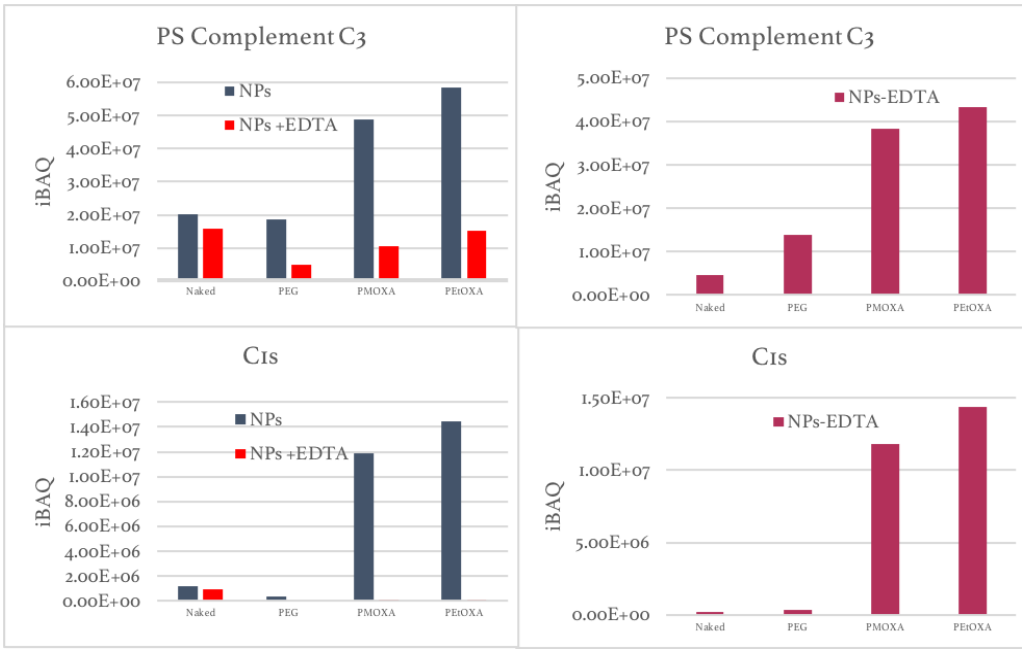

Figure 33: Specific polypeptide abundance of certain complement proteins with SiO_2-NPs in pig serum with chelating agents (EDTA). The panels on the left represent the change in abundance between the pig serum and serum supplemented with EDTA. On the right, panels indicate the absolute value when normalized against EDTA. The iBAQ score on the left of the graph corresponds to the sum of all the peptides intensities divided by the number of observable peptides of a protein. The peptides listed are in descending abundance corresponding to serum with SiO_2-NPs without EDTA after the elimination of proteins with peptide number <4 and elimination of contaminants (keratins, dermicidins, and hornerin).

Complement activation via cleavage of C3

Given that C3 is the most versatile molecule of the complement cascade and the common link between all three cascades, studying the functional properties of the C3 molecule would allow us to better understand the human complement system with the different ORMOSIL particles, but also how different animal models, which are necessary in scientific works, interact with C3 and thus the complement cascade. C3a, a 9 kDa anaphylatoxin, and C3b is generated upon complement activation and subsequent cleavage of C3. The convergence of the three complement pathways occurs around the conversion of C3 to C5 convertase activated by C3 convertase by the binding of C3b which ultimately leads to the formation of the membrane attack complex (MAC). Therefore, in order to determine whether complement is activated by PMOXA-coated NPs and PEtOXA-coated ORMOSIL nanoparticles, the C3 cleavage product C3a which is released into solution, was detected by Western blot. Therefore, we analyzed the protein corona formed on the nanoparticles after being incubated for 20 min at 37 °C in human, mouse, and pig serum. The supernatant was collected as C3a is released into solution upon cleavage in addition to recovering the NPs following ultracentrifugation and washings to be used as a negative control as those samples would not contain any C3a. Gel electrophoresis under non-reducing conditions was performed, and after transfer to 0.45 μm nitrocellulose the blotted bands were immunodetected with a specific rabbit anti-human C3a Mab and subsequently visualized with peroxidase labeled goat anti-rabbit IgG antibodies and further analyzed by densitometry. Based on the Western blot analysis and densitometry quantifications (Figure 34), C3a amounts released following particle and human serum incubation for 20 min at 37 °C shows a significant increase in free C3a in the media following PMOXA-coated NPs (37%) and PEtOXA-coated NPs (36%) particle incubation compared to positive control samples. In fact, C3a levels are two times higher in pig serum than in human serum where free C3a is increased for PMOXA-coated NPs by 72% and

PEtOXA-coated NPs by 69% in pig serum compared to the positive control. Western blot further revealed C3a is activated roughly the same by PEtOXA-coated and PMOXA-coated NPs when using the same amount of particles. However, in mouse the C3a signal was well below the detectable amount to do any analysis, although shotgun and in gel digestion further support the lack of C3a activation.

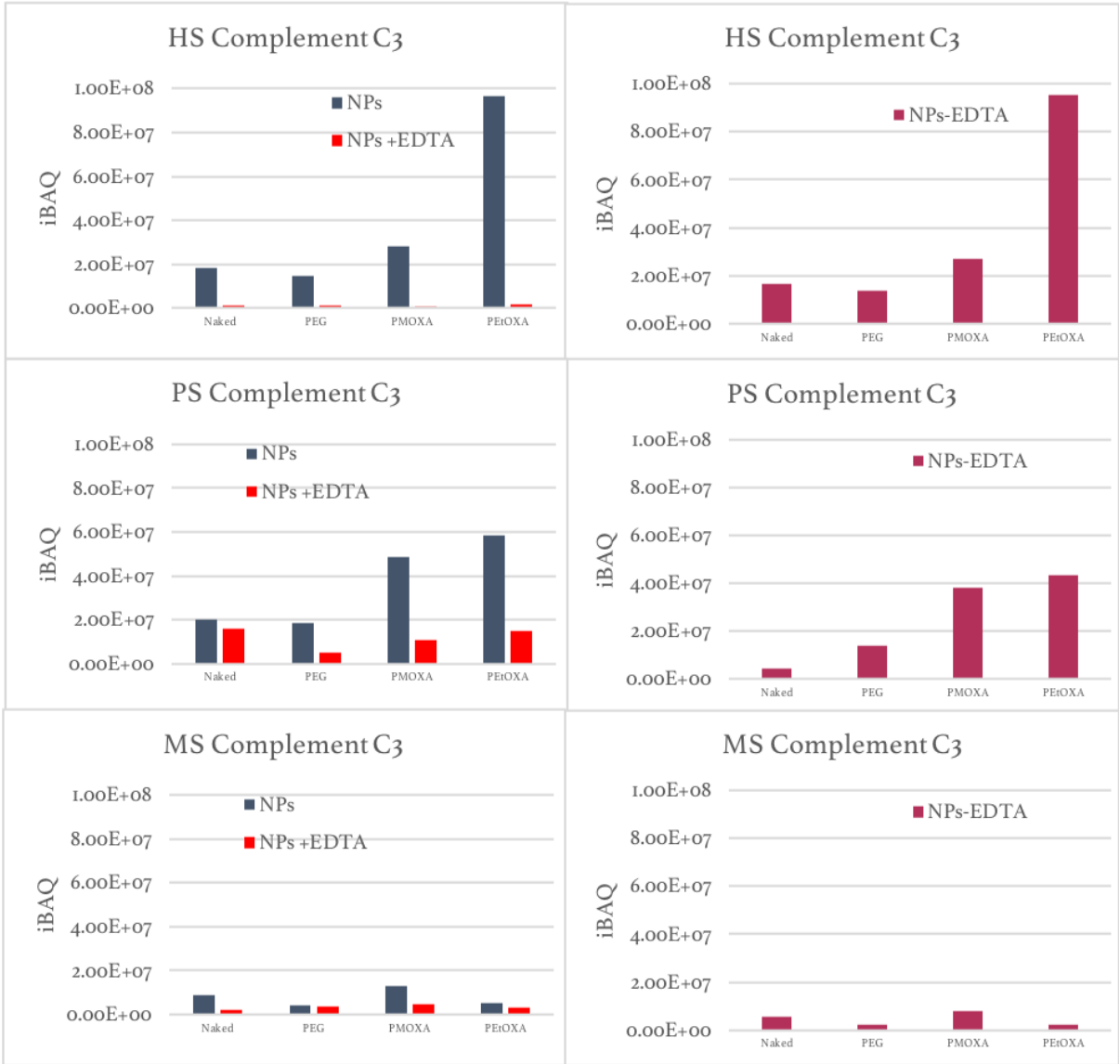

Figure 34: Specific polypeptide abundance of complement C3 protein with SiO_2-NPs in human, mouse, and pig serum with chelating agents (EDTA). The panels on the left represent the change in abundance between the human, mouse, and pig serum and serum supplemented with EDTA. On the right, panels indicate the absolute value when normalized against EDTA. The iBAQ score on the left of the graph corresponds to the sum of all the peptides intensities divided by the number of observable peptides of a protein. The peptides listed are in descending abundance corresponding to serum with SiO_2-NPs without EDTA after the elimination of proteins with peptide number <4 and elimination of contaminants (keratins, dermicidins, and hornerin).

These results obtained from Western blots against C3a, an indicator of C3 activation and therefore complement activation, support the hypothesis that in human serum, PMOXA-coated and PEtOXA-coated ORMOSIL nanoparticles greatly activate complement via opsonization of complement system proteins. In MS, there was no C3 activation, suggesting that the addition of nanoparticles does not activate the complement system (Figure 35).

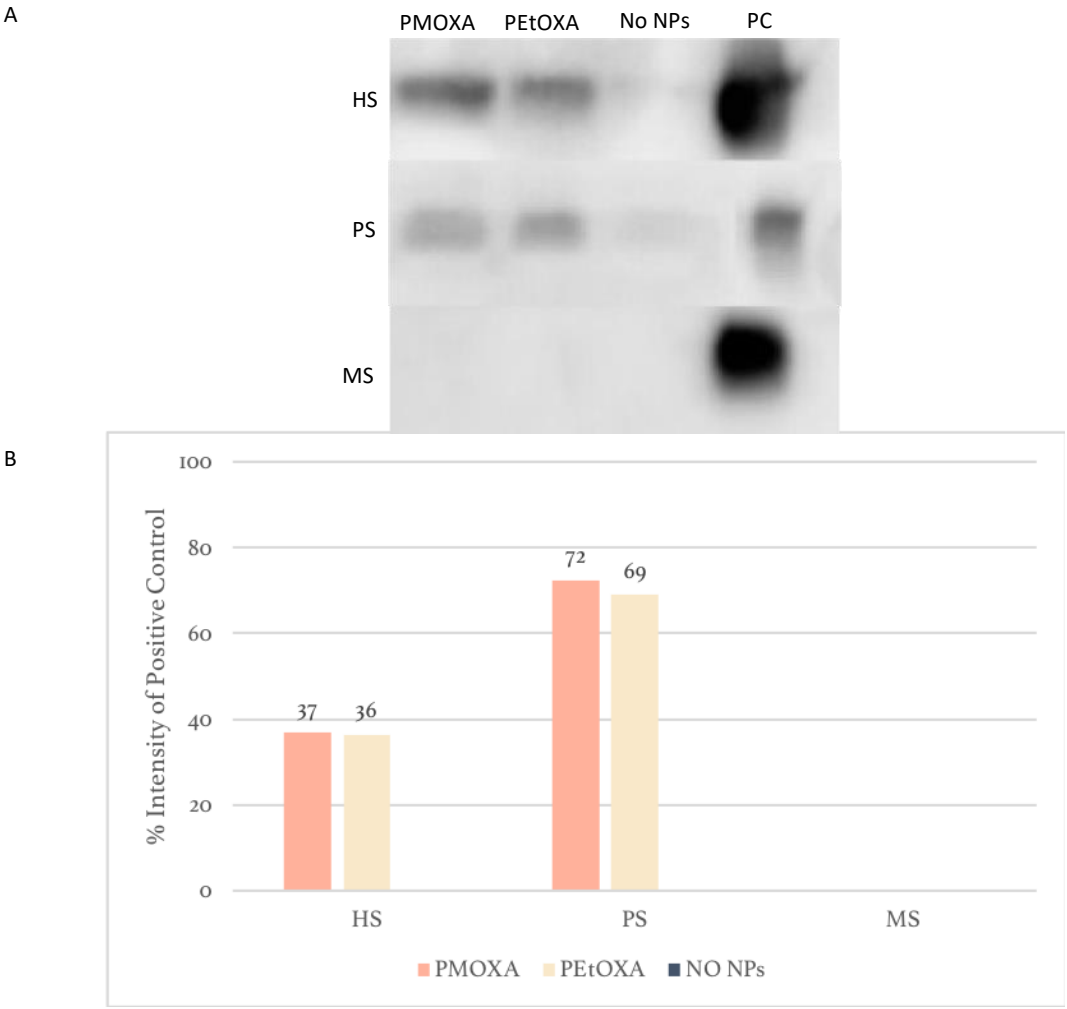

Figure 35: Western Blot analysis of complement activation via C3 cleavage into C3a (9kDa) by PMOXA and PEtOXA coated SiO_2-NPs. (A) 800 ug/mL of SiO_2-NPs were incubated for 20 minutes at 37 °C in 70% HS, MS, or PS. Equal samples volumes of either supernatants and washed pellets were analyzed by SDS-PAGE (12%). After transfer to 0.45 µm nitrocellulose the blotted bands were immunodetected with a specific rabbit anti-human C3a Mab and subsequently visualized with peroxidase labeled goat anti-rabbit IgG antibodies. (B) A semi-quantitative estimation of the amount of the indicated proteins associated with NPs were obtained by densitometry of the corresponding SDS-PAGE bands. Data were normalized against the positive control (PC) where the percentage of the PC was plotted.

It is well known that C1q and C2 mouse complement proteins involved in the classical pathway can malfunction and improper storage and handling of serum can cause protein degradation and complement deactivation. For that reason, in order to control complement activity, sera were treated with Zymosan to be used as a positive control since it is a well-known activator of the complement system. Therefore, we can conclude the sera used in these studies are in fact functional with an intact complement system and thus the results produced represent an actual difference between mouse and human complement activation. In addition, as the C3a antibody is polyclonal, we can exclude recognition issues and can reason the lack of C3a is due to no C3 cleavage indicating a lack of opsonization of PMOXA-coated and PEtOXA-coated NPs in MS with complement proteins. This is in congruence with confocal microscopy data performed with the same batches of sera in the Western Blot experiments, where there was no phagocytic cellular uptake by macrophages in mouse serum supporting the absence of immune activation.

Similarly to human serum, pig serum showed an increase in C3a, which is in line with the confocal microscopy and flow cytometry data, which quantifies NP-cell association, demonstrating how PMOXA-coated and PEtOXA-coated NPs activates cellular uptake, at times even higher than in human serum. This observation can be explained by complement activation via either of the three pathways or partially by a pathway independent of C3. This can transpire where complement is activated by an additional bypass pathway that acts independently of C3 such as activation by thrombin which acts as a C5 convertase to generate C5a and mediate pathology, bypassing C3 convertase, or by Fcɣ receptors (FcɣRs) which recognize immunoglobulin G (IgG) thus releasing either activating or inhibitory intracellular signals via the interaction of the Fc portion of antibody molecules. In fact, mass spectrometry data (Table 2) of PEtOXA-coated NPs with PS showing a presence of prothrombin, the

precursor to thrombin, suggests complement activation by pig serum could be a combination of both a C3 and C3a independent pathway activation.

We further looked into the abundance of C3 in all three species compared to samples with EDTA. Figure 34 demonstrates the amount of C3 present in the protein corona upon nanoparticle incubation with serum. It is apparent that C3 is much more prolific in PMOXA-coated and PEtOXA-coated NPs in both human and pig serum, yet for mouse serum, there is a high, uniform decrease in C3 content. Therefore, complement is not activated by MS in either particles, and PMOXA-coated and PEtOXA-coated NPs in PS activates complement which is supported by other analytical methods but does not always go through C3 complement mediated activation.

Activation of the lectin complement pathway by SiO_2-NPs

Given the proteomic findings concerning the involvement of ficolins in nanoparticle recognition in pig serum, we wanted to probe ficolin further to determine the possible underlying mechanism. It is known the acid-amide side chain arrangement is essential for the specificity of sugar binding of membrane C-type lectin receptors (CLRs). Mannose recognizes glutamic acid-asparagine residues whereas galactose recognizes glutamine-aspartic acid residues, indicating in a mannose-binding lectin activation, galactose does not compete and therefore will not affect the activation of the lectin pathway. Given this, galactose was proposed as an internal control to probe activation of the lectin complement pathway. Furthermore, given CLRs recognize their ligands by a carbohydrate-recognition domain (CRD) via binding to mannose and/or N- Acetylglucosamine among others discussed previously, we decided to use mannose and N- Acetylglucosamine sugars to compete with MBLs in lectin pathway activation mediated by ficolin. In order to further probe the role of the lectin pathway of complement activation by the nanoparticles' surface to prevent uptake by primary human macrophages, we performed competition assays with 25 mM or 50 mM sugar inhibitors incubated with particles and pig serum. We also compared human serum as well which was found not to contain ficolin like pig serum did, therefore human would be used as a further control (Figure 38). In fact, data from the competition assay seems to support the major role of ficolins in the lectin pathway of complement activation by PMOXA-coated and PEtOXA-coated NPs. In the case of PMOXA-coated NPs (Figure 37C), 25 mM mannose reduced ficolin binding by 26.5% and 25 mM N- Acetylglucosamine reduced ficolin binding by 17%. However, the biggest effect was seen using 50 mM N-Acetylglucosamine as it marginally reduced ficolin deposition (Figure 37C) by 65.5%. Ficolin was not deposited on uncoated SiO_2-NPs (Figure 37A) and showed no inhibition by any of the monosaccharides. PEGylated NPs had almost no ficolin deposition too (Figure

37B) as well as having no inhibition by monosaccharides. PEtOXA-coated nanoparticles also showed no sensitivity to monosaccharides inhibitors with 25 mM mannose and 50 mM N-Acetylglucosamine marginally reduced ficolin deposition (Figure 37D). Therefore, 25 mM sugars had no effect on NP binding and only 50 mM N-Acetylglucosamine showed marginal effects with PMOXA-coated NPs. Furthermore, gels (Figure 38) with human serum showed no ficolin binding and no reduction upon sugar supplementation thereby confirming previous results. As the sugars were only introduced to the cells for a 3 hr incubation, the cells' phagocytic activity was not impaired with high sugar concentrations as it was found to be if cells were cultured in high sugar environments.[131] These results support the idea that ficolin and therefore the lectin pathway is involved in complement activation.

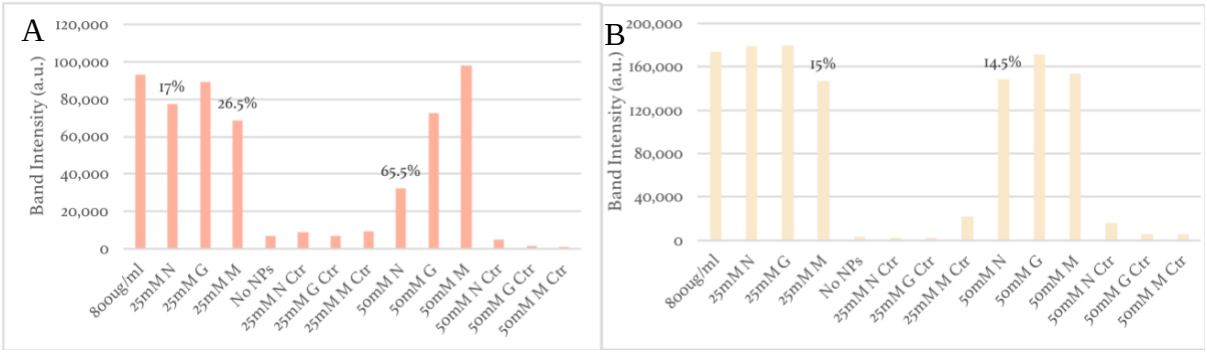

Figure 36: Densitometric analysis to examine the corona protein levels absorbed onto (A) PMOXA and (B) PEtOXA ORMOSIL SiO_2-NPs. Following silver staining, a semi-quantitative estimation of the relative amount of the ficolin bands found, were determined by densitometry.

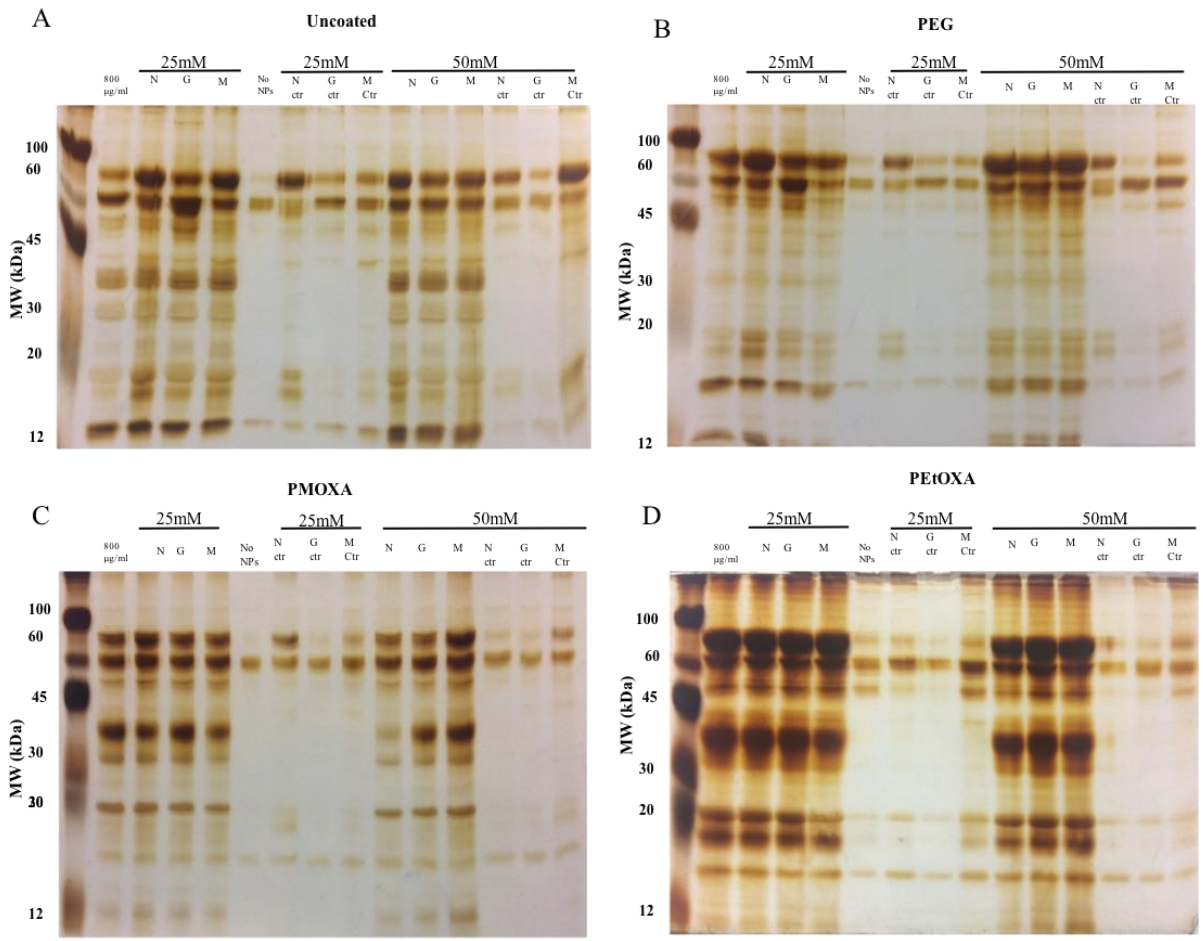

Figure 37: SDS-PAGE analysis of monosaccharide inhibition of the complement lectin pathway activation by SiO_2-NPs. 25 mM or 50 mM sugar inhibitors N-Acetylglucosamine, Mannose, or Galactose were incubated with 800 µg/mL of (A) Uncoated (B) PEG (C) PMOXA (D) PEtOXA SiO_2-NPs were incubated for 20 minutes at 37 °C in 70% PS, washed and analyzed by SDS-PAGE (12%). Equal sample volumes were loaded onto an SDS-PAGE and stained by silver nitrate. On the left-hand side of each image, the values indicate the MW in kDa of the molecular weight standard polypeptides used in the gel.

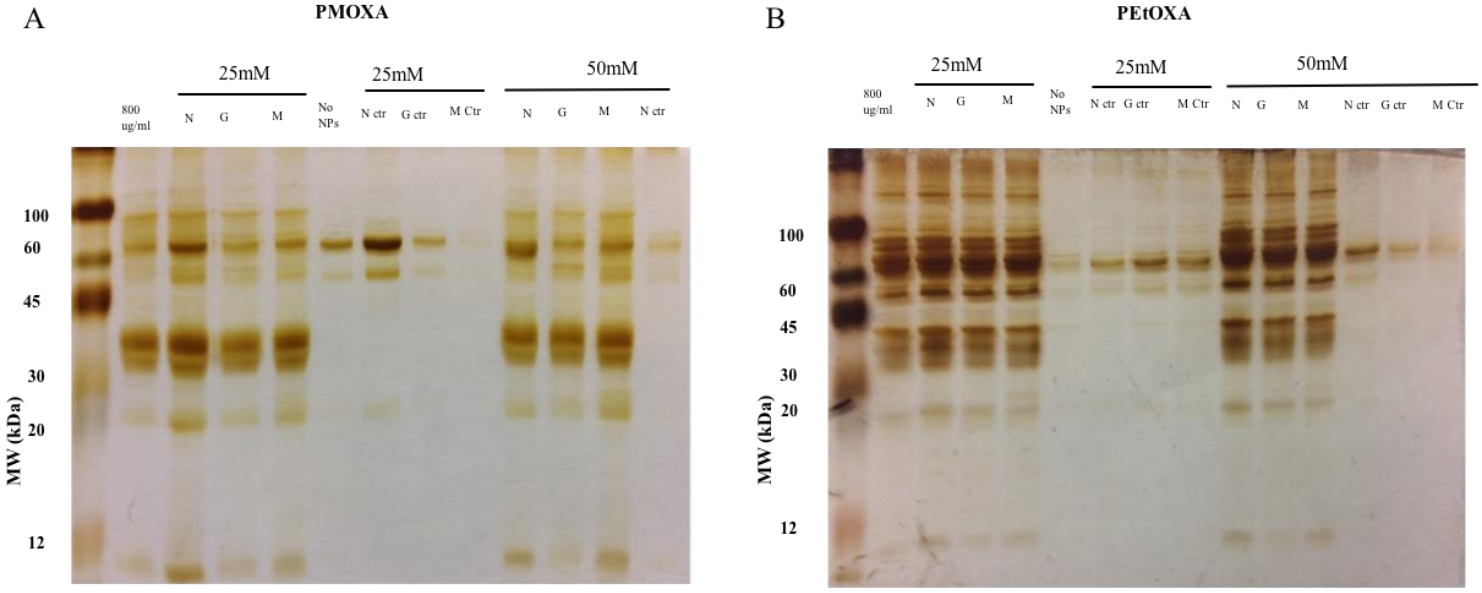

Figure 38: SDS-PAGE analysis of the pattern of HS proteins adsorbed on SiO_2-NPs in the presence of sugar inhibitors. 25 mM or 50 mM sugar inhibitors N-Acetylglucosamine, Mannose, or Galactose were incubated with 800 µg/mL of (A) PMOXA or (B) PEtOXA for 20 minutes at 37 °C in 70% HS, washed and analyzed by SDS-PAGE (12%). Equal sample volumes were loaded onto an SDS-PAGE and stained by silver nitrate. On the left-hand side of each image, the values indicate the MW in kDa of the molecular weight standard polypeptides used in the gel.

We also performed confocal microscopy (Figure 39) with human macrophages incubated for 3 hours at 37 °C in pig serum (PS), in the presence of 800 ug/mL nanoparticles diluted 10X in culture medium either supplemented with 25 mM sugar inhibitors or without (mock control sample), and then inspected. Figure 39A illustrates uncoated nanoparticle's evident low cytoplasmic signal which supports previous confocal experiments (Figure 17 and Figure 19). However, with the addition of 25 mM sugar inhibitors, neither N- Acetylglucosamine nor mannose reduced the fluorescent signal of uncoated nanoparticles, being equal to that of the internal control of galactose and of uncoated in un-supplemented PS conditions. PEGylated nanoparticles demonstrated an increase in cell capture in un-supplemented PS conditions compared to uncoated, but similarly there was no effect with the addition of sugars (Figure 39B). However, conversely PMOXA--coated NPs (Figure 39C) displayed similar cytoplasmic signal as uncoated NPs, which is in contrast to previous findings. Furthermore, there was no effect with the addition of 25 mM sugars. PEtOXA-coated NPs, which demonstrated high ficolin binding by SDS-PAGE analysis of the protein corona composition in PS, now showed reduced fluorescence with 25 mM N-Acetylglucosamine condition in contrast to the internal control of galactose and PEtOXA-coated NPs in normal PS (Figure 39D). The fact 25mM sugar inhibitors were used and were seen to be ineffective at competing with ficolin binding, can indicate a higher concentration of sugars are required to see an affect as in SDS PAGE. However, cells were not viable with 50 mM sugars due to undesirable osmotic changes. Therefore, any cellular experiments such as functional studies with cells or confocal were unfeasible as they required a low sugar concentration which was below the threshold to see an effect.

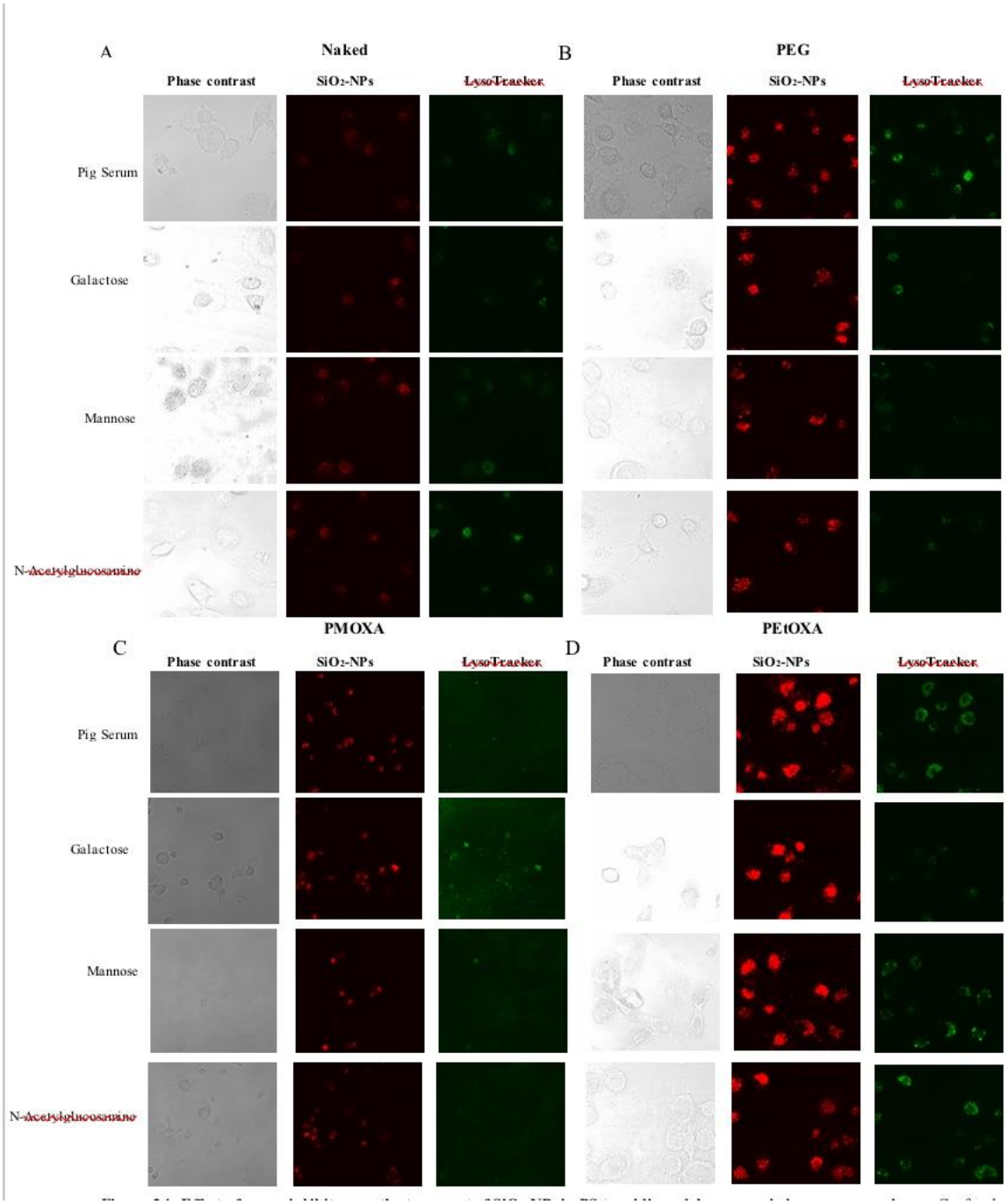

Figure 39: Effect of sugar inhibitors on the transport of SiO_2-NPs in PS to acidic endolysosomes in human macrophages. Confocal images of human macrophages treated at 37 °C for 3 hr with 80 µg/ml (A) Uncoated (B) PEG (C) PMOXA (D) PEtOXA SiO_2-NPs in RPMI medium with 25 mM sugars N-Acetylglucosamine, Mannose, or Galactose were incubated (indicated to the left of the boxes), stained with LysoTracker green.

Flow cytometry was performed with primary human monocytes isolated from healthy blood donors and macrophages differentiated from monocytes in order to probe the impact of serum from multiple species on coated nanoparticle cellular association with serum proteins. Given the presence of ficolin was only observed in PMOXA-coated and PEtOXA-coated NPs from the inhibition assay, we decided to specifically look at the association between these polymers and lectin complement activation with human phagocytes. In congruence with the inhibition assay and confocal images, 25 mM N-Acetylglucosamine supplemented PS was seen to be only slightly effective at preventing cellular uptake of PMOXA-coated and PEtOXA-coated NPs (Figure 40), where the effect is marginal and not significant. Until this point, 25 mM sugars were tested which was also used to probe the corona composition as well as Ficolin in pig serum. Effective protocols to study the effect of sugars with cells should be designed in order to probe the effect of higher sugar concentrations on competition with ficolin with particle phagocytosis. For example, particles can be incubated with sugars to form the corona with ficolin binding competition, however cells do not need to be supplemented with sugars as the inhibition of ficolin will have already occurred in the initial incubation. Therefore, high concentrations of sugars can be used without affecting cell viability.

Figure 40: The effect of sugar inhibitors on SiO_2-NPs cellular association with serum proteins from multiple species in human monocyte and macrophage cells. Following a 20 min incubation at 37 °C in 70% serum and 25 mM sugars N-Acetylglucosamine, Mannose, or galactose with 80 µg/ml SiO_2-NPs were incubated for 3 hours at 37 °C with human monocyte and macrophage cells. The cells were subsequently analyzed by flow cytofluorimetry to measure nanoparticle-associated fluorescence. Data are mean ± standard error of the mean (n = 3). Values above the bars indicate cell association expressed as the mean Fluorescence Intensity.

Due to the fact that 25 mM sugars showed no influence on ficolin binding and 50 mM showed limited effect, we decided to probe ficolin binding using 100 mM sugar inhibitors against PMOXA-coated NPs as they showed to have the greatest sensitivity to ficolins. SDS-PAGE analysis accompanied by Western Blot against ficolin revealed an intense reduction in ficolin by 54% via Silver staining analysis and 60% using Western Blotting when 100 mM of N-Acetylglucosamine was incubated in pig serum with PMOXA-coated NPs (Figure 41 and Figure 42). On one hand, it appears ficolin has a stronger binding specificity towards PEtOXA-coated NPs rather than PMOXA-coated NPs, therefore there would be less

competition from the sugars. On the other hand, ficolin binding might occur through another binding site which does not favor N-Acetylglucosamine and therefore no competition would arise either, or the interaction between PEtOXA-coated NPs with ficolin is non-specific. Therefore, we wanted to know if ficolin binding is actually involved in complement activation.

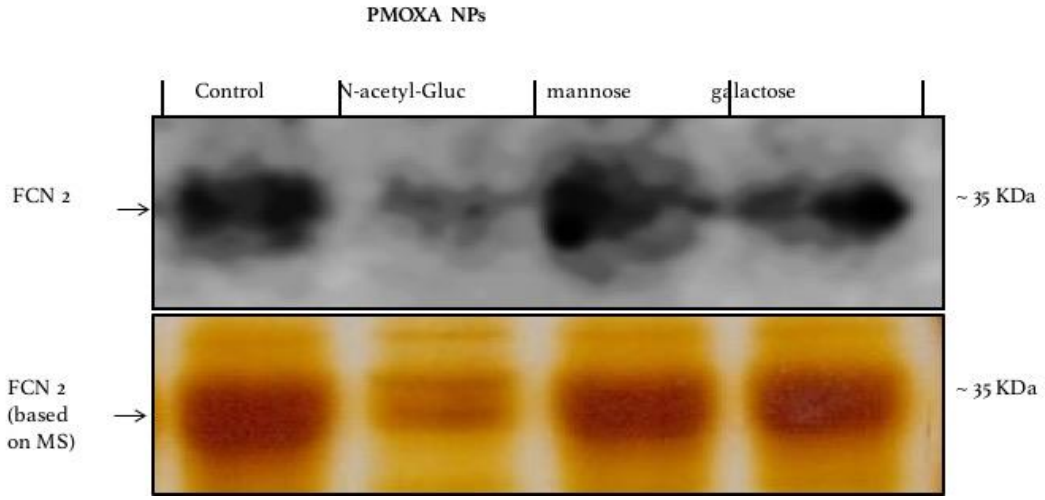

Figure 41: SDS-PAGE analysis of the pattern of PS proteins adsorbed on PMOXA SiO_2-NPs in the presence of 100 mM sugar inhibitors. 100 mM sugar inhibitors N-Acetylglucosamine, Mannose, or Galactose were incubated with 800 µg/mL of PMOXA for 20 minutes at 37 °C in 70% PS, washed and analyzed by SDS-PAGE (12%). Equal sample volumes were loaded onto an SDS-PAGE and stained by silver nitrate (Below). Western Blot analysis was performed against ficolin 2 (Above). After transfer to 0.45 µm nitrocellulose the blotted bands were immunodetected with a specific Rabbit anti-human Ficolin 2 Mab and subsequently visualized with peroxidase labeled goat anti-rabbit IgG antibodies.

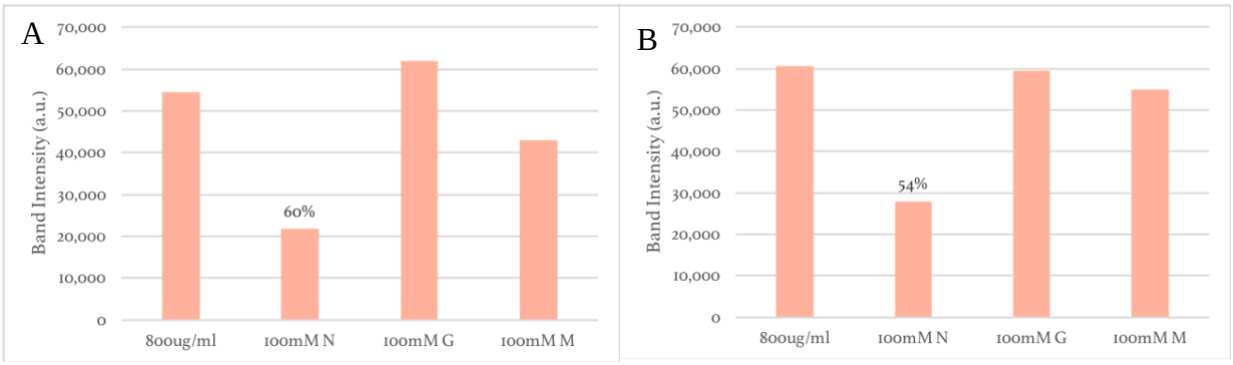

Figure 42: Densitometric analysis to examine the corona ficolin levels absorbed onto PMOXA-coated ORMOSIL SiO_2-NPs analyzed by (A) WB and (B) silver staining. Following silver staining, a semi-quantitative estimation of the relative amount of the ficolin bands found, were determined by densitometry.

In order to discern the effect of ficolin binding on C3 activation, we performed a series of SDS-PAGE analyses both in the presence of 100 mM N-Acetylglucosamine as well as in 0 °C and 37 °C with PMOXA-coated and PEtOXA-coated NPs (Figure 43). It is known that protein binding kinetics, protein interactions, and binding potentials are all greatly temperature dependent as well as enzymatic activity which will influence C3 cleavage and subsequent activation thus the reason for temperature comparison in this experiment. For both nanoparticles, there is a lack of C3b as well as a reduction in ficolin at 0 °C. Ficolin binding is inhibited by 100 mM N-Acetylglucosamine at 37 °C with PMOXA-coated NPs but not PEtOXA-coated NPs. However, complement activation via C3b presence is not inhibited for both PMOXA-coated and PEtOXA-coated NPs thereby indicating that although there is such a huge presence of ficolin in PS for both coated particles, ficolin does not play a role in complement activation and subsequent particle clearance via phagocytosis.

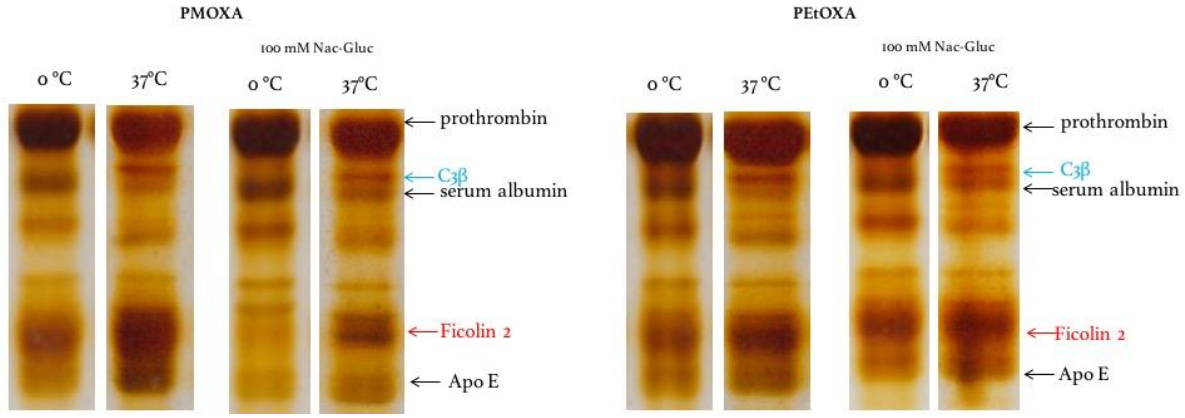

Figure 43: SDS-PAGE analysis of the pattern of PS proteins adsorbed on PMOXA-coated and PEtOXA-coated SiO_2-NPs in the presence of 100 mM sugar inhibitors and different temperatures. 100 mM sugar inhibitors N-Acetylglucosamine, Mannose, or Galactose were incubated with 800 μg/mL of PMOXA -coated or PEtOXA- coated NPs for 20 minutes at either 0 °C or 37 °C in 70% PS, washed and analyzed by SDS-PAGE (12%). Equal sample volumes were loaded onto an SDS-PAGE and stained by silver nitrate

Subsequently, we asked ourselves given that ficolin is in fact binding to our particles, given that N-Acetylglucosamine is able to compete with ficolin binding, and finally given that this binding has no effect on C3 activation, can we determine which binding site ficolin is using to bind the nanoparticles and can we determine a substrate that would compete with ficolin binding and disrupt C3. Furthermore, could ficolin enhance phagocyte capture of PMOXA/PEtOXA-coated NPs via complement opsonization, as it is the case for bacteria clearance? To answer these questions, we decided on using the competitor sucrose octasulfate (SOS), given that SOS can bind heparin similarly to ficolins, which are able to bind acetylated ligands, demonstrated by the carbohydrate N-Acetylglucosamine, but they are also capable of binding DNA, ligands shared with mouse ficolin-B, and with immobilized heparin, a highly sulfated molecule as well. Furthermore, it has been found SOS competes with ficolin binding, therefore we hypothesized SOS could compete with ficolin for binding to our coated particles.[132] It has also been shown that SOS competes less efficiently for ficolin 2 binding to acetylated BSA than to heparin which indicates that acetylated ligands are displaced less easily.[133] Therefore, we hypothesized that SOS and N-Acetylglucosamine might be binding ficolin in different binding sites. Using SOS as a binding competitor at varying concentrations, we probed its efficiency at preventing ficolin binding to PMOXA-coated and PEtOXA-coated NPs. Interestingly, SDS-PAGE analysis revealed that SOS does not decrease ficolin binding (Figure 44) at either 3 concentration titrations of SOS. However, surprisingly, C3b was reduced with 20 mM SOS incubated with PMOXA-coated NPs and as low as 5 mM with PEtOXA-coated NPs. Given that there are 4 binding sites on ficolin, S1-4 where it was identified that S3 binds sulfate and phosphate groups, and S1 was found to bind acetyl groups, we can conclude from our results that N- Acetylglucosamine is favored to bind at S1, and SOS, which is sulfated, preferably binds S3. Therefore, this indicates that our NPs bind to ficolin via S1 and therefore SOS, which binds at S3, would not affect binding.

However, the fact that C3b is reduced upon SOS introductions indicates that SOS-bound ficolin reduces complement, indicating the binding site S3 is potentially involved in nanoparticle recognition and immune responses. Possible other binding sites might play a role in complement activation as well as other protein-protein interactions that can arise upon changing polymers' surfaces. Although we cannot speculate for sure which mode of action ficolin is involved in complement activation, we can conclude binding to particles does not occur via the S1 binding site and that ficolin binding through this site does not affect complement activation. Furthermore, binding is particle specific where even slight variations in polymer chains contribute to significant alterations in biological function. It has been well documented that nanoparticle surface camouflaging with polymers such as PEG or polyoxazolines can provide stealthing effects to impede macrophage recognition, thus increasing the particle's longevity in the blood. However, studies have also shown that these polymers may catalyze complement depending on surface polymer configuration. Therefore, altering the polymer's architecture on the particle's surface from a flat to mushroom- brush configuration, was seen to switch complement from the classical, C1q-dependent pathway to a lectin pathway in human serum.[134] Binding sites are dependent on the particle's repetitive recognition patterns on the surface which can be altered by changes in surface density, possibly creating new binding sites which may affect complement activation. Previously, it was shown that PEG chains share structural similarities with d-mannose/ N-Acetylglucosamine in the terminal regions, thus indicating when in mushroom-brush configuration, PEG is able to form dynamic "pathogen-mimicking" clusters which allows for lectin pathway activation via MBL, ficolin, or CL11 docking. Yet, not only was it shown that the surface of the particle dictates which complement pathway is activated, it was also shown that lectin pathway activation can be modified through binding of different lectin pathway initiating molecules such as favoring MBL over Ficolin 2 or visa versa.[135] In addition, it was

also shown that although ficolin 3 does not recognize substrates *in vivo*, it is the most abundant ficolin in human serum and the most potent activator of the lectin pathway *in vitro*.[40] Therefore, not only is the surface of the particle important at dictating lectin activation but also the initiating molecules themselves play an important role in determining complement initiation. For these reasons, our results are in line with previous literature to the extent that ficolin binds preferentially to the surface of PEtOXA-coated NPs and to a lesser extent to PMOXA-coated NPs, where the different bindings can be attributed to variations in polymer chains. PMOXA-coated NPs are acylated proteins, similar to N-Acetylglucosamine, whereas PEtOXA-coated NPs are propanoyl proteins thus possibly binding alternative binding sites. However, our results diverge from previous literature where we found that although ficolin docking is inhibited in PMOXA-coated NPs, C3b is not, indicating complement activation is independent of ficolin binding. Perhaps this high level of ficolin is just an artifact of the serum itself as pig serum is found to have ficolin levels more than 10X higher than in humans or mice. This could explain the intense ficolin docking to our particles via weaker binding interactions, yet, does not affect C3 cleavage and complement activation. Furthermore, as ficolin is known to bind like C1q does, directly acting as an opsonin for apoptotic cells clearance, ficolin might also bind the coated particles in such a way, or perhaps direct binding of C1q is responsible for particle clearance in pig serum as with human serum or could complex with ficolin in order to mediate binding. Further experiments are required to fully investigate the role of ficolin in particle binding and capture however the importance of our results lies in the fact there are distinct differences between PMOXA-coated and PEtOXA-coated nanoparticle uptake as well as the way in which they interact and activate potential complement pathways. This distinction is not only physio-chemical specific to the polymer, but to also the species in which the polymer is tested in.

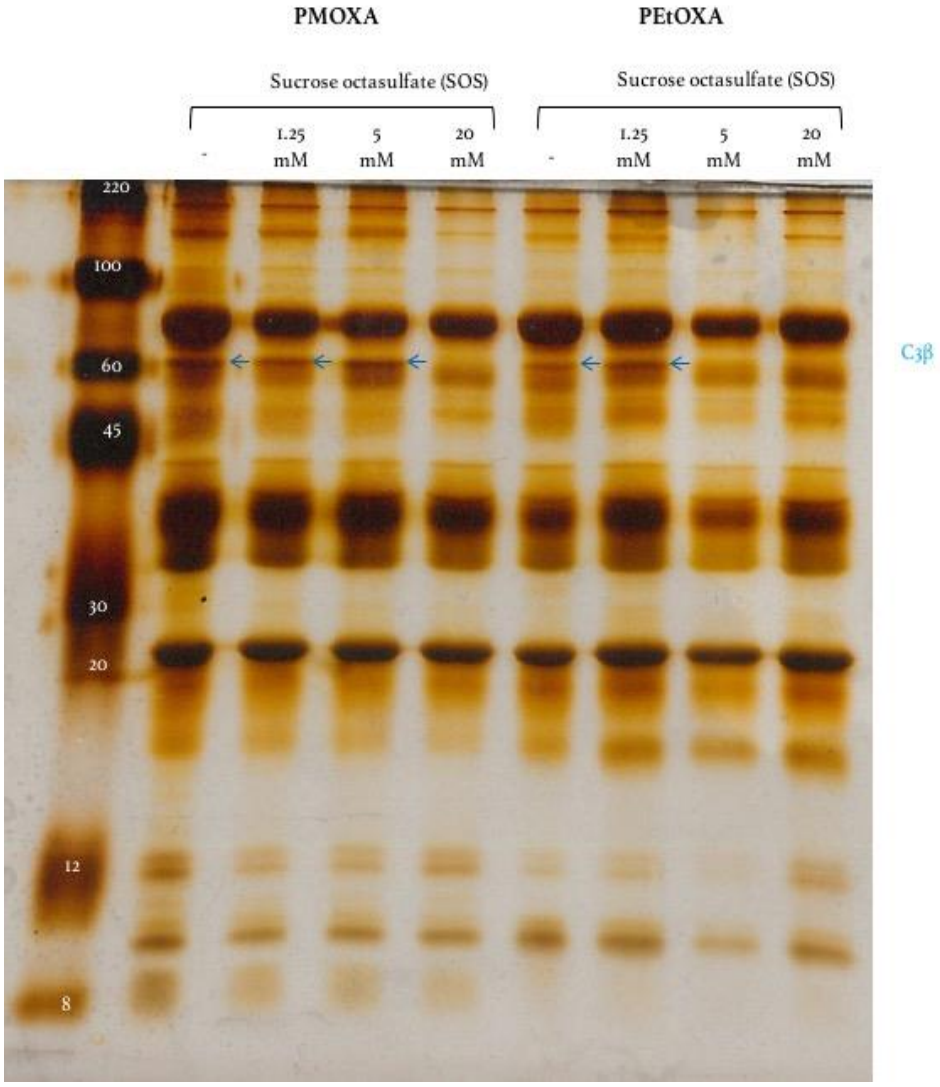

Figure 44: SDS-PAGE analysis of the pattern of PS proteins adsorbed on PMOXA-coated and PEtOXA-coated SiO_2-NPs in the presence of different concentrations of sucrose octasulfate (SOS) inhibitors. 1.5 mM, 5 mM, or 20 mM SOS inhibitors were incubated with 800 μg/mL of PMOXA-coated and PEtOXA-coated SiO_2-NPs for 20 minutes at 37 °C in 70% PS, washed and analyzed by SDS-PAGE (12%). Equal sample volumes were loaded onto an SDS-PAGE and stained by silver nitrate. Complement C3b is marked by blue arrows.

Conclusions:

Nanoparticles are undoubtedly an important tool, utilized in a wide variety of biomedical fields and theranostic nanomedicine from imaging and sensing to drug delivery. However, in order to optimize their efficacy, nanoparticle platforms must be designed in a way which limits cytotoxicity and optimizes biocompatibility for safe medical use. We have demonstrated coating ORMOSIL nanoparticles with PMOXA and PEtOXA polymers, which provides "stealthing" effects in murine conditions, effectively activates the complement system in human and pig environments. We have shown the extent of C3, C4b, C9, and properdin deposition on PEtOXA-coated NPs and to a lesser extent PMOXA-coated NPs in human serum, which correlates to the extent of phagocytosis by human macrophages. In addition, C3 deposition in pig serum with PMOXA-coated and PEtOXA-coated NPs along with functional studies, exhibit similar activation as in human conditions although mouse serum does not seem to activate complement given the lack of C3 activation supported by proteomic and functional studies. We suggest in order to probe the compatibility of the nanomaterial with the human immune system preclinically, it is highly beneficial to do so with human materials, instead of depending on non-human species such as murine models. Given that Poly(2-oxazoline) (POZ) has been proposed as an alternative polymer for PEG as they are easier to synthesize and can incorporate varying monomers to tailor the nanoparticle for specific applications, future perspective should focus on further modification of POZs in order to evade recognition by components of the human innate immune system.

Section 2: Gold

Physiochemical characterization of Au-NPs

Because of the versatility and physicochemical properties of gold nanoparticles, new opportunities for therapeutic treatments have been of increasing focus. At first, when the nanoparticles are introduced into circulatory system, the plasma proteins are the first to form the corona, dominated by albumin, the most abundant protein in serum (55%) along with apolipoproteins, fibrinogen, and immunoglobulins. However, similar to silica nanoparticles, when exposed to plasma or serum, unwanted side effects occur from protein interactions with the particle's corona triggering immunogenicity, cytotoxicity, platelet aggregation, or altering blood coagulation pathways.[97] Gold particles themselves can trigger coagulation as the van der Waals forces between two metal nanoparticles leads towards coagulation or they can trigger coagulation via interactions with plasma proteins based on their surface charge. For example, anionic surfaces initiate coagulation due to the fact that the intrinsic coagulation pathway is activated by anionic physiological surfaces, extracellular matrix, or aggregated platelets. Our initial characterization of four gold nanoparticles can be seen in Figure 45 where gold nanoparticles, roughly 10 nm in diameter, were conjugated with different thiols thus giving rise to four, separately charged particles: positive (cationic), negative (anionic), neutral, and zwitterionic. Nanoparticles were analyzed by NMR *in situ,* their core characterized by TEM analysis, and the organic monolayer was studied by thermogravimetric analysis (data not shown). In contrast with ORMOSIL particles where the surface characteristics remained similar except for the polymer, gold nanoparticles were designed so their chemical-physical features would be altered and therefore allow us to probe the effects of charge, thiol density…etc on our system.

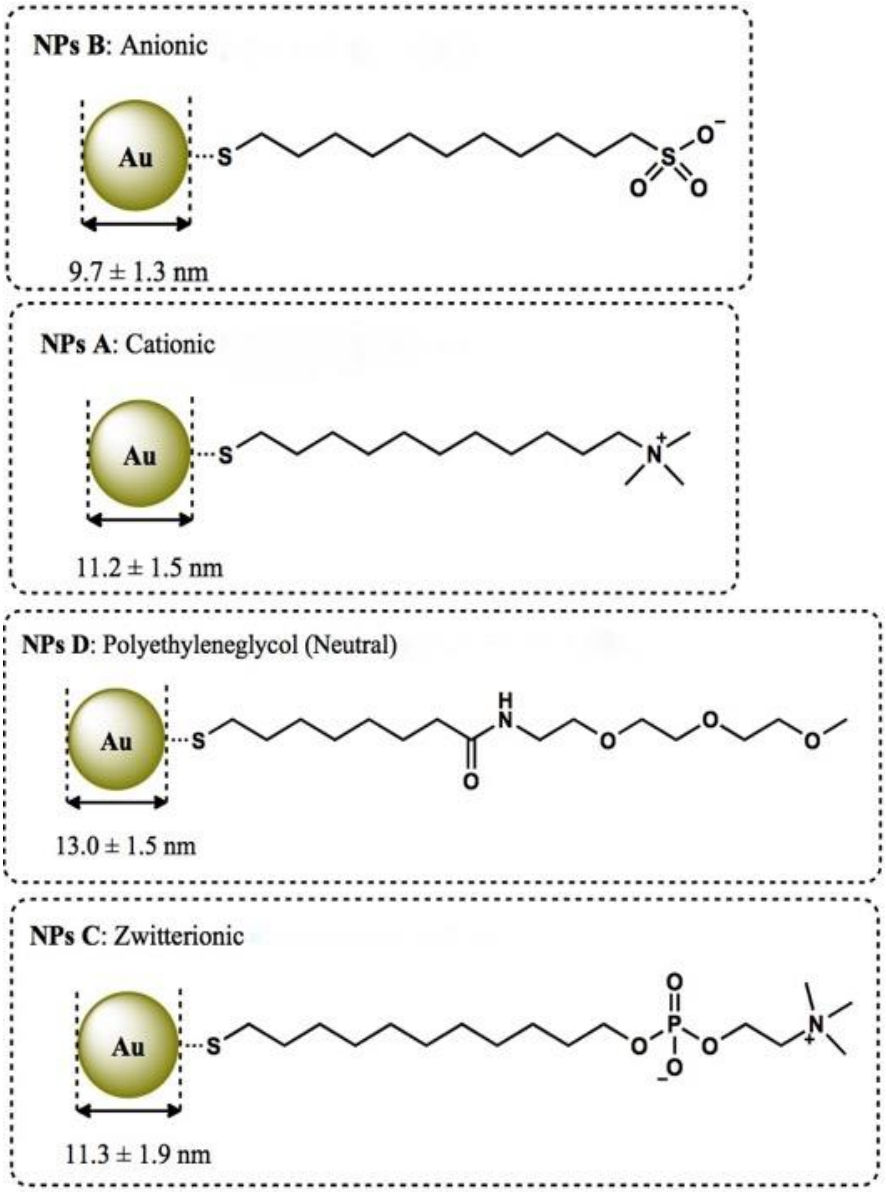

Figure 45: Chemical structures of the thiols constituting mixed-monolayer gold nanoparticles.

We have previously demonstrated the importance of corona composition on the ultimate fate of nanosystems as well as predicting the way in which the immune systems responds to particle administration. Furthermore, although the complement and the coagulation systems are two distinct protein networks, they both are involved in the first line of defense against pathogens and the inflammatory response as well as having a few points in the cascade which link these two pathways together. Therefore, we analyzed the protein corona formed on the

10 nm cationic, anionic, neutral, and zwitterionic nanoparticles incubated for 10 min at 37 °C in human plasma supplemented with 15 mM calcium chloride to activate the coagulation system in order to elucidate the protein differences in a pro-coagulant environment. Interestingly, to date, the coagulation cascade has never been probed previously using conditions which mimic those seen in the human system, for example, with full calcium, required for coagulation to occur as human plasma is supplemented with citrate or heparin in order to be obtained. Thus, although quite experimentally difficult as margins of error must be in the seconds, we decided to probe coagulation activation by the four gold nanoparticle in human plasma resembling the solution which the nanoparticle will first encounter upon administration in the human body.

Following NP recovery and thorough ultracentrifugation washings, gel electrophoresis under non-reducing conditions was performed, where the proteins were revealed by silver nitrate staining and further analyzed by MS spectrometry after in-gel digestions of major electrophoretic bands obtained in the SDS-PAGE. The major electrophoretic bands are quite distinct between the four gold particles as with SiO_2-NPs, however the amount of proteins are much reduced (Figure 46). This is likely because the gold nanoparticles are 10 times smaller in diameter and smaller NPs experience greater changes in hydrodynamic diameter with the formation of the protein corona as well as clot strength decreasing with particle size. Furthermore, it was demonstrated *in vitro* that neutrally charged particles have a much lower opsonization rate than charged particles and the kinetics of the corona formation depends greatly on physical-chemical properties of the particle, such as size and surface ligands.[136]

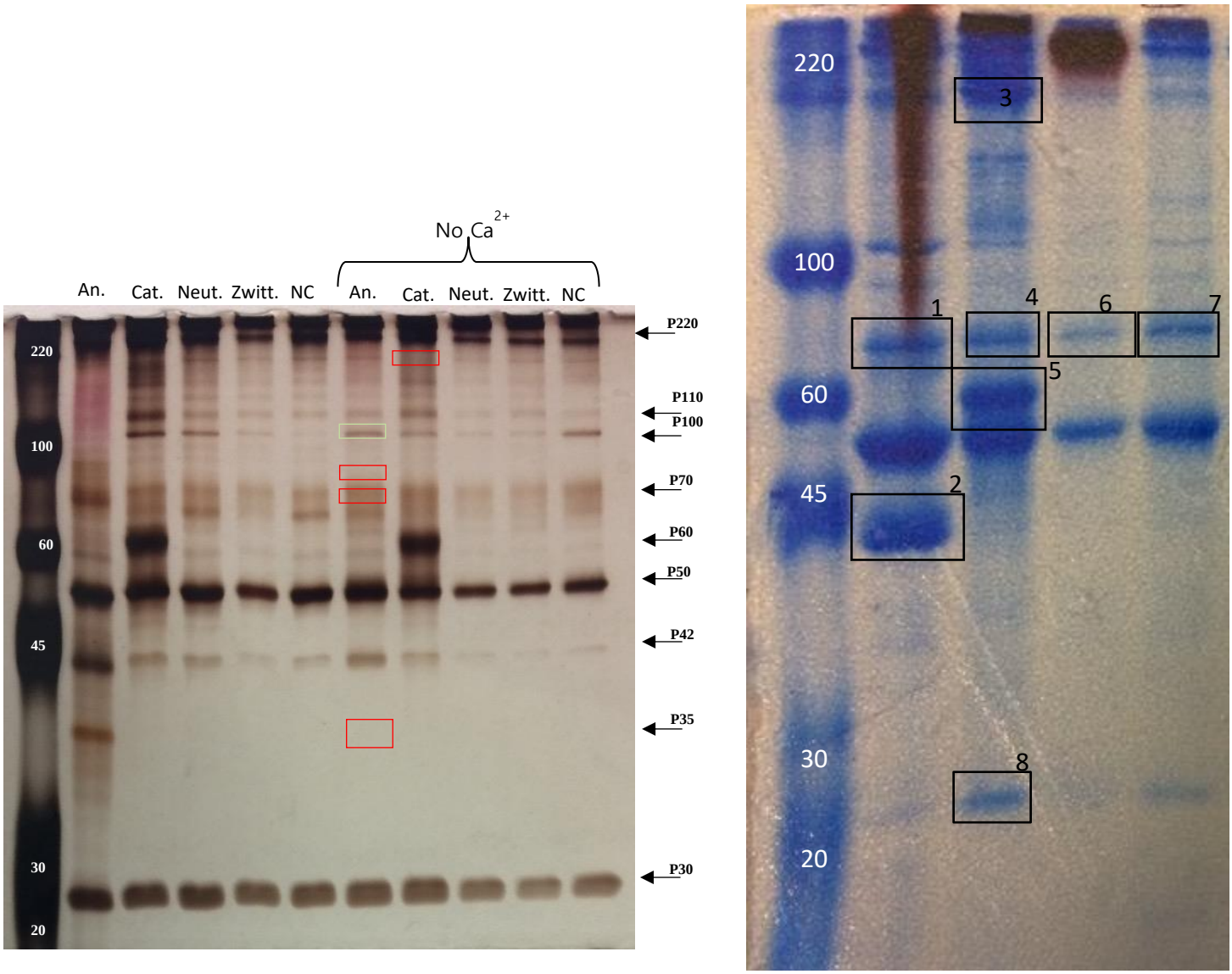

Figure 46: SDS-PAGE analysis of the pattern of proteins adsorbed onto anionic, cationic, neutral, and zwitterionic Au-NPs. 200 μg/mL gold nanoparticles were incubated for 10 minutes at 37 °C in 70% citrated human plasma supplemented with 15 mM $CaCl_2$, washed and analyzed by SDS-PAGE (12%) in reducing conditions. Equal sample volumes were loaded onto an SDS-PAGE and stained by (A) silver nitrate and (B) Coomassie to undergo in gel digestion for LC MS/MS. Red brackets indicate bands which disappeared in no Ca^{2+} conditions and green brackets indicate bands which appeared in no calcium conditions but were absent in full calcium plasma. The main protein bands found (arrows), are labeled by their rough apparent molecular weight in kDa (pxx).

Table 3: Serum proteins from different species bound to PEtOXA amorphous silica nanoparticle surface identified by tandem mass spectrometry analysis.

Band #	Protein	MW (kDa)
1	Prothrombin	68.7
2	Apolipoprotein H	38
3	C4b	190
4	Prothrombin	68.7
5	Hyaluronan-binding protein	62
6	Prothrombin	68.7
7	Prothrombin	68.7
8	Apolipoprotein A	28.3

The purple color which is smeared throughout the upper lane for anionic particles is due to high molecular weight complexes of aggregated particles which under normal circumstances would not leave the loading lane, but is forced to travel down its lane due to its negative charge, leaving parts of the complex behind as it does so. Normal gold nanoparticles are a deep red color but as they become more aggregated, they turn more purple/blue. The major electrophoretic bands common between all four particles are p220, p110, p100, p70, p50, p42, and p30. However, there are differences in intensities as seen for p42 which is more prominent for anionic nanoparticles than for the others. This is also the case for p110 and p100 which is more intense for cationic NPs. The bands at p35 for anionic and p60 for cationic are the two distinct bands which are unique to those particles. Furthermore, p35 disappears when calcium is absent, indicated by the red box, but as the band is not able to be stained using Coomassie, mass analysis was not able to be performed on this band. Although p60 is specific for cationic, it however is not calcium dependent and is present even when calcium is chelated. Interestingly, the band corresponding to p100 which is quite faint with anionic NPs, appears much more intense without calcium.

In order to determine the polypeptide composition of proteins bound to the particles and therefore specific interactions of specific coatings, we decided to perform semi-quantitative estimations by label-free methods after liquid chromatography-tandem mass spectrometry (LC-MS/MS) analysis (Table 3). The main corona components included the expected common circulating blood proteins, coagulation and complement factors, such as prothrombin, C4b, and Apo A. Proteins bound to anionic NPs which were detectable with Coomassie staining included Apo H (38 kDa) at p42 whereas p60 for cationic was identified as Hyaluronan-binding protein (62 kDa), which is also known as Factor VII Activating Protease (FSAP).

FSAP is a single chain zymogen which undergoes autoactivation to be converted to a two chain form connected by a disulfide bond and is proteolytically active, consisting of a 46 kDa heavy chain and a 29 kDa light chain. The heavy chain is further cleaved in the N-terminal section around 18 kDa. FSAP activates the coagulation Factor VII, thus instigating coagulation independently of tissue factor as well as being able to cleave fibrinogen and high-molecular-weight kininogen.[137] Given the specificity of FSAP to cationic particles, we decided to perform a dose dependent gel to determine the binding specificity of FSAP to the gold Au-NPs (Figure 47). In non-reducing conditions, as expected, there is only one band corresponding to FSAP single chain at 60 kDa visible only for concentrations above 200 ug/mL. However, in reducing conditions, first fragments corresponding to the heavy chain of FSAP can be seen at 45 kDa at 50 ug/mL as well as second and third fragments at 29 kDa and 18 kDa at 100 ug/mL and 25 ug/mL respectively. This indicates FSAP is activated in plasma containing cationic particles. We wanted to validate the SDS PAGE findings using western blot against FSAP which continued to support the fact in reducing conditions, FSAP is activated, however the fragments can only be seen at 50 ug/mL or higher (Figure 48).

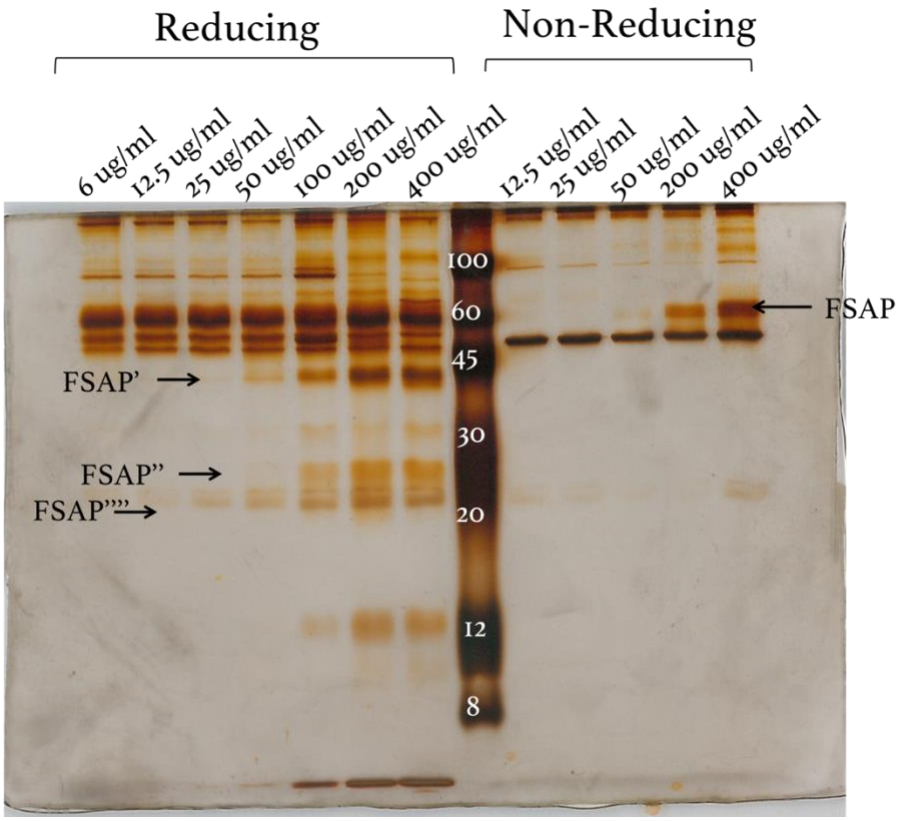

Figure 48: SDS-PAGE analysis of the pattern of FSAP proteins adsorbed on cationic Au-NPs. Cationic gold nanoparticles were incubated at the indicated concentrations for 15 minutes at 37 °C in 70% citrated human plasma supplemented with 15 mM $CaCl_2$, washed and analyzed by SDS-PAGE (12%) in reducing and non-reducing conditions. Equal sample volumes were loaded onto an SDS-PAGE and stained by silver nitrate.

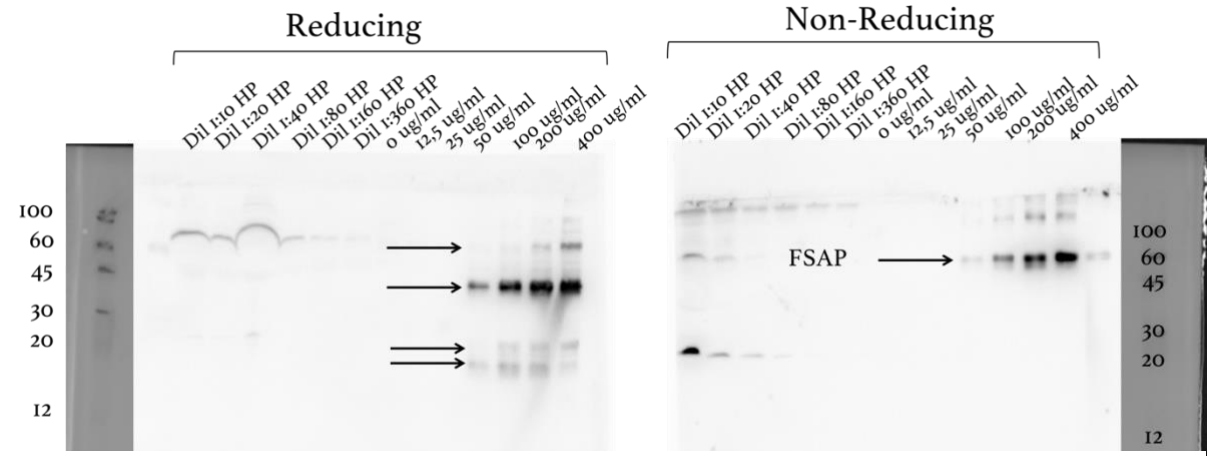

Figure 47: Western Blot analysis of FSAP activation by varying concentration of cationic Au-NPs. Different concentrations of Au-NPs were incubated for 10 minutes at 37 °C in 70%. Equal samples volumes of washed pellets were analyzed by SDS-PAGE (12%). After transfer to 0.45 µm nitrocellulose the blotted bands were immunodetected with a specific rabbit polyclonal anti FSAP Ab and subsequently visualized with peroxidase labeled goat anti-rabbit IgG antibodies.

Because coagulation is very much time dependent[138], we decided to characterize the protein corona formation in 70% human plasma supplemented with 15 mM calcium chloride incubated with 200 μg/mL cationic particles at varying time points. Comparing samples with particles in reducing and non-reducing conditions to control samples without particles incubated for the same time periods, we found even at time zero, FSAP is present as well as activated FSAP fragments, which are not present in non-reducing conditions (Figure 49 and Figure 50). This can be explained by autoactivation of FSAP which is promoted by endogenous Glycosaminoglycans (GAGs), such as heparin.[139] FSAP is also known to release nucleosomes from secondary necrotic cells via a plasmin-like protease which is induced by human plasma.[140] Nucleosomes are roughly 10 kDa in size where only histones and nucleosomes can activate FSAP in plasma. H1 and H3 are able to be degraded by FSAP. [141] Furthermore, as histones are highly positively charged where highly negative plasma proteins including heparin, pentraxin 3, C-reactive protein, and inter- α inhibitor protein are all able to bind to and neutralize them, we propose FSAP is binding to our 10 nm cationic particles mistaking them for nucleosomes. As we can see in Figure 49, Densitometric analysis of all activated fragments of FSAP deposition on the cationic Au-NPs shows that intensity of FSAP fragments increases with incubation time which is consistent with previous studies.

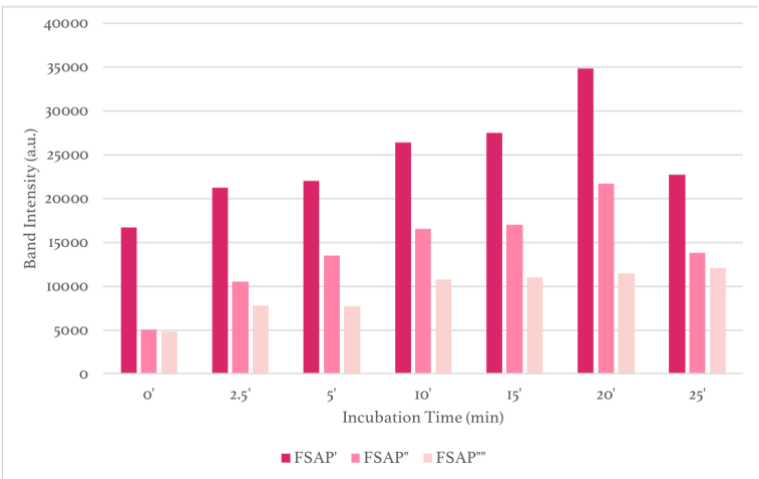

Figure 49: Densitometric quantification (arbitrary units) of SDS PAGE analysis of FSAP', FSAP", and FSAP"" binding to engineered NPs (200 μg/mL) on incubation with 15 mM calcium supplemented citrated human plasma. Following SDS PAGE, semi-quantitative estimation of the relative amount of the main FSAP protein bands found were determined by densitometry and represented in histograms.

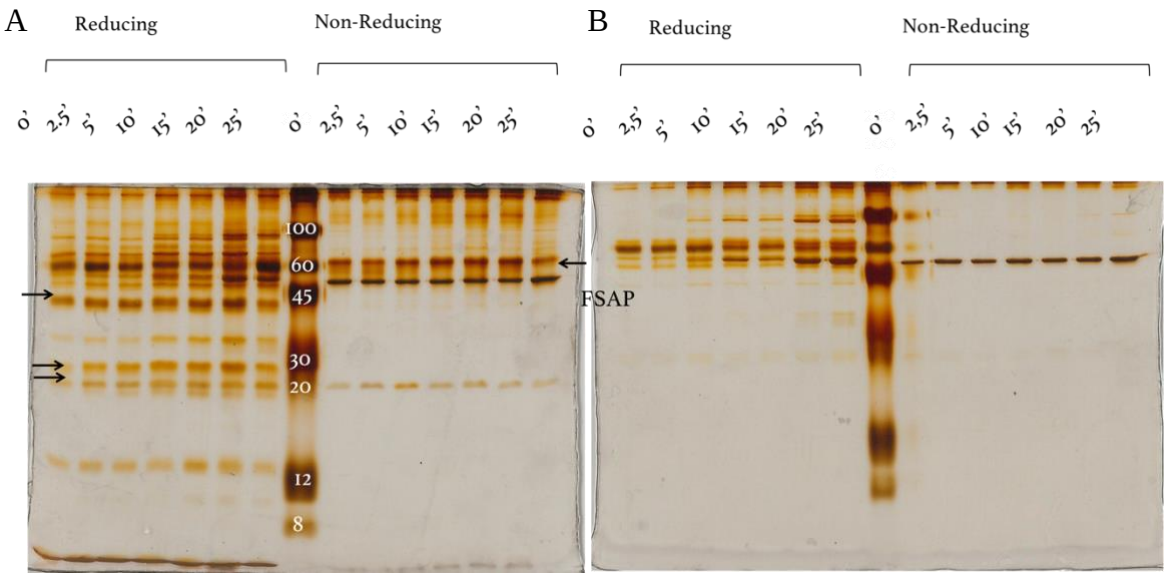

Figure 50: SDS-PAGE analysis of the pattern of FSAP proteins adsorbed on cationic Au-NPs. (A) Cationic Au-NPs (200 μg/mL) were incubated for the indicated amount of time at 37 °C in 70% HP, washed and analyzed by SDS-PAGE (12%). Equal sample volumes were loaded onto an SDS-PAGE and stained by silver nitrate. (B) Samples were compared to conditions without particles and represented our control groups.

Given these findings, we decided to probe the kinetics of coagulation in a concentration dependent manner. Figure 51A demonstrates a biphasic curve of coagulation activation by zwitterionic, neutral, and anionic particles where at the lower concentrations to 25 ug/mL activated coagulation, however at 25 ug/mL they became slightly less activating, and as the concentration increased above 50 ug/mL, the trend leveled off. Similarly, silica nanoparticles shown in Figure 51B, steadily activated coagulation as the concentration increased. Conversely, cationic Au-NPs showed a biphasic curve where at concentrations below 100 ug/mL, the particles enhanced coagulation whereas above 100 ug/mL the nanoparticles became inhibitory. Thus, despite the proposed activation role of FSAP in the coagulation cascade and according to some studies in the C cascade, FSAP-gold NPs complexes inhibited the clotting time of human isolated plasma and did not generate C3a after a short (max 15 min) incubation time.

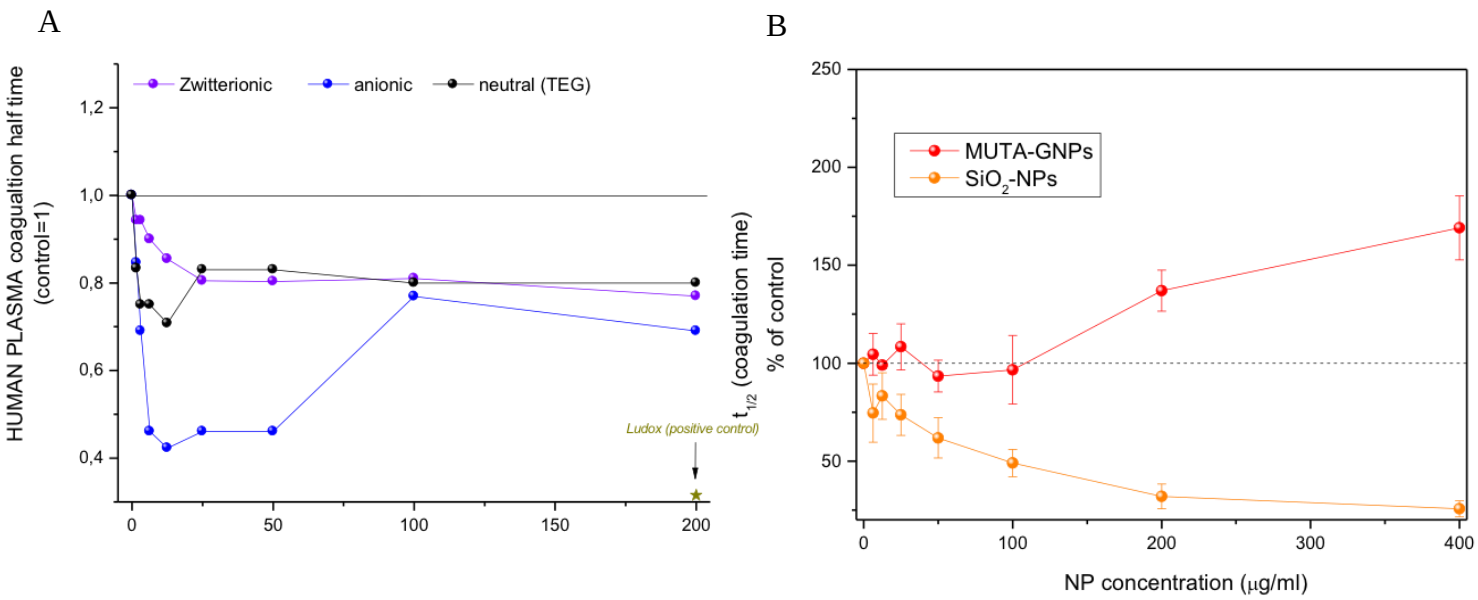

Figure 51: Coagulation kinetics of clot formation in citrated human plasma with 15 mM $CaCl_2$. Curves tracking changes in the clot formation via changes in optical density of A) Anionic, neutral, and zwitterionic Au-NPs and B) Cationic Au-NPs and SiO_2-NPs in relation so control samples (black line).

Conclusions:

In line with previous thinking, the surface charge of the particle is important for dictating the ultimate function of the particle. We have shown specific protein binding favoring one charge over another based solely on surface charge. Anionic appears to favor Apo H whereas cationic particles bind Apo A and FSAP. In addition, further probing the effect of FSAP and particle-protein binding, we have found FSAP and activated fragments of FSAP are in fact bound to the surface of the cationic particles when incubated in human plasma supplemented with calcium. The levels of FSAP increases with particle concentration as well as plasma incubation time. However, although FSAP is an activator of coagulation factor VII, FSAP-gold NPs complexes inhibited the clotting time of human isolated plasma. Because we looked at plasma supplemented with calcium, parameters which mimic those in the human body, we can understand more accurately the way in which particles activate the immune system when administered into the body. Similarly to ORMOSIL outcomes, gold nanoparticles must be tested in conditions which most closely represent those seen clinically or the particles could potentially have severely adverse reactions in patients.

Chapter 3: Methods

1. Nanoparticles synthesis and characterization

Solvents were purified by standard methods. All commercially available reagents and substrates were used as received. Silica nanoparticles are synthesized by base catalyzed polymerization of silicon alkoxides in an ethanol/water solution (the Stober protocol). PEGylated ORMOSIL nanoparticles are prepared by ammonia-catalyzed co-polymerization of vinyltriethoxysilane (VTES) following a modification of the Prasad procedure in an aqueous solution of co-micelles of a non-ionic surfactant and n-butanol. O-(2-aminoethyl)-O'-methylpolyethylene glycol (MPEG2000-amine, 150 mg, 0.075 mmol, 1 equiv) is dissolved in 1.5 mL of dry dichloromethane. Then 42 mg of K_2CO_3 (0.300 mmol, 4 equiv) and 98 µl of 2-(4-chlorosulfonylphenyl) ethyltrimethoxysilane (50% solution in dichloromethane, 0.15 mmol, 2 equiv) are added. Stirring occurs for 3 hr at 40 ℃, in a Schlenk tube under N_2 atmosphere. Following filtration and evaporation, the residue is dissolved in 1 mL of ethanol. 14 mL of cold tert-butyl methyl ether and centrifuged at 4 ℃ precipitates the product. Following repetition 3 times of purification, the precipitate is dried under vacuum (85%). PMOXA and PEtOXA coated ORMOSIL nanoparticles are prepared by N-(2-aminoethyl)-poly(2-methyloxazoline) (PMOXA3800-amine, 363 mg, 0.097 mmol, 1 equiv) and equivalent for PEtOXA is dissolved in 1.5 mL of dry dichloromethane. Then 54 mg of K_2CO_3 (0.388 mmol, 4 equiv) and 126 µl of 2-(4-chlorosulfonylphenyl) ethyltrimethoxysilane (50% solution in dichloromethane, 0.194 mmol, 2 equiv) are added. Stirring occurs for 3 hr at 40 ℃, in a Schlenk tube under N_2 atmosphere. Following filtration and evaporation, the residue is dissolved in 1 mL of ethanol. 14 mL of cold tert-butyl methyl ether and centrifuged at 4 ℃ precipitates the product. Following repetition 3 times of purification, the precipitate is dried under vacuum (80%). Ultrafiltration was used to filter

uncoated particles using a 50 mL Amicon Ultra 15 centrifugal filter, using a cellulose membrane with a cut-off of 100,000 Da. For purification of coated particles, centrifugation (12000 rpm, 10 min, 3 times) in 15 mL centrifuge tubes was used. Dynamic Light Scattering (DLS) and UV-Visible spectra and kinetic traces were used to confirm the formation of the nanoparticles, hydrodynamic particle size, and zeta potential on a Malvern Zetasizer Nano-S equipped with a HeNe laser (633 nm) and a Peltier thermostatic system for DLS, and with a Cary 50 spectrophotometer equipped with thermostated multiple cell holders for UV-vis. Measurements were performed at 25 °C in water or PBS buffer at pH 7.0. Transmission Electron Microscopy (TEM) was recorded on a Jeol 300PX instrument where a drop of sample was allowed to evaporate in a sample grid. NMR spectra were recorded using a Bruker AV III 500 spectrometer operating at 500 MHz for ^{1}H, 125.8 MHz for ^{13}C. Chemical shifts are reported relative to internal Me4Si. MALDI spectra were recorded with an AB SCIEX MALDI TOF/TOF, and α-Cyano-4-hydroxycinnamic acid (CHCA) was used as the matrix. Thermogravimetric analysis (TGA) was used to measure the stoichiometry to calculate the percent mass of the substance in the sample as well as the polymer footprint by running 100 µl of the nanoparticle solution, using a Q5000 IR model TA instrument from 30 to 1000 °C under a continuous air flow.

Rhodamine labeling of particles occurred following previous protocols.[142] Covalent bonding of the fluorophore to silica occurred via the functionalization of the rhodamines with a triethoxysilane group. Synthesis occurred by dissolving the following in 4.16 mL of mQ water, in a thermostated reaction vessel at 30 °C: 833 µl of Brij35P (30 mM, pH 2), 150 µl of n-butanol, rhodamine B-Si (10 mM in DMSO) and the appropriate amount of vinyl-triethoxysilane (VTES). For 30 min, stirring occurred and then 10 µl of aqueous ammonium hydroxide (15% solution) was added. Another stirring occurred for 2 hr at 30 °C, where the particles were pelleted and collected by centrifugation and washed with 3 x 5 mL of milliQ

water (12000 rpm, 10 min, 3 times). Conversely, uncoated particles were transferred to a 50 mL Amicon Ultra 15 centrifugal filter, followed by the addition of 10 mL of mQ water and centrifuged until reaching a final volume of 5 mL (2900 rpm, 10 min, 3 times). Final solutions are filtered using a 0.45 μm membrane filter and stored at 4 °C. Rhodamine concentrations were in the 0.1-0.3% w/w range determined from absorbance λ = 567 nm (after scattering contribution subtraction) using the molar extinction coefficient (ε) of 9.5×10^4 $cm^{-1}M^{-1}$.

2. Isolation and culture of cells.

2.1 Human Peripheral blood mononuclear cells (PBMC)

PBMC were isolated from buffy coats, obtained anonymously from healthy donors (Padova, Italy), by centrifugation over a Ficoll-Hypaque (Amersham Biosciences, UK) step gradient followed by a Percoll (Amersham Biosciences, UK) gradient and suspended in RPMI-1640 (Invitrogen, CA, USA) supplemented with 100 U/mL penicillin and 100 μg/mL streptomycin (Invitrogen, CA, USA). For human PMNs purification, after centrifugation of buffy coats through Ficoll-Hypaque gradient, red blood cells contained in the bottom fraction were eliminated by dextran sedimentation, followed by hypotonic lysis and washing with PBS. The percentage of contaminating cells were <5%. Unless otherwise specified, monocytes and PMNs were kept at 37 °C in a humidified atmosphere containing 5% (v/v) CO_2 in RPMI-1640 supplemented with antibiotic and 10% FCS (Euroclone, Italy, endotoxin <0.3 EU/mL). To differentiate macrophages, human monocytes were incubated for 7 days with 100 ng/mL of macrophage colony-stimulating factor (M-CSF, Peprotech, UK) in RPMI 1640 (Invitrogen, CA, USA) supplemented with 20% (v/v) fetal calf serum, FCS, (Euroclone, Italy, endotoxin < 0.3 EU/mL), and antibiotics (100 U/mL penicillin, and 100 μg/mL streptomycin).

2.2 Pig monocyte and macrophage cell isolation

Primary pig monocytes and macrophages were prepared following an established protocol.[143] Venous blood was taken from healthy pigs and immediately anticoagulated with 3.8% tri-sodium citrate (9:1 of blood: citrate) for a total of ~500 mL total blood collection. The Buffy coat was extracted by layering aliquoted blood onto PBS in 50 mL flacon tubes and centrifuged for 15 min at 1,200 g without brake. Buffy Coat was further diluted and layered (25 mL) over aliquots 15 mL lymphoprep while inclining the falcon tube as to not mix the blood. Centrifuge for 25 min at 1,200 x g with no brake and remove the mononuclear cell layer into a fresh 50 mL centrifuge tube. Add PBS and centrifuge 10 min at 600 x g with brake on in order to remove any remaining Ficoll and resuspend the pellet in PBS or RPMI. Centrifuge at 400 x g with brake on. Resuspend the pellet RPMI, count the cells in a haemocytometer where 1 to 2.10e6 PBMC can be obtained per mL of pig whole blood.

To differentiate macrophages, pig monocytes were prepared as with human monocytes where they were incubated for 7 days with 100 ng/mL of macrophage colony-stimulating factor (M-CSF, Peprotech, UK) in RPMI 1640 (Invitrogen, CA, USA) supplemented with 20% (v/v) fetal calf serum, FCS, (Euroclone, Italy, endotoxin < 0.3 EU/mL), and antibiotics (100 U/mL penicillin, and 100 μg/mL streptomycin).

2.3 Mouse macrophage cell isolation

Primary mouse macrophages were prepared and isolated from mice bone marrow. Mice were sacrificed and following dissection, the pelvic and femoral bones were collected and all the remaining tissue on the bones were removed. The ends of the bones were cut off, and bone marrow was expelled via washing with Iscove's modified Dulbecco's medium (IMDM, Thermo Fisher Scientific, MA, USA). Red blood cells were then lysed with ammonium-chloride-potassium lysis buffer (5 min, RT), leukocytes were recovered, and mononuclear

phagocytic precursor cells were propagated for 7 days with 10 ng/mL M-CSF (Miltenyi, Germany) in RPMI1640 with 10% FBS medium. One-half of the medium was replaced with fresh medium after 4 days. Adherent cells were detached by trypsin (0.5%) digestion.

The RAW 264.7 is a macrophage-like cell line derived from tumors induced in male BALB/c mice by the Abelson murine leukemia virus. Growth medium was warmed for 15 to 20 min in a 37° C water bath and the vial of RAW cells were thoroughly immersed in water bath until only partially frozen fraction remained. Cells were extracted with a pipette and into a 75 cm^2 flask. Cells were maintained at 37 °C, in a humidified atmosphere, with 5% CO_2. After the cells have adhered, approximately 6 hours, aspirate the old medium and add 15 mL of fresh medium. When the cells are 80% confluent, they were passed into a new vessel with fresh medium.

3. Serum preparation

3.1 Human

Venous blood was taken from healthy human volunteers (Padova, Italy) and collected into BD Vacutainer clot activator tube (Becton Dickinson, NJ, USA). Experiments with human sera were performed under local guidelines. Clotting was performed at room temperature, where blood samples were then centrifuged at 1,250g for 5 min to obtain sera. Collected sera were aliquoted, frozen in liquid nitrogen, and stored at -80 °C. Before use, all serum was thawed at 37 °C for 30 min.

3.2 Mouse

Whole blood from 12 adult, healthy male and female BALB/c mice were collected via severing the jugular vein following anesthetization. Clotting and retraction was allowed to take place spontaneously at room temperature (around 20 °C) following procedures outlined

in Lachmann.[129] The initial centrifugation was carried out at 3000 g for 5 min at room temperature and the serum extracted. A second, high speed, centrifugation was performed to remove all red and white cell fragments at 20,000 g for 2 min. The serum was removed from this second centrifugation, aliquoted and frozen with liquid nitrogen, and stored at -80 °C for future use. Before use, all serum was thawed at 37 °C for 30 min.

3.3 Porcine

Venous blood was taken from healthy pigs where clotting and retraction was allowed to take place spontaneously at room temperature (around 20 °C) following procedures outlined in Lachmann.[129] After clotting at room temperature, blood samples were centrifuged at 1,250g for 5 min to obtain sera. Collected sera were aliquoted, frozen in liquid nitrogen, and stored at -80 °C. Before use, all serum was thawed at 37 °C for 30 min.

4. Confocal Microscopy

Confocal microscopy filters out-of-focus light creating images which have higher contrast, clarity, and detection sensitivity. This is achieved as the specimen is optically sectioned with a shallow depth of field (0.5–1.5 μm), allowing information to be collected from a well-defined plane. One or more points of laser light is sharply focused in all three directions: *x*, *y*, and *z*, *and then* passes through a pinhole in front of the camera to remove out-of-focus light. In order to detect nanoparticles with fluorescence techniques, ~100 nm diameter nanoparticles were conjugated with rhodamine dye (red, λexc 570 nm and λem 590 nm). During synthesis, the nanoparticles allow for covalent grafting of the dye to the silica, hindering the possibility of dye leaking from the nanoparticles.

Intracellular distribution of fluorescent NPs was assessed by confocal microscopy where human macrophages ($2x10^6$) were seeded on glass slides and washed with PBS (Invitrogen, CA, USA). 70% (v/v) human serum (HS), pig serum (PS), or mouse serum (MS), were incubated with 800 μg/mL (unless otherwise stated) uncoated, PEGylated, PMOXA-coated, or PEtOXA-coated NPs first in the absence of cells for 20 min at 37 °C and then incubated with cells after a 10-fold dilution in protein-free culture medium for 3 h at 37 °C. The media was removed following incubation, and cells were washed with PBS, and incubated for 30 min with 75 nM LysoTracker Green DND-26 (Invitrogen, CA, USA) for endolysosomal staining and then directly analyzed by confocal microscopy (Leica SP2, Germany). ImageJ software were used to analyze images. For control experiments NP were incubated in PBS.

5. Flow Cytometry

70% (v/v) human serum (HS), pig serum (PS), or mouse serum (MS), were incubated with 800 μg/mL (unless otherwise stated) uncoated, PEGylated, PMOXA-coated, or PEtOXA-coated NPs first in the absence of cells for 20 min at 37 °C and then incubated with cells after a 10-fold dilution in protein-free culture medium for 3 h at 37 °C. Cells were than washed with PBS, resuspended in FACS buffer (1% FBS in PBS), and analyzed by cytofluorimetry (FACSCantoII, Becton Dickinson, NJ, USA). Data were analyzed by FACSDiva software (Becton Dickinson, NJ, USA) and expressed as MFI (mean fluorescence intensity) values, normalized based on intrinsic quantum yield of different NPs types and batches. Certain experiments were performed with 10 mM EGTA/2 mM $MgCl_2$ or 10 mM EDTA or with 25 mM-100 mM of D-mannose, N-acetylglucosamine (inhibitors of lectin complement pathway) or D-galactose (as control). Dilution occurred as above in culture medium.

6. Proteomics:

6.1 Shotgun

Sera were thawed by incubation under stirring at 37 ℃ for 30 min. 75% (v/v) serum was further incubated with 800 ug/mL (or as stated) NPs under stirring at 37 ℃ for 20 min. The NP-serum mixture was washed via centrifugation and resuspension three times with 1 mL of ice-cold PBS pH 7.4, or PBS supplemented with 10mM $EDTA^{2+}$ or 10mM $EGTA^{2+}$ /2.5mM $MgCl_2$ or with D-mannose, N-acetylglucosamine (inhibitors of lectin complement pathway) or D-galactose (as control), and centrifuged for 30 min, 21,000 g at 4 ℃. Determination of the amount of protein was done according to the standard Bradford Assay (Biorad, CA, USA) with Bovine serum albumin (BSA) as a standard. Following incubation and centrifugation, NP-protein pellets were resuspended in 8 M urea/50 mM NH_4HCO_3 (Sigma, MO, USA). 5 mM TCEP (Sigma, MO, USA) was added to reduce disulfide bonds for 30 min, and alkylated with 40 mM iodacetamide (Fluka, Mexico) at room temperature in the dark. The content of urea was brought to 6 M with 50 mM NH_4HCO_3, and 1 to 100% (w/w) of LysC (Promega Co., WI, USA) was added to each sample for 6 hr at 37 ℃. Following experiment (20 min incubation with NPs at 37℃, centrifuge 3x at 13,000 at 4℃) resuspend final pellet in 40 ul of 8 M Urea in 50 mM NH_4HCO_3 (Sigma, MO, USA). 5 mM TCEP was added to reduce disulfide bonds for incubate for 30 min at RT, and alkylated with 40 mM iodacetamide (Fluka, Mexico) for 45 min at RT in the dark. The content of urea was brought to 6 M with 50 mM NH_4HCO_3, and 1:100% (w/w) of LysC (Promega Co., WI, USA) was added to each sample for 6 h at 37 ℃. The content of urea was brought to 1.2 M by dilution with 50 mM NH_4HCO_3.1:50% (w/w) of sequencing grade modified trypsin (Promega Co., WI, USA) was added to samples where digestion was carried out at 37 ℃ overnight. Samples were centrifuged at 18,000g for 30 min at 4℃ to recover supernatant. Samples were then dried under vacuum and suspended in 24 μL of 3% (v/v) acetonitrile/0.1% (v/v) formic acid. Next,

2 µL of each samples were analyzed by LC-MS/MS on a LTQ-Orbitrap XL mass spectrometer (ThermoFisher Scientific) coupled online to a nano-HPLC Ultimate 3000 (Dionex –ThermoFisher Scientific) as described earlier.[144] Peptides were loaded onto a pico-frit column (New Objective, NJ, USA) packed in-house with C18 material (Aeris Peptide 3.6 mmXBC18; Phenomenex, CA, USA) using a flow rate of 8 µL/min, and separated at a flow rate of 250 nL/min with a linear gradient of acetonitrile/0.1% (v/v) formic acid from 3% to 40% in 45 min. Ion source capillary temperature was 200 °C and spray voltage was set to 3% to 40% in 45 min. Ion source capillary temperature was 200 °C and spray voltage was set to 1.2-1.3 kV. The instrument operated in a data-dependent mode with a full scan at 60,000 resolution on the Orbitrap followed by MS/MS fragmentation in the linear trap of the four most intense ions.

6.2 In gel digestion and Mass-spec

Following initial experiments described above, and SDS PAGE gels (Section 7), the bands, stained with Coomassie, were excised from the gel and washed with 50% v/v acetonitrile (ACN) in 0.1 M NH_4HCO_3 and vacuum-dried. The proteins were reduced for 30 min at 56 °C with 10 mM DTT in 0.1 M NH_4HCO_3. The DTT solution was replaced with 55 mM iodacetamide in 0.1 M NH_4HCO_3 for 20 min at 25 °C in the dark. 50% ACN in 0.1 M NH_4HCO_3 was used to wash the dried gel pieces and then they were swollen in 15 µL of digestion buffer containing 25 mM NH_4HCO_3 and 12.5 ng/µL trypsin (Promega Co., WI, USA) and incubated overnight at 37 °C. Following the protocol described by Kin *et al*, tryptic peptides were extracted and analyzed by LC-MS/MS on a 6520 Q-TOF mass spectrometer (Agilent Technologies, CA, USA) coupled to a chip-based chromatographic interface. MALDI spectra were recorded with an AB SCIEX MALDI TOF/TOF, and α-Cyano-4-hydroxycinnamic acid (CHCA) was used as the matrix. MS/MS spectra were

searched against the SwissProt database, with the Mammalia taxonomy filter (June 2014 version, Taxonomy Mammalia, 66370 peptide entries). Enzyme specificity was set to trypsin/P with 2 missed cleavages, using a mass tolerance window of 20 ppm for parent mass and 0.6 Da for fragment ions. Carbamidomethylation of cysteine was set as fixed modification and methionine oxidation as variable modification. Proteins were considered positive hits if at least 2 peptides per protein were identified with high confidence ($p < 0.05$).

7. SDS-PAGE (PolyAcrylamide Gel Electrophoresis) and Western Blots

Sera were thawed by incubation under stirring at 37 °C for 30 min. 70% (v/v) serum was further incubated with NPs under stirring at 37 °C for 20 min. The NP-serum mixture was washed via centrifugation and resuspension three times with 1 mL of ice-cold PBS pH 7.4, or PBS supplemented with 10 mM $EDTA^{2+}$ or 10 mM $EGTA^{2+}$ /2.5 mM $MgCl_2$ or with D-mannose, N-acetylglucosamine (inhibitors of lectin complement pathway) or D-galactose (as control), and centrifuged for 30 min, 21,000 g at 4 °C. Pellets were dissolved in 25 µL of loading sample buffer (62.5 mM Tris-HCl, pH 6.8, 2% w/v SDS, 25% v/v glycerol, 0.01% w/v bromophenol blue, with or without β-mercaptoethanol). After heating at 95 °C for 5 min equal volumes (12 µL) of samples were subjected to SDS-PAGE in 12% acrylamide gels. Mock samples were always performed with serum protein in the absence of NPs exactly the same way the previous samples were prepared, to estimate nonspecific protein background. Proteins were stained with silver nitrate or with colloidal Coomassie G-250 in case of mass spectrometry analysis.

As for Gold NPs, anionic, cationic, neutral, or zwitterionic Au-NPs at indicated concentrations were incubated for 10 min at 37 °C in 70% citrated human plasma supplemented with 15 mM $CaCl_2$.

7.1 Colloidal Coomassie G-250 Staining

Gels were fixed for 18 hr in 50% methanol 2% H_3PO_4, rinsed 3 times for 30 min with water, and incubated for 1 hr in a solution containing 34% methanol, 2% H_3PO_4 and 17% $(NH_4)_2SO_4$. Staining was performed for 3 days in 34% methanol, 2% H_3PO_4, 17% $(NH_4)_2SO_4$ and 0.066% Coomassie G-250, and it was followed by de-staining in water for additional 3 days.

7.2 Silver Staining

Gels were fixed for 30 min in 50% methanol 10% acetic acid, incubated for 15 min in 5% methanol 1% acetic acid, washed 3 times with water and exposed for 90 seconds to thiosulfate solution (200 μg/mL $Na_2S_2O_3$ pentahydrate). After extensive washing with water, gels were incubated in the dark for 30' with 2 g/l $AgNO_3$, rinsed and developed for 5'-15' with a solution containing 60 mg/mL Na_2CO_3, 4 μg/mL $Na_2S_2O_3$ pentahydrate and 0.01875% formaldehyde. Reaction was stopped with 6% acetic acid.

7.3 Densitometry

Following SDS-PAGE (PolyAcrylamide Gel Electrophoresis) and Western Blot procedure as described in section 7, band intensities of NP associated proteins were estimated using Image J software after subtraction of the lane background from the calculations.

The area under the peak of identified peptides for each composition of the NPs corona is calculated and estimates the amount of protein by averaging the area.

7.4 Western Blot

In order to control complement activity, 25 µL of HS were treated with 6.25 µL of Zymosan (25 mg/mL, Sigma, MO, USA, prepared as described by manufacturer's instructions) for 30 min at 37 °C to be used as a positive control. 25 mM EDTA was used to stop the reaction. Following experimental incubation as described above, 1.6 µL of each sample were mixed with 38.4 µL of water and 6.7 µL of loading buffer without β-mercaptoethanol, and 15 µL of sample was loaded onto a 12% gel. Proteins were transferred on a PVDF membrane (Biorad, CA, USA) (100 V, 200 mA, 1 h). After membranes blocking for 1 hr at RT with 5% nonfat dry milk in TBS 0.1% Tween, primary antibodies were diluted in 1% nonfat dry milk in TBS and were added to the membranes overnight at 4 °C. Membranes were washed three times with TBS 0.1% Tween, incubated 1 hr with secondary antibodies, washed 4 times and developed using enhanced chemiluminescence by Huvitec (Eppendorf, Germany).

8. Coagulation kinetics

HP was incubated for 15 min at 37 ℃ to thaw. 80% HP +15 mM $CaCl_2$ was added to 96 well flat bottom plate. Particles at varying concentrations depending on experiment was added to the wells and mixed rapidly both manually and in the spectrophotometer for 5 seconds prior to readings. Lag time from calcium addition to HP until first reading was 3min. Optical Density was measured at 405 nm for 1 hr with readings every 1 min at 37 ℃.

Chapter 4: Perspectives

The area of biomedicine and nanotechnology is quite vast and encompasses a wide variety of research. My thesis work specifically pertains to the field of nanomedicine where NPs are utilized as drug delivery vehicles for the purpose of targeted drug delivery. Our data directly effects the preclinical trials of NPs including testing models and design of the NP itself. According to our research, current testing methods of NPs for drug delivery have many shortcomings, the most important being the way in which the NP interacts with interspecies complement proteins. As I have mentioned in chapter 1, it is crucial to improve specific drug-delivery methods in order for the NP systems to transfer into clinical effectiveness. Most drugs in biotechnology are limited by their poor solubility, high toxicity, high dosage requirements, aggregation, poor solubility, nonspecific delivery, *in vivo* degradation, and short circulating half-lives. However, drugs coupled with nanoparticles increase the drugs' theranostic abilities. Polymer coatings increase the NP-drug complex's bioavailability as well as decreases immune response and clearance. Our data pertains to this area by specifically studying certain polymer coatings and suggesting alternatives to current standards. Most significantly is the failure of Poly(2-oxazolines) to inhibit complement activation in humans and pigs as well as their ability to inhibit in mice. These results should affect the way in which we study NPs in the lab before bringing them to clinical trials with patients.

I have effectively demonstrated that coating ORMOSIL nanoparticles with PMOXA and PEtOXA polymers, which provides "stealthing" effects in murine conditions, effectively activates the complement system in human and pig environments. However, there were some limitations in experimental design which should be addressed. Firstly, although we suggested the potential role of ficolins in NP capture, further experiments are required to fully investigate the mechanism of ficolin in particle binding and capture. Effective protocols to

study the effect of sugars with cells should be designed in order to probe the effect of higher sugar concentrations on competition with ficolin with particle phagocytosis. For example, particles can be incubated with sugars to form the corona with ficolin binding competition. Therefore, cells do not need to be supplemented with sugars as the inhibition of ficolin will have already occurred in the initial incubation. Thus, high concentrations of sugars can be used without affecting cell viability.

Secondly, all experiments utilized pooled pig and mouse sera from multiple donors. However, we demonstrated previously in this lab NPs in human serum are captured differently depending on the blood donor from which the serum came from. Therefore, it would be quite interesting to study the variability in phagocytosis of specific porcine donors. The size of mice and the amount of blood that can be extracted from one mouse does not make it possible to look at an individual's complement response.

Thirdly, I have demonstrated ORMOSIL NPs behave similarly in pig serum as they do with human serum. This indicates complement proteins are either the same in both species or they interact with the NPs in a similar manner or mechanism. Further experiments with pig macrophages would be useful in supporting the previous findings discussed in this thesis including additional confocal microscopy and additional flow cytometry.

Fourthly, in order to probe the compatibility of the nanomaterial with the human immune system preclinically, it is highly beneficial to do so with human materials, instead of depending on non-human species such as murine models. Given Poly(2-oxazoline) (POZ) has been proposed as an alternative polymer for PEG as they are easier to synthesize and can incorporate varying monomers to tailor the nanoparticle for specific applications, future perspectives should focus on further modifications of POZs in order to evade recognition by components of the human innate immune system. Poly(2-isopropyl-2-oxazoline) (PPrOXA)

has been proposed as another polymer with side-chains of different variants of propyl which like PMOXA and PEtOXA are water-soluble or thermoresponsive polymers, however PPrOXA is semi-crystalline instead of amorphous. This difference could possibly change the way in which PPrOXA interacts with complement proteins and thus clearance by the immune system.

Furthermore, the shape of the surface is known to activate complement in different ways, for example spheres and short filomicelles are more rapidly taken up by cells than are longer filaments examined under fluid flow conditions because longer filaments are extended by the flow.[76] This indicates the internalization of nonspherical particles occurs via different mechanisms of endocytosis. Although such particles have already been tested in labs, they have not been tested using the serum of varying species nor cross-tested them with different polymers. It would be interesting to test nonspherical particles in the conditions we tested our spherical NPs and see if any particles would become more stealth.

Finally, my thesis focused on *in vitro* interactions between the NPs and serum proteins, however, in order to utilized NPs in the biomedical field, *in vivo* studies are particularly important. Since the most common model to study NPs is the mouse, it would be interesting to test the stealth abilities of the four ORMOSIL NPs *in vivo* in mice. Yet, more interestingly would be to test the NPs in a porcine model as it replicated the trends seen in humans *in vitro*. The most obvious difference between the mouse and humans is size where mice are about 2,500 times smaller than humans. Size is correlated with metabolic rates and the variations between mice and humans can manifest in anatomic, physiologic, and biochemical differences. Furthermore, different composition and properties of cellular components results in different strategies in immune responses. Thus, looking at the way in which the NPs

behave and interact with porcine cells would better characterize the NPs for future use in clinical trials in humans.

Although I have already proposed the pig as a great alternative to mice, purely out of my own personal curiosity, I would be highly interested in looking into particle behavior in rabbit and monkey models. Although I do not have access to them for any *in vivo* studies, sera could be purchased to conduct *in vitro* experiments, replicating what I've done with mice and pigs.

List of Figures and Tables:

Bibliography

1. Salata, O. Applications of nanoparticles in biology and medicine. *J. Nanobiotechnology* **2,** 3 (2004).
2. McNamara, K. & Tofail, S. A. M. Nanoparticles in biomedical applications. *Adv. Phys. X* **2,** 54–88 (2017).
3. Bangham, A. D. Liposomes: the Babraham connection. *Chem. Phys. Lipids* **64,** 275–285 (1993).
4. Gregoriadis, G. & Ryman, B. E. Liposomes as Carriers of Enzymes or Drugs: a New Approach to the Treatment of Storage Diseases. *Cell* 8–10 (1971).
5. Akbarzadeh, A. *et al.* Liposome: classification, preparation, and applications. *Nanoscale Res. Lett.* **8,** 102 (2013).
6. Lila, A. S. A., Ishida, T. & Allen, T. M. in *Handbook of Nanobiomedical Research: Fundamentals, Applications and Recent Developments* **3,** 1–53 (2014).
7. Allen, T. M. & Cullis, P. R. Liposomal drug delivery systems: From concept to clinical applications. *Adv. Drug Deliv. Rev.* **65,** 36–48 (2013).
8. Gregoriadis, G. Drug entrapment in liposomes. *FEBS Lett.* **36,** 292–296 (1973).
9. Scherphof, G., Roerdink, F., Waite, M. & Parks, J. Disintegration of phosphatidylcholine liposomes in plasma as a result of interaction with high-density lipoproteins. *Biochim. Biophys. Acta - Gen. Subj.* **542,** 296–307 (1978).
10. Kimelberg H.K., Tracy T.F., Biddlecome S.M., B. R. S. The effect of entrapment in liposomes on the in vivo distribution of 3H - methotrexate in a primate. *Cancer Res.* **36,** 2949 – 2957 (1976).
11. Sessions, P. Liposomes in the therapy of infectious diseases and cancer. *J. Cell. Biochem.* **38,** 244–262 (1988).
12. Hamad-Schifferli, K. How can we exploit the protein corona? *Nanomedicine* **8,** 1–3 (2013).
13. Proffitt, R. *et al.* Liposomal blockade of the reticuloendothelial system: improved tumor imaging with small unilamellar vesicles. *Science (80-.).* **220,** 502–505 (1983).
14. Blume, G. & Cevc, G. Liposomes for the sustained drug release in vivo. *Biochim. Biophys. Acta - Biomembr.* **1029,** 91–97 (1990).
15. Klibanov, A. L., Maruyama, K., Torchilin, V. P. & Huang, L. Amphipathic polyethyleneglycols effectively prolong the circulation time of liposomes. *FEBS Lett.* **268,** 235–237 (1990).
16. Immordino, M. L., Dosio, F. & Cattel, L. Stealth liposomes: review of the basic science, rationale, and clinical applications, existing and potential. *Int. J. Nanomedicine* **1,** 297–315 (2006).
17. MG, K., V, K. & F, H. History and Possible Uses of Nanomedicine Based on Nanoparticles and Nanotechnological Progress. *J. Nanomed. Nanotechnol.* **06,** (2015).
18. Moghimi, S. M. & Szebeni, J. Stealth liposomes and long circulating nanoparticles: critical issues in pharmacokinetics, opsonization and protein-binding properties. *Prog. Lipid Res.* **42,** 463–478 (2003).
19. James, N. D. *et al.* Liposomal doxorubicin (Doxil): An effective new treatment for Kaposi's sarcoma in AIDS. *Clin. Oncol.* **6,** 294–296 (1994).
20. García, K. P. *et al.* Zwitterionic-Coated "Stealth" Nanoparticles for Biomedical Applications: Recent Advances in Countering Biomolecular Corona Formation and Uptake by the Mononuclear Phagocyte System. *Small* **10,** 2516–2529 (2014).
21. Brannon-Peppas, L. Recent advances on the use of biodegradable microparticles and nanoparticles in controlled drug delivery. *Int. J. Pharm.* **116,** 1–9 (1995).
22. Bharti, C., Gulati, N., Nagaich, U. & Pal, A. Mesoporous silica nanoparticles in target drug delivery system: A review. *Int. J. Pharm. Investig.* **5,** 124 (2015).
23. Kong, M. *et al.* Biodegradable Hollow Mesoporous Silica Nanoparticles for Regulating Tumor Microenvironment and Enhancing Antitumor Efficiency. *Theranostics* **7,** 3276–3292 (2017).
24. Meng, H. *et al.* Use of a Lipid-Coated Mesoporous Silica Nanoparticle Platform for Synergistic Gemcitabine and Paclitaxel Delivery to Human Pancreatic Cancer in Mice. *ACS Nano* **9,** 3540–3557 (2015).
25. Malachin, G., Lubian, E., Mancin, F., Papini, E. & Tavano, R. Combined Action of Human Commensal Bacteria and Amorphous Silica Nanoparticles on the Viability and Immune Responses of Dendritic Cells. *Clin. Vaccine Immunol.* **24,** e00178-17 (2017).
26. Xia, X., Kupferschmidt, N. & Garcia-Bennett, A. E. in *Handbook of Nanobiomedical Research: Fundamentals, Applications and Recent Developments* 75–96 (2014). doi:10.1142/9789814520652_0054
27. Tang, L. & Cheng, J. Nonporous silica nanoparticles for nanomedicine application. *Nano Today* **8,** 290–312 (2013).
28. Mero, A. *et al.* Synthesis and characterization of poly(2-ethyl 2-oxazoline)-conjugates with proteins and drugs: Suitable alternatives to PEG-conjugates? *J. Control. Release* **125,** 87–95 (2008).
29. Psychogios, N. *et al.* The Human Serum Metabolome. *PLoS One* **6,** e16957 (2011).
30. Kumar, H., Kawai, T. & Akira, S. Pathogen Recognition by the Innate Immune System. *Int. Rev. Immunol.* **30,** 16–34 (2011).
31. Szeto, G. L. & Lavik, E. B. Materials design at the interface of nanoparticles and innate immunity. *J. Mater. Chem. B* **4,** 1610–1618 (2016).
32. Forrester, J. V., Dick, A. D., McMenamin, P. G., Roberts, F. & Pearlman, E. in *The Eye* 370–461.e2 (Elsevier, 2016). doi:10.1016/B978-0-7020-5554-6.00007-1
33. Zipfel, P. F. & Skerka, C. Complement regulators and inhibitory proteins. *Nat. Rev. Immunol.* **9,** 729–740 (2009).
34. Thomas, S. N. *et al.* Engineering complement activation on polypropylene sulfide vaccine nanoparticles. *Biomaterials* **32,** 2194–2203 (2011).
35. Kishore, U. & Reid, K. B. . C1q: Structure, function, and receptors. *Immunopharmacology* **49,** 159–170 (2000).
36. Almitairi, J. O. M. *et al.* Structure of the C1r–C1s interaction of the C1 complex of complement activation. *Proc. Natl. Acad. Sci.* **115,** 768–773 (2018).
37. Merle, N. S., Church, S. E., Fremeaux-Bacchi, V. & Roumenina, L. T. Complement System Part I - Molecular

Mechanisms of Activation and Regulation. *Front. Immunol.* **6,** 262 (2015).
38. Devine, D. V. in *Blood Banking and Transfusion Medicine* 30–42 (Elsevier, 2007). doi:10.1016/B978-0-443-06981-9.50008-9
39. Moghimi, S. M. & Simberg, D. Complement activation turnover on surfaces of nanoparticles. *Nano Today* **15,** 8–10 (2017).
40. Bartlomiejczyk, M. A., Swierzko, A. S., Brzostek, A., Dziadek, J. & Cedzynski, M. Interaction of lectin pathway of complement-activating pattern recognition molecules with Mycobacteria. *Clin. Exp. Immunol.* **178,** 310–319 (2014).
41. Krarup, A., Thiel, S., Hansen, A., Fujita, T. & Jensenius, J. C. L-ficolin Is a Pattern Recognition Molecule Specific for Acetyl Groups. *J. Biol. Chem.* **279,** 47513–47519 (2004).
42. Le, Y., Lee, S. ., Kon, O. . & Lu, J. Human <scp>l</scp> -ficolin: plasma levels, sugar specificity, and assignment of its lectin activity to the fibrinogen-like (FBG) domain. *FEBS Lett.* **425,** 367–370 (1998).
43. Tan, S. M. *et al.* Improvements on the purification of mannan-binding lectin and demonstration of its Ca(2+)-independent association with a C1s-like serine protease. *Biochem. J.* **319 (Pt 2,** 329–32 (1996).
44. Le, Y., Tan, S. ., Lee, S. ., Kon, O. . & Lu, J. Purification and binding properties of a human ficolin-like protein. *J. Immunol. Methods* **204,** 43–49 (1997).
45. Brady, A. M., Spencer, B. L., Falsey, A. R. & Nahm, M. H. Blood Collection Tubes Influence Serum Ficolin-1 and Ficolin-2 Levels. *Clin. Vaccine Immunol.* **21,** 51–55 (2014).
46. Drickamer, K. Engineering galactose-binding activity into a C-type mannose-binding protein. *Nature* **360,** 183–186 (1992).
47. Dambuza, I. M. & Brown, G. D. C-type lectins in immunity: recent developments. *Curr. Opin. Immunol.* **32,** 21–27 (2015).
48. Rosbjerg, A., Genster, N., Pilely, K. & Garred, P. Evasion Mechanisms Used by Pathogens to Escape the Lectin Complement Pathway. *Front. Microbiol.* **8,** 1–7 (2017).
49. Ali, Y. M. *et al.* The Lectin Pathway of Complement Activation Is a Critical Component of the Innate Immune Response to Pneumococcal Infection. *PLoS Pathog.* **8,** e1002793 (2012).
50. Endo, Y., Matsushita, M. & Fujita, T. The role of ficolins in the lectin pathway of innate immunity. *Int. J. Biochem. Cell Biol.* **43,** 705–712 (2011).
51. Janssen, B. J. C., Christodoulidou, A., McCarthy, A., Lambris, J. D. & Gros, P. Structure of C3b reveals conformational changes that underlie complement activity. *Nature* **444,** 213–216 (2006).
52. Seifert, P. S., Messner, M., Roth, I. & Bhakdi, S. Analysis of complement C3 activation products in human atherosclerotic lesions. *Atherosclerosis* **91,** 155–162 (1991).
53. Shahini, N. *et al.* The alternative complement pathway is dysregulated in patients with chronic heart failure. *Sci. Rep.* **7,** 42532 (2017).
54. Oikonomopoulou, K., Ricklin, D., Ward, P. A. & Lambris, J. D. Interactions between coagulation and complement—their role in inflammation. *Semin. Immunopathol.* **34,** 151–165 (2012).
55. Gordon, S. M. & Remaley, A. T. High density lipoproteins are modulators of protease activity: Implications in inflammation, complement activation, and atherothrombosis. *Atherosclerosis* **259,** 104–113 (2017).
56. Yun, S.-H., Sim, E.-H., Goh, R.-Y., Park, J.-I. & Han, J.-Y. Platelet Activation: The Mechanisms and Potential Biomarkers. *Biomed Res. Int.* **2016,** 1–5 (2016).
57. Hirata, T. & Narumiya, S. in *Advances in Immunology* **116,** 143–174 (Elsevier Inc., 2012).
58. Wood, J. P., Ellery, P. E. R., Maroney, S. A. & Mast, A. E. Biology of tissue factor pathway inhibitor. *Blood* **123,** 2934–2943 (2014).
59. Amara, U. *et al.* in 68–76 (2008). doi:10.1007/978-0-387-78952-1_6
60. Puy, C. *et al.* Activated factor XI increases the procoagulant activity of the extrinsic pathway by inactivating tissue factor pathway inhibitor. *Blood* **125,** 1488–1496 (2015).
61. Sanfins, E., Augustsson, C., Dahlbäck, B., Linse, S. & Cedervall, T. Size-Dependent Effects of Nanoparticles on Enzymes in the Blood Coagulation Cascade. *Nano Lett.* **14,** 4736–4744 (2014).
62. Bassendine, M. F. *et al.* HCV and the hepatic lipid pathway as a potential treatment target. *J. Hepatol.* **55,** 1428–1440 (2011).
63. Dominiczak, M. H. & Caslake, M. J. Apolipoproteins: metabolic role and clinical biochemistry applications. *Ann. Clin. Biochem.* **48,** 498–515 (2011).
64. Lange, S., Dodds, A. W., Gudmundsdóttir, S., Bambir, S. H. & Magnadóttir, B. The ontogenic transcription of complement component C3 and Apolipoprotein A-I tRNA in Atlantic cod (Gadus morhua L.)—a role in development and homeostasis? *Dev. Comp. Immunol.* **29,** 1065–1077 (2005).
65. Qie, Y. *et al.* Surface modification of nanoparticles enables selective evasion of phagocytic clearance by distinct macrophage phenotypes. *Sci. Rep.* **6,** 26269 (2016).
66. Boyette, L. B. *et al.* Phenotype, function, and differentiation potential of human monocyte subsets. *PLoS One* **12,** e0176460 (2017).
67. Tamás, R. Understanding th Mysterious M2 macrophage through activation markers and effector mechanism. *Mediators Inflamm.* **2015,** 16 (2015).
68. Shi, C. & Pamer, E. G. Monocyte recruitment during infection and inflammation. *Nat. Rev. Immunol.* **11,** 762–774 (2011).
69. Jakubzick, C. V., Randolph, G. J. & Henson, P. M. Monocyte differentiation and antigen-presenting functions. *Nat. Rev. Immunol.* **17,** 349–362 (2017).
70. Chow, A., Brown, B. D. & Merad, M. Studying the mononuclear phagocyte system in the molecular age. *Nat. Rev. Immunol.* **11,** 788–798 (2011).

71. Idzkowska, E. *et al.* The Role of Different Monocyte Subsets in the Pathogenesis of Atherosclerosis and Acute Coronary Syndromes. *Scand. J. Immunol.* **82,** 163–173 (2015).
72. Zhang, X. Gold Nanoparticles: Recent Advances in the Biomedical Applications. *Cell Biochem. Biophys.* **72,** 771–775 (2015).
73. Lai, W. *et al.* Interaction of gold and silver nanoparticles with human plasma: Analysis of protein corona reveals specific binding patterns. *Colloids Surfaces B Biointerfaces* **152,** 317–325 (2017).
74. Fleischer, C. C. & Payne, C. K. Secondary Structure of Corona Proteins Determines the Cell Surface Receptors Used by Nanoparticles. *J. Phys. Chem. B* **118,** 14017–14026 (2014).
75. Longmire, M., Choyke, P. L. & Kobayashi, H. Clearance properties of nano-sized particles and molecules as imaging agents: considerations and caveats. *Nanomedicine* **3,** 703–717 (2008).
76. Geng, Y. *et al.* Shape effects of filaments versus spherical particles in flow and drug delivery. *Nat. Nanotechnol.* **2,** 249–255 (2007).
77. Chen, H., Zou, P., Connarn, J., Paholak, H. & Sun, D. Intracellular dissociation of a polymer coating from nanoparticles. *Nano Res.* **5,** 815–825 (2012).
78. Kreyling, W. G. *et al.* In vivo integrity of polymer-coated gold nanoparticles. *Nat. Nanotechnol.* **10,** 619–623 (2015).
79. Jeon, S. ., Lee, J. ., Andrade, J. . & De Gennes, P. . Protein-surface interactions in the presence of polyethylene oxide. *J. Colloid Interface Sci.* **142,** 149–158 (1991).
80. Ulbrich, K. *et al.* Targeted Drug Delivery with Polymers and Magnetic Nanoparticles: Covalent and Noncovalent Approaches, Release Control, and Clinical Studies. *Chem. Rev.* **116,** 5338–5431 (2016).
81. Singh, R. & Lillard, J. W. Nanoparticle-based targeted drug delivery. *Exp. Mol. Pathol.* **86,** 215–223 (2009).
82. Singh, N. *et al.* Bioresponsive Mesoporous Silica Nanoparticles for Triggered Drug Release. *J. Am. Chem. Soc.* **133,** 19582–19585 (2011).
83. Pan, D. *et al.* Contact-facilitated drug delivery with Sn2 lipase labile prodrugs optimize targeted lipid nanoparticle drug delivery. *Wiley Interdiscip. Rev. Nanomedicine Nanobiotechnology* **8,** 85–106 (2016).
84. Lockman, P. R., Mumper, R. J., Khan, M. A. & Allen, D. D. Nanoparticle Technology for Drug Delivery Across the Blood-Brain Barrier. *Drug Dev. Ind. Pharm.* **28,** 1–13 (2002).
85. Barik, T. K., Sahu, B. & Swain, V. Nanosilica-from medicine to pest control. *Parasitol. Res.* **103,** 253–258 (2008).
86. Napierska, D., Thomassen, L. C. J., Lison, D., Martens, J. A. & Hoet, P. H. The nanosilica hazard: another variable entity. *Part. Fibre Toxicol.* **7,** 39 (2010).
87. Rio-Echevarria, I. M. *et al.* Highly PEGylated silica nanoparticles: "ready to use" stealth functional nanocarriers. *J. Mater. Chem.* **20,** 2780 (2010).
88. Liberman, A., Mendez, N., Trogler, W. C. & Kummel, A. C. Synthesis and surface functionalization of silica nanoparticles for nanomedicine. *Surf. Sci. Rep.* **69,** 132–158 (2014).
89. Finnie, K. S., Bartlett, J. R., Barbé, C. J. A. & Kong, L. Formation of Silica Nanoparticles in Microemulsions. *Langmuir* **23,** 3017–3024 (2007).
90. Pissuwan, D., Niidome, T. & Cortie, M. B. The forthcoming applications of gold nanoparticles in drug and gene delivery systems. *J. Control. Release* **149,** 65–71 (2011).
91. Link, S.-S. & El-Sayed, M. A. Shape and size dependence of radiative, non-radiative and photothermal properties of gold nanocrystals. *Int. Rev. Phys. Chem.* **19,** 409–453 (2000).
92. Yeh, Y.-C., Creran, B. & Rotello, V. M. Gold nanoparticles: preparation, properties, and applications in bionanotechnology. *Nanoscale* **4,** 1871–1880 (2012).
93. Huang, X. & El-Sayed, M. A. Gold nanoparticles: Optical properties and implementations in cancer diagnosis and photothermal therapy. *J. Adv. Res.* **1,** 13–28 (2010).
94. Amendola, V., Pilot, R., Frasconi, M., Maragò, O. M. & Iatì, M. A. Surface plasmon resonance in gold nanoparticles: a review. *J. Phys. Condens. Matter* **29,** 203002 (2017).
95. Das, M., Shim, K. H., An, S. S. A. & Yi, D. K. Review on gold nanoparticles and their applications. *Toxicol. Environ. Health Sci.* **3,** 193–205 (2011).
96. Xia, H., Bai, S., Hartmann, J. & Wang, D. Synthesis of monodisperse quasi-spherical gold nanoparticles in water via silver(I)-assisted citrate reduction. *Langmuir* **26,** 3585–3589 (2010).
97. Ajdari, N., Vyas, C., Bogan, S. L., Lwaleed, B. A. & Cousins, B. G. Gold nanoparticle interactions in human blood: a model evaluation. *Nanomedicine Nanotechnology, Biol. Med.* **13,** 1531–1542 (2017).
98. Knop, K., Hoogenboom, R., Fischer, D. & Schubert, U. S. Poly(ethylene glycol) in Drug Delivery: Pros and Cons as Well as Potential Alternatives. *Angew. Chemie Int. Ed.* **49,** 6288–6308 (2010).
99. Salmaso, S. & Caliceti, P. in *Peptide and Protein Delivery* 247–290 (Elsevier, 2011). doi:10.1016/B978-0-12-384935-9.10011-2
100. Tavano, R. *et al.* Procoagulant properties of bare and highly PEGylated vinyl-modified silica nanoparticles. *Nanomedicine* **5,** 881–896 (2010).
101. Turecek, P. L., Bossard, M. J., Schoetens, F. & Ivens, I. A. PEGylation of Biopharmaceuticals: A Review of Chemistry and Nonclinical Safety Information of Approved Drugs. *J. Pharm. Sci.* **105,** 460–475 (2016).
102. Veronese, F. M. & Pasut, G. PEGylation, successful approach to drug delivery. *Drug Discov. Today* **10,** 1451–1458 (2005).
103. Branch, D. Long-term stability of grafted polyethylene glycol surfaces for use with microstamped substrates in neuronal cell culture. *Biomaterials* **22,** 1035–1047 (2001).
104. Pidhatika, B. *et al.* Comparative Stability Studies of Poly(2-methyl-2-oxazoline) and Poly(ethylene glycol) Brush Coatings. *Biointerphases* **7,** 1 (2012).
105. Bludau, H. *et al.* POxylation as an alternative stealth coating for biomedical applications. *Eur. Polym. J.* **88,** 679–

688 (2017).
106. Sedlacek, O., Monnery, B. D., Filippov, S. K., Hoogenboom, R. & Hruby, M. Poly(2-Oxazoline)s - Are They More Advantageous for Biomedical Applications Than Other Polymers? *Macromol. Rapid Commun.* **33,** 1648–1662 (2012).
107. Wilson, P., Ke, P. C., Davis, T. P. & Kempe, K. Poly(2-oxazoline)-based micro- and nanoparticles: A review. *Eur. Polym. J.* **88,** 486–515 (2017).
108. AOI, K. Polymerization of oxazolines. *Prog. Polym. Sci.* **21,** 151–208 (1996).
109. de la Rosa, V. R. Poly(2-oxazoline)s as materials for biomedical applications. *J. Mater. Sci. Mater. Med.* **25,** 1211–1225 (2014).
110. Viegas, T. X. *et al.* Polyoxazoline: Chemistry, Properties, and Applications in Drug Delivery. *Bioconjug. Chem.* **22,** 976–986 (2011).
111. Mansfield, E. D. H., Sillence, K., Hole, P., Williams, A. C. & Khutoryanskiy, V. V. POZylation: a new approach to enhance nanoparticle diffusion through mucosal barriers. *Nanoscale* **7,** 13671–13679 (2015).
112. Dawson, H. D. *et al.* Structural and functional annotation of the porcine immunome. *BMC Genomics* **14,** 332 (2013).
113. Michael Holers, V., Kinoshita, T. & Molina, H. The evolution of mouse and human complement C3-binding proteins: divergence of form but conservation of function. *Immunol. Today* **13,** 231–236 (1992).
114. Mair, K. H. *et al.* The porcine innate immune system: An update. *Dev. Comp. Immunol.* **45,** 321–343 (2014).
115. de Bruijn, M. H. & Fey, G. H. Human complement component C3: cDNA coding sequence and derived primary structure. *Proc. Natl. Acad. Sci.* **82,** 708–712 (1985).
116. Perlman, R. L. Mouse Models of Human Disease: An Evolutionary Perspective. *Evol. Med. Public Heal.* eow014 (2016). doi:10.1093/emph/eow014
117. Hulbert, A. J. The links between membrane composition, metabolic rate and lifespan. *Comp. Biochem. Physiol. - A Mol. Integr. Physiol.* **150,** 196–203 (2008).
118. Fedeli, C. *et al.* The functional dissection of the plasma corona of SiO 2 -NPs spots histidine rich glycoprotein as a major player able to hamper nanoparticle capture by macrophages. *Nanoscale* **7,** 17710–17728 (2015).
119. Butler, J. E. Bovine immunoglobulins: An augmented review. *Vet. Immunol. Immunopathol.* **4,** 43–152 (1983).
120. Izak-Nau, E., Voetz, M., Eiden, S., Duschl, A. & Puntes, V. F. Altered characteristics of silica nanoparticles in bovine and human serum: the importance of nanomaterial characterization prior to its toxicological evaluation. *Part. Fibre Toxicol.* **10,** 56 (2013).
121. Martinez, M. N. Factors Influencing the Use and Interpretation of Animal Models in the Development of Parenteral Drug Delivery Systems. *AAPS J.* **13,** 632–649 (2011).
122. Molina, H. *et al.* Markedly impaired humoral immune response in mice deficient in complement receptors 1 and 2. **93,** 3357–3361 (1996).
123. Kobayashi, C. *et al.* Features of a Newly Cloned Pig C1 Esterase Inhibitor. *J. Biochem.* **140,** 421–427 (2006).
124. Moghimi, S. . & Patel, H. . Serum-mediated recognition of liposomes by phagocytic cells of the reticuloendothelial system – The concept of tissue specificity. *Adv. Drug Deliv. Rev.* **32,** 45–60 (1998).
125. Lesniak, A. *et al.* Effects of the Presence or Absence of a Protein Corona on Silica Nanoparticle Uptake and Impact on Cells. *ACS Nano* **6,** 5845–5857 (2012).
126. Aoyama, M. *et al.* Clusterin in the protein corona plays a key role in the stealth effect of nanoparticles against phagocytes. *Biochem. Biophys. Res. Commun.* **480,** 690–695 (2016).
127. Lundqvist, M. *et al.* Nanoparticle size and surface properties determine the protein corona with possible implications for biological impacts. *Proc. Natl. Acad. Sci.* **105,** 14265–14270 (2008).
128. Ohashi, T. & Erickson, H. P. Oligomeric Structure and Tissue Distribution of Ficolins from Mouse, Pig and Human. *Arch. Biochem. Biophys.* **360,** 223–232 (1998).
129. Lachmann, P. J. Preparing serum for functional complement assays. *J. Immunol. Methods* **352,** 195–197 (2010).
130. Klickstein, L. B. *et al.* Human C3b/C4b receptor (CR1). Demonstration of long homologous repeating domains that are composed of the short consensus repeats characteristics of C3/C4 binding proteins. *J. Exp. Med.* **165,** 1095–112 (1987).
131. Pavlou, S., Lindsay, J., Ingram, R., Xu, H. & Chen, M. Sustained high glucose exposure sensitizes macrophage responses to cytokine stimuli but reduces their phagocytic activity. 1–13 (2018). doi:10.1186/s12865-018-0261-0
132. Laffly, E. *et al.* Human ficolin-2 recognition versatility extended: An update on the binding of ficolin-2 to sulfated/phosphated carbohydrates. *FEBS Lett.* **588,** 4694–4700 (2014).
133. Garlatti, V. *et al.* Structural insights into the innate immune recognition specificities of L- and H-ficolins. *EMBO J.* **26,** 623–633 (2007).
134. Hamad, I. *et al.* Distinct Polymer Architecture Mediates Switching of Complement Activation Pathways at the Nanosphere−Serum Interface: Implications for Stealth Nanoparticle Engineering. *ACS Nano* **4,** 6629–6638 (2010).
135. Moghimi, S. M., Wibroe, P. P., Wu, L. & Farhangrazi, Z. S. Insidious pathogen-mimicking properties of nanoparticles in triggering the lectin pathway of the complement system. *Eur. J. nanomedicine* **7,** 263–268 (2015).
136. Owens III, D. & Peppas, N. Opsonization, biodistribution, and pharmacokinetics of polymeric nanoparticles. *Int. J. Pharm.* **307,** 93–102 (2006).
137. Stavenuiter, F. *et al.* Factor seven activating protease (FSAP): does it activate factor VII? *J. Thromb. Haemost.* **10,** 859–866 (2012).
138. Soulban, G., Labrecque, G. & Barbeau, G. Time-Dependent Variations in the Coagulation Factors II, VII, IX, and X in Young and Elderly Volunteers. *Chronobiol. Int.* **12,** 206–213 (1995).
139. Kannemeier, C. *et al.* Factor VII and single-chain plasminogen activator-activating protease. *Eur. J. Biochem.* **268,** 3789–3796 (2001).

140. Zeerleder, S. *et al.* Nucleosome-releasing factor: a new role for factor VII-activating protease (FSAP). *FASEB J.* **22,** 4077–4084 (2008).
141. Sperling, C., Maitz, M. F., Grasso, S., Werner, C. & Kanse, S. M. A Positively Charged Surface Triggers Coagulation Activation Through Factor VII Activating Protease (FSAP). *ACS Appl. Mater. Interfaces* **9,** 40107–40116 (2017).
142. Rampazzo, E. *et al.* Energy Transfer from Silica Core−Surfactant Shell Nanoparticles to Hosted Molecular Fluorophores †. *J. Phys. Chem. B* **114,** 14605–14613 (2010).
143. Kapetanovic, R. & Fairbairn, L. Macrophages Isolation in Pig (Monocyte, Peritoneal, Alveolar, and Bone-Marrow). *Rosl. Inst.* 5–9 (2009).
144. Gerotto, C., Franchin, C., Arrigoni, G. & Morosinotto, T. In Vivo Identification of Photosystem II Light Harvesting Complexes Interacting with PHOTOSYSTEM II SUBUNIT S. *Plant Physiol.* **168,** 1747–1761 (2015).

Appendix

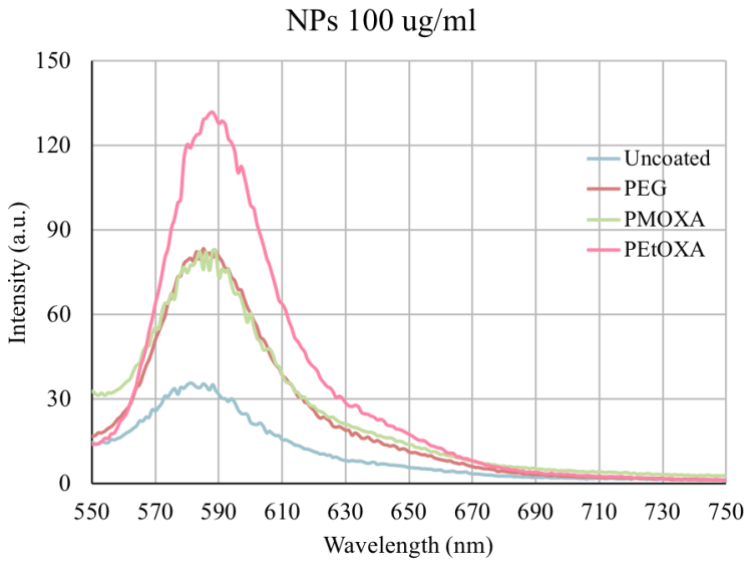

Figure 52: UV-VIS Spectral Analysis of 100 ug/L Uncoated, PEGylated, PMOXA-coated, and PEtOXA- coated ORMOSIL NPs in Water. Rhodamine concentration was determined from absorbance λ= 567 nm (after scattering contribution subtraction) using the molar extinction coefficient (ε) of 9.5×14⁴ cm^{-1} M^{-1}.

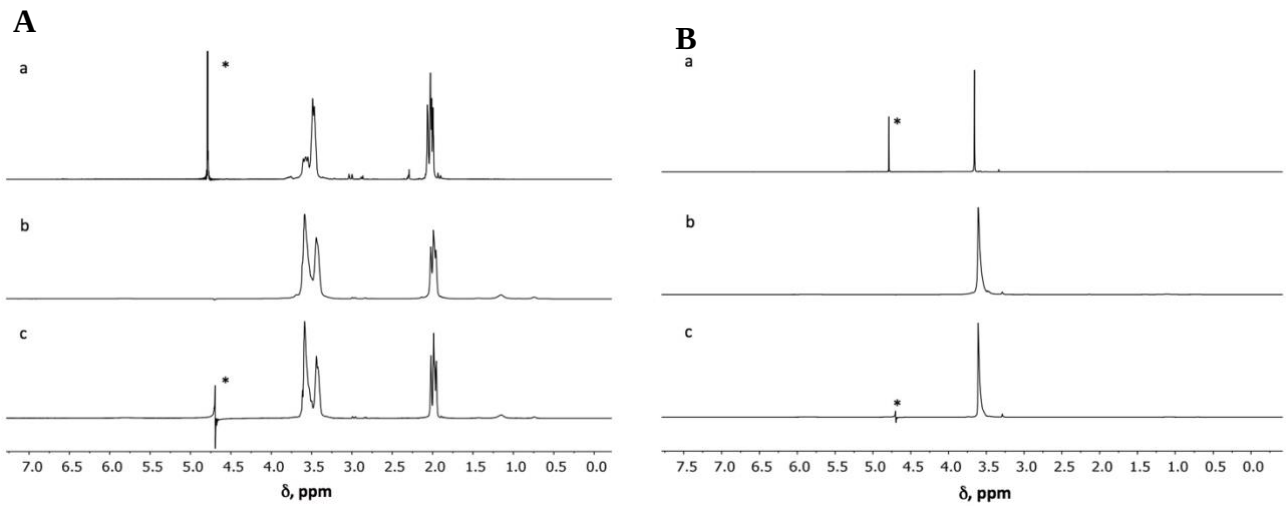

Figure 53: A) ^{1}H-NMR (500 MHz) subspectrum of a) PMOXA-amine in D_2O, b) PMOXA-coated NPs in D_2O /H_2O 1:9, (H_20 signal was suppressed), c) Diffusion filtered spectrum of b. B) ^{1}H-NMR (500 MHz) subspectrum of a) PEG-OMe in D_2O, b) PEGylated NPs in D_2O / H_20 1:9, (H_20 signal was suppressed), c) Diffusion filtered spectrum of b. (indicates the residual solvents.)*